Methods and models for the concept design of liquefied natural gas fuel systems on ships

Jonas Thiaucourt

THESE DE DOCTORAT DE

L'ÉCOLE CENTRALE DE NANTES

COMUE UNIVERSITE BRETAGNE LOIRE

ECOLE DOCTORALE N° 602
Sciences pour l'Ingénieur
Spécialité : *« Energétique-Thermique-Combustion »*

Par
Jonas THIAUCOURT

Méthodes et modèles pour l'étude de faisabilité des navires propulsés au gaz naturel liquéfié

Thèse présentée et soutenue à Nantes, le 30 septembre 2019
Unité de recherche : UMR 6598
Laboratoire de recherche en Hydrodynamique, Energétique et Environnement Atmosphérique

Rapporteurs avant soutenance

Laura A. Pellegrini	Professeure, Ecole Polytechnique de Milan
Christelle Perilhon	Maitre de conférences HDR, Conservatoire National des Arts et Métiers (CNAM)

Composition du Jury

Président	Sofiane Khelladi	Professeur, Arts et Métiers ParisTech
Examinateur	Gordon Paker	Professeur, Université Technologique du Michigan
Dir. de thèse	Jean-François Hétet	Professeur, Ecole Centrale de Nantes
Co-dir. de thèse	Etienne Delaire	Docteur, Ecole Nationale Supérieure Maritime
	Pascal Robert	Docteur, Ecole Nationale Supérieure Maritime

Contents

Abstract

Methods and models for the concept design of liquefied natural gas fuel systems on ships

In proportion to the ton of cargo, shipping is a relatively "clean" transportation mode. Nevertheless, due to trade intensification, its share in the global greenhouse gas (GHG) emissions should increase. Aware that GHG adverse effects are a major concern for humanity, united nation member states impose, via the international maritime organization, a regulatory framework so that this vital sector remains sustainable. Ambitious short (2020) and medium (2050)-term goals are set. According to the weak version of Porter's hypothesis, strict environmental regulations encourage innovations. Hence, in the shipping industry, solutions flourish among which the use of natural gas as a fuel. To save space on-board, natural gas is stored at low temperature (around 111 K) under its liquid form known as Liquefied Natural Gas (LNG).

On a thermodynamic basis, the unavoidable heat leaks into the cryogenic tanks cause variations of the:

- tank pressure;
- natural gas quality at engine inlet.

Depending on the ship's operational profile, those two phenomena will impact significantly the LNG as a fuel option relevance. One major bottleneck slowing the uptake of LNG as a marine fuel is the lack of methods and models to perform, at a concept design level, the feasibility study.

In response, this thesis proposes 0D models to assess, from the operational profile, the:

1. tank pressure evolution;
2. natural gas quality evolution at engine inlet.

In the first part, models are proposed to simulate heat leaks into the tanks, LNG vaporization, ageing (the alteration of natural gas thermophysical properties by a differentiate vaporization of its compounds) and methane number evolution at engine inlet.

Then, the models are put together and applied on a case study. The case study is brought by a freight company.

Keywords: Liquefied Natural Gas (LNG), Natural gas fueled ship, IGF Code, Boil-off, Cryogenic fuel.

Abstract in French

Méthodes et modèles pour l'étude de faisabilité des navires propulsés au gaz naturel liquéfié

Rapporté à la tonne de fret, le trafic maritime est un mode de transport relativement « propre ». Néanmoins, par l'intensification des échanges mondiaux, sa part dans les émissions de Gaz à Effet de Serre (GES) est appelée à augmenter. Conscients des effets néfastes associés aux GES, les pays membres des nations unies, via l'organisation maritime internationale, imposent le cadre réglementaire pour que ce secteur demeure écologiquement acceptable. Des objectifs ambitieux sont établis à court et moyen terme (2020 et 2050). Or, d'après l'hypothèse faible de Porter, fixer des objectifs environnementaux sans imposer les moyens à mettre en œuvre favorise l'innovation. Aussi, dans l'industrie du « shipping », les solutions fleurissent au premier rang desquelles figure l'emploi du gaz naturel en tant que combustible. Afin de minimiser son encombrement à bord, le gaz naturel est stocké à basse température (autour de -162°C) sous la forme de Gaz Naturel Liquéfié (GNL).

D'un point de vue thermodynamique, les inévitables infiltrations thermiques à travers les parois des réservoirs cryogéniques entraînent une variation:

- de la pression dans le réservoir;
- et de la qualité du gaz à l'admission moteur.

Selon le schéma d'exploitation navire, ces deux grandeurs impactent significativement la pertinence de l'option GNL. Or, un des freins au développement du GNL comme combustible marin est le manque d'outils et méthodes pour réaliser ces études de faisabilité technico-économique en phase d'avant-projet navire.

En réponse, cette thèse propose un ensemble de modèles 0D qui, à partir d'un profil opérationnel, permettent d'évaluer:

1. l'évolution de la pression dans les réservoirs;
2. l'évolution de la qualité du gaz à l'admission moteur.

Dans une première partie, des modèles sont proposés pour simuler les infiltrations thermiques à travers le réservoir, l'évaporation du GNL, son vieillissement (altération des propriétés du gaz par évaporation différenciée des composés) et l'évolution du taux de méthane à l'admission moteur.

Puis, les modèles sont assemblés à travers une étude de faisabilité technico-économique. Le cas d'étude est apporté par un acteur du transport maritime.

Mots-clés: Gaz Naturel Liquéfié (GNL), Navire gaz, Code IGF, Boil-off, Combustible cryogénique

Acknowledgments

"On ne juge pas le Cyborg à son ossature, je veux faire le tour de ma planète comme les anneaux de Saturne" - Nekfeu

Je tiens à remercier l'École Centrale de Nantes et l'École Nationale Supérieure Maritime qui ont financé cette thèse. Je remercie également le laboratoire LHEEA et particulièrement l'équipe TSM pour leur accueil bienveillant durant ces trois années de thèse.
J'exprime ma gratitude à ma famille et mes amis pour leur soutien sans failles.

Thesis organization

The present document is mainly composed of an introduction, two parts (a modeling part and a practical application part) and a conclusion.

The introduction presents the thesis context. An area of concern is highlighted. Then, the doctorate objectives are set and a literature review is performed. Based on the literature review, a need for further investigations is identified, justifying this research work.

The first part presents the modeling of two phenomenon: self-pressurization in cryogenic tanks and liquefied natural gas ageing. In each case, the models are compared with experiments from literature. Then, a meta-model is proposed to assess the methane number at engine inlet.

The second part combines the models developed in the first part through a case study. The case is proposed by a french freight company. More precisely, the study addresses the technical feasibility of a fuel system concept.

A general conclusion closes the corpus of the thesis and proposes new work perspectives.

Thesis organization in French

Ce document est composé d'une introduction, de deux parties (une partie consacrée aux modèles puis une partie dédiée à leur mise en œuvre pratique) et d'une conclusion.

L'introduction présente le contexte général de la thèse. Une problématique est mise en évidence. Puis, les objectifs de la thèse sont explicités et un état de l'art est proposé. D'après l'étude des travaux existants, un besoin de recherches supplémentaire est identifié, ce qui justifie ce doctorat.

La première partie propose des modèles pour deux phénomènes: l'autopressurisation des réservoirs cryogéniques et le vieillissement du gaz naturel. Pour chaque phénomène, les modèles sont comparés avec des données expérimentales issues de la littérature. Puis, un meta-modèle est proposé pour calculer l'indice de méthane à l'admission moteur.

La deuxième partie combine ces modèles à travers un cas d'étude. Le cas est apporté par une entreprise française de transport et l'étude se concentre sur la faisabilité technique d'un circuit combustible.

Une conclusion générale termine ce document dans laquelle des nouveaux développements sont proposés.

List of Figures

List of Tables

Introduction

Highlights

- Environmental regulations drive shippers toward liquefied natural gas as a fuel.
- Despite a strong growth (+20% increase in orders last year), liquefied natural gas fueled ships is still a niche market (<1% of the global fleet).
- The lack of dedicated tools and methods to assess the relevance of using liquefied natural gas during concept design is slowing transition to a low carbon business.
- Since the topic of implementing liquefied natural gas as a ship fuel is a new trend, open academic literature is scarce.

Contents

In this part, first, concerns about the environmental impact of shipping are presented. In reaction to these concerns, the ever-tightening regulations regarding ship exhaust emissions are detailed. The weak version of the Porter hypothesis states that strict environmental regulations stimulate innovation. Therefore, the third section briefly exposes solutions for compliance among which figures natural gas as a fuel.

Then, to grasp fully and interpret correctly its potential as a fuel for ships, basic knowledge regarding natural gas especially under its liquefied form is presented. After, an overview of the current fleet is proposed, highlighting it is still a niche market. Some remaining challenges are underlined, especially for medium-sized companies specialized in the design of vessels up to 100 m in length.

In response, the thesis scope and objectives are explicitly set. In the last section, a literature review is performed. Because it is a recent and small market, there is very few open literature dedicated to basic design tools and methods for natural gas fuel systems on vessels up to 100 m. This research work seeks to make a contribution to fulfill this gap.

Background

Environmental and health concerns

Environmental concern

In 1988, the United Nations Environment Program (UNEP) and the World Meteorological Organization (WMO), two agencies from the United Nations (UN) created the Intergovernmental Panel on Climate Change (IPCC) to provide governments with a comprehensive summary of what is known about the drivers of climate change, its impacts and future risks, and how adaptation and mitigation can reduce those risks. IPCC reports are a key input into international climate change negotiations. In 2014, the IPCC completes its fifth report. The summary for policymakers certifies warming of the climate system:

> *"Warming of the climate system is unequivocal, and since the 1950s, many of the observed changes are unprecedented over decades to millennia. The atmosphere and ocean have warmed, the amounts of snow and ice have diminished, and sea level has risen."[14]*

According to the IPCC, human activities play a major part in climate change:

> *"Anthropogenic Greenhouse Gas (GHG) emissions have increased since the pre-industrial era, driven largely by economic and population growth, and are now higher than ever. This has led to atmospheric concentrations of carbon dioxide, methane and nitrous oxide that are unprecedented in at least the last 800,000 years. Their effects, together with those of other anthropogenic drivers, have been detected throughout the climate system and are extremely likely*[1] *to have been the dominant cause of the observed warming since the mid-20th century."[14]*

Aware that climate change and its adverse effects are a major concern for humanity, UN member states manifest, through the United Nations Framework Convention on Climate Change (UNFCCC), their will to limit, among others, anthropogenic GHG:

> *"The ultimate objective of this Convention and any related legal instruments that the Conference of the Parties may adopt is to achieve, in accordance with the relevant provisions of the Convention, stabilization of GHG concentrations in the atmosphere at a level that would prevent dangerous anthropogenic interference with the climate system. Such a level should be achieved within a time frame sufficient to allow*

[1] probability>95%

ecosystems to adapt naturally to climate change, to ensure that food production is not threatened and to enable economic development to proceed in a sustainable manner."[15]

To describe how much global warming a given type and amount of GHG may cause it is usually compared to carbon dioxide (CO_2). An equivalent carbon dioxide (CO_2 *eq.*) unit is used [14].

In 2010, among five major economic sectors, 14.3% of the GHG emissions worldwide were caused by the transport sector, 14% by direct emissions and 0.3% by indirect emissions (see table 1). Among those 14.3%, 11% are due to shipping and inland water transport. Yet, international shipping transports more than 80%[2] of global trade to peoples and communities all over the world and emits no more than about 2% of the total GHG emissions. Hence, it is the most carbon-efficient way to transport goods on a CO_2 *eq.*/tonne/km basis [16].

Still the maritime industry is under regulatory pressure to greatly reduce its emissions for two main reasons:

- First, because international trade is planned to grow over the coming decades thanks to globalization. Shipping is expected to develop to sustain international business. Consequently, GHG emissions associated to shipping are projected to increase significantly. Depending on future economic and energy developments, scenarios project an increase by 50% to 250% in the period up to 2050 [16]. Actions on efficiency and emissions can mitigate the emissions growth, although all scenarios but one project emissions in 2050 to be higher than in 2012.

- Secondly, because GHG emissions go hand in hand with other pollutants, notably air pollutants threatening human health [17].

[2]http://www.imo.org/en/About/Pages/Default.aspx, visited in February 2019

Indirect emissions	25	%
AFOLU[a]	24	%
Buildings	6.4	%
Transport	14	%
Industry	21	%
Other energy sectors	9.6	%
Total	100	%

(a) Direct emissions

AFOLU	0.87	%
Buildings	12	%
Transport	0.3	%
Industry	11	%
Other energy sectors	1.4	%
Total	25.57	%

(b) Indirect emissions

[a]Agriculture, Forestry, Other Land Use

Table 1: Total anthropogenic GHG emissions distribution by economic sectors in 2010. On the right, indirect emissions shares (in % of total anthropogenic GHG emissions) from electricity and heat production are attributed to sectors of final energy use, based on [9]

Health concern

According to the World Health Organization (WHO) website[3]:

> *"Air pollution is contamination of the indoor or outdoor environment by any chemical, physical or biological agent that modifies the natural characteristics of the atmosphere. Household combustion devices, motor vehicles, industrial facilities and forest fires are common sources of air pollution… Outdoor and indoor air pollution cause respiratory and other diseases, which can be fatal."*

CO_2 has negligible direct effects on health and is not considered as an air pollutant. Without being exhaustive, major air pollutants are:

- Nitrogen Oxides (NO_x);
- Sulfur Oxides (SO_x);
- Particulate Matter (PM);
- Volatile Organic Compounds (VOC);
- Carbon monoxide (CO).

[3]https://www.afro.who.int/health-topics/air-pollution, visited in February 2019

15%/13% of the total anthropogenic NO_x/SO_x emissions are due to shipping [18]. Those pollutants constitute a small fraction of diesel engine exhaust gases (see table 2), yet their impact on human health is significant. Indeed, 70% of ships air pollutants are released at less than 400 km from the shore [19] while nearly 2.4 billion people (about 40% of the world's population) live within 100 km of the coast [20]. As a result, in 2007, shipping-related emissions were responsible for approximately 60,000 cardiopulmonary and lung cancer deaths annually, at a global scale, with impacts concentrated in coastal regions on major trade routes [21]. Most mortality effects are seen in Asia and Europe where high populations and high shipping-related PM concentrations coincide. The aforementioned study concluded that under current regulations and with the expected growth in shipping activity, annual mortalities could increase by 40% between 2007 and 2012.

For the sake of clarity, environmental and health concerns have been presented as two distinct issues. However, they are deeply linked. For instance, Nitrogen dioxide (NO_2) is a GHG causing also strong acid rains and lung diseases. Because the effects of climate change endanger humanity, CO_2 can also be considered as an air pollutant. Both problems are a result of the same context. Policy makers are aware of this strong connection. For example, this global vision lies entirely within the section 202(a) of the US Clean Air Act (CAA) (federal law):

> *"The Administrator finds that the current and projected concentrations of the six key well-mixed greenhouse gases—carbon dioxide, methane, (...) —in the atmosphere threaten the public health and welfare of current and future generations."*

To make sure the shipping sector addresses those environmental and health issues, policy makers have been implementing since the 60's an ever-tightening international regulation framework. The regulation framework is detailed in the next section.

N_2	Nitrogen	74.30	%
O_2	Oxygen	11.25	%
H_2O	Water	8.10	%
CO_2	Carbon dioxide	6.0	%
-	Minor compounds	0.35	%

(a) Major compounds

NO_x	Nitrogen oxides	48	%
SO_x	Sulfur oxides	43	%
HC	Hydrocarbons	6	%
CO	Carbon monoxide	2	%
-	Soots, ashes	1	%

(b) Details of minor compounds

Table 2: Exhaust gas composition (% mass fraction) for a Diesel four strokes marine engine using HFO with 3% of sulfur on a mass basis, from [10]

Regulatory context

International regulatory framework

As a specialized agency of the UN, the International Maritime Organization (IMO) is the global standard-setting authority for the safety, security and environmental performance of international shipping. Its main role is to create a regulatory framework for the shipping industry that is fair and effective, universally adopted and implemented. In other words, its role is to create a level playing-field so that ship operators cannot address their financial issues by simply cutting corners and compromising on safety, security and environmental performance. This approach also encourages innovation and efficiency[4]. Of the 51 treaty instruments for the regulation of international shipping IMO has adopted so far, 21 are directly environment-related. Among them figures the International Convention for the Prevention of Pollution from Ships (MARPOL), initiated in 1973, amended by the Protocols of 1978 and 1997 and kept updated with amendments. The MARPOL convention addresses pollution from ships by oil; by noxious liquid substances carried in bulk; harmful substances carried by sea in packaged form; sewage; garbage and the prevention of air pollution from ships (including GHG). Regulations regarding air pollution and GHG emissions are contained in the annex VI entitled "Prevention of Air Pollution from Ships". This annex entered into force on 19 May 2005. A revised version, with significantly tightened emissions limits, was adopted in October 2008 and entered into force in July 2010. The annex targets, among others, emissions linked to the combustion process in internal combustion engines, notably:

- CO_2;
- SO_x;
- PM;
- NO_x.

Constraint levels vary significantly for each pollutant.

Carbon dioxide Regarding CO_2, MARPOL introduces a design standard, known as the Energy Efficiency Design Index (EEDI), to apply to new ships built from 2013. The standard has a baseline - the average efficiency of ships built between 1999 and 2009 - and sets the maximum amount of CO_2 permitted per ship type and size in order to carry a unit of transport work (i.e. CO_2/tonne/km). To boost the future design efficiency of new ships, the IMO regulation sets 3 targets, known

[4]http://www.imo.org/en/About/Pages/Default.aspx, visited in February 2019

as phases, each progressively requiring less energy (and thus CO_2) to perform the same amount of transport work. The EEDI phases for new ships are detailed below:

- Phase 0 - ships built between 2013-2015 are required to have a design efficiency at least equal to the baseline;
- Phase 1 - ships built between 2015-2020 are required to have a design efficiency, at least, 10% below the reference line;
- Phase 2 - ships built between 2021-2025 are required to have a design efficiency, at least, 20% below the reference line;
- Phase 3 - ships built after 2025 are required to have a design efficiency, at least, 30% below the reference line.

It is to note, analysis based on IMO data reveals that most ships in all class categories already comply with the 30% improvement required by the Phase 3 target [22]. The EEDI has long been criticized by environmental groups as too lax. CO_2 emissions regulations in shipping are, so far, easy to comply for shipowners. Conversely, regulations concerning SO_x, PM and NO_x are much more challenging and will be detailed below.

Sulfur oxides and particulate matters SO_x emissions, and to a lesser extent PM, are dependent on the sulfur content of the fuel. The major abatement method for these two pollutants has been limiting the sulfur content of the fuel [23]. Further control of PM emissions is more difficult as it requires changes in the design of the engine and/or treatment of the engine exhaust gas. Measures to reduce these emissions can increase fuel consumption and the associated CO_2 emissions. Regulation 14 (annex VI MARPOL) introduces a global calendar (see table 3) on fuel sulfur content limit with tighter restrictions in designated Sulfur Emission Control Areas (SECAs) (see figure 2). SECAs are:

- the Baltic Sea;
- the North Sea;
- the English Channel;
- the North American and Canadian coasts and Hawaii;
- an area around Puerto Rico (American common wealth) and the American Virgin Islands.

Negotiations at IMO to establish new protected areas are ongoing. For instance, in 2017, the French prime minister declared: "France will ask IMO to create a SECA in the Mediterranean sea"[24]. The global 0.50% sulfur cap will enter into force in 2020, and more than 70,000 ships will be affected by the regulation. This is a division by seven of the sulfur limit. With less than twelves months to go until it comes into force, shippers are assessing options for compliance. At first glance, the solution is clear: switch to any fuel with less than 0.5% sulfur. However, signatory states can authorize, via regulation 4 of the annex, other solutions judged as "equivalent". This is how the installation of exhaust gas treatment plants, scrubbers, are now widely accepted as an alternative sulfur reduction method. Other systems, such as desulfurization units are on-track to penetrate this new market (see figure 1).

Year of application	Sulfur limit in fuel in % of mass fraction	
	Global	SECA
2000	4.5	1.5
2010	4.5	1.0
2012	3.5	1.0
2015	3.5	0.1
2020	**0.5**	0.1

Table 3: The sulfur limit in fuel worldwide and in SECAs with the year of application

(a) Installation of an exhaust gas treatment plant: a scrubber, from [25]

(b) Compact sulfur reduction unit, from [26]

Figure 1: Two technologies on the new market of sulfur reduction equivalent methods

Nitrogen oxides NO_x originate from combustion of the nitrogen in the air and in the fuel.Their production rises exponentially with combustion temperature. MARPOL, annex VI, regulation 13 limits NO_x emissions (in g/kWh) depending on:

- the navigation area;
- the ship construction date (or the last major conversion date);
- the engine rated speed.

A marine diesel engine is defined as any reciprocating internal combustion engine. The regulation concerns all engine with a power above 130 kW on-board. There are two exceptions: engines used solely for emergencies and engines on a ship operating solely within the waters of the state in which they are flagged. The later exception only applies if these engines are subject to an alternative NO_x control measure. Concerning navigation areas, a tighter restriction is set in designated NO_x Emission Control Areas (NECAs) (see figure 2). NECAs are:

- for ships built (or last major conversion) after 2016:
  - the North American and Canadian coasts and Hawaii;
  - an area around Puerto Rico (American common wealth) and the American Virgin Islands.
- for ships built (or last major conversion) after 2021 the above areas plus:
  - the Baltic Sea;
  - the North Sea;
  - the English Channel.

The thresholds are referred to as Tier I, II and III. Tier I and II are global requirements while Tier III is the more stringent requirement for NECAs. They are computed depending on the engine rated speed (n in rpm), as shown in table 4.

Tier	Applies to ships built (or with major revision) after	NO_x limit (g/kWh)		
		$n < 130$	$130 \leq n < 1999$	$n \geq 2000$
I	2000	17	$45n^{-0.2}$	9.8
II	2011	14.4	$44n^{-0.23}$	7.7
III	2016/2021	3.4	$9n^{-0.2}$	2.0

Table 4: NO_x emission limits

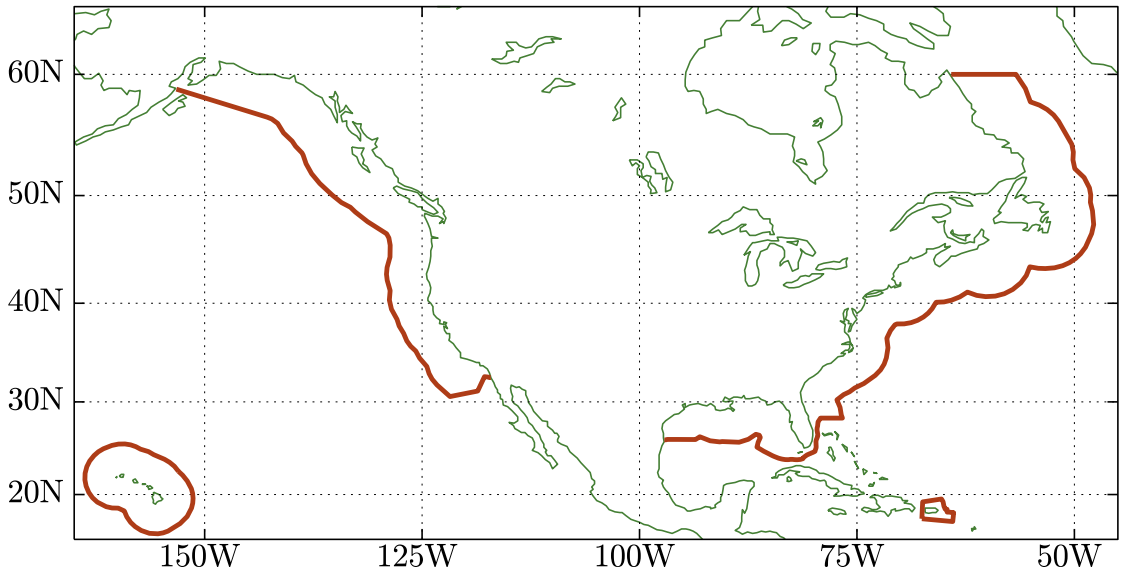

(a) Map of SECAs and NECAs - Miller cylindrical projection

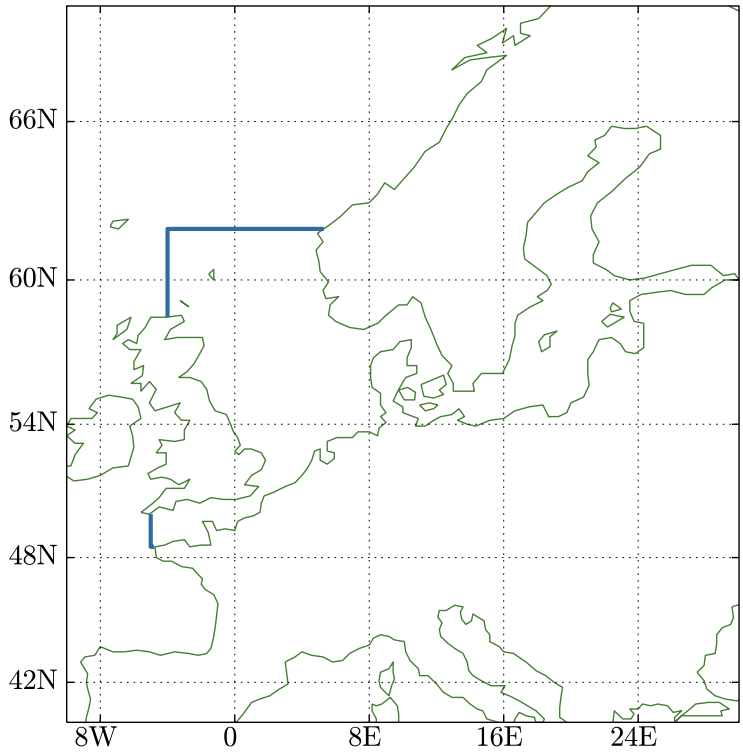

(b) Map of SECAs and future NECAs (2021) - Miller cylindrical projection

Figure 2: Map of SECAs and NECAs. They are defined by enclosed geodesic lines connecting coordinates defined by the IMO

Elements on the european, national and local regulatory framework

All responsibility for the implementation of public international laws is assumed by member states. IMO has for long recognized the onerous burden on flag states in the performance of their obligations and has incorporated clauses in the conventions authorizing states to delegate some of its duties to recognized organizations, mainly classification societies [27].

At a national or local level, standards can be stricter than the international norms. For instance, the Environmental Protection Agency (EPA) is adopting more stringent exhaust emission standards for large marine diesel engines as part of a coordinated strategy to address emissions from all ships that affect U.S air quality. At a local level, the port of Rotterdam authority rewards vessels that have a Green Award with discounts on the port dues. The Green Award is a certificate that is issued by the independent Green Award Foundation to shipping companies that have made additional investments in their vessels and crews to improve their environmental and safety performances. Some key ports[5] have committed themselves to reduce GHG by joining the World Ports Sustainability Program (WPSP). The WPSP members rely on an environmental index, the Environmental Ship Index (ESI), to identify and reward seagoing ships that perform better-than-standards in reducing air emissions.

The economic literature has long recognized that regulation can be a powerful stimulus to innovation. Environmental regulations induce a need for finding new ways of doing things. Hence, they boost the need for higher Research and Development (R&D) allocation and eco-innovations flourish. This effect is commonly known as the weak Porter hypothesis (1995): strict environmental regulations encourage innovations.

In the next section, the main solutions available for the shipping industry to comply with MARPOL above-mentioned regulations are detailed.

Solutions for compliance

While not attempting to present an exhaustive list, this section aims to illustrate ways to comply with the above-mentioned regulations. All the solutions do not present the same Technology Readiness Level (TRL) nor the same efficiency and reaching compliance may imply to combine those options (see table 5). Moreover, for decision-makers, a compliance strategy is more than a technical solution. It implies weighting emissions output, Capital Expenditures (CAPEXs) and Operational Expenditures (OPEXs). Nevertheless, excluding the non-compliance option, from ship-specific calculations studies [28][29], three approaches arise:

[5]list of ports available at http://www.environmentalshipindex.org/Public/Home

1. Some solutions focus on exhaust-gas treatments. This is the case for scrubbers or Exhaust Gas Re-circulation (EGR) systems.

2. Other solutions rely on internal engine modifications such as the Miller cycle with water injection.

3. Some reflections promote a fuel switch from Heavy Fuel Oil (HFO) toward Ultra Low Sulfur Fuel Oil (ULSFO), low sulfur Marine Diesel Oil (MDO), methanol, hydrogen or natural gas.

Abatement technology/measure	Emission reduction (%)			
	SO_x	NO_x	PM	CO_2
Basic modifications on 2 strokes, low speed engine	0	-20	0	0
Advanced engine modifications	0	-30	0	0
Direct water injection	0	-50	0	0
Humid air motors	0	-70	0	0
Exhaust gas re-circulation + scrubbing	-93	-35	-63	0
Selective catalytic reduction (2.7 % m/m sulfur fuel)	0	-90	0	0
Sea water scrubbing	-75	0	-25	0
Fuel switch (from 2.7 to 1.5 % sulfur m/m HFO)	-44	0	-18	0
Fuel switch (from 2.7 to 0.5 % sulfur m/m HFO)	-81	0	-20	0
Fuel switch (from 0.5 to 0.1 % sulfur m/m MDO)	-80	0	0	0
natural gas (Otto cycle, low pressure)	-90	-80	-100	-20

Table 5: Gas emission reduction resulting from operating with different emission control systems compared to the use of natural gas, based on [11]

All alternative fuels are accompanied by benefits and challenges [30]. Among the possible solutions, natural gas is perceived as a serious short-term candidate to fuel the shipping industry [31]. To better understand to what extend is the adoption of natural gas as a fuel for ships a strong trend, a selection of knowledge regarding natural gas as a marine fuel is proposed in the next section.

Natural gas as a marine fuel

Basics

This section introduces basic knowledge regarding LNG. However, if the reader feels familiar with these topics, skipping this part would not interfere with the understanding of the next parts.

Composition and thermophysical properties Natural gas is an odorless, colorless mixture of several gases, mainly methane (CH_4) together with other hydrocarbon species: ethane (C_2H_6), propane (C_3H_8),butane (C_4H_{10}) and traces of other gases such as nitrogen (N_2). To save space on-board, natural gas is usually stored in insulated tanks under its liquid form (at around 111 K) known as Liquefied Natural Gas (LNG). As a cryogenic liquid, the natural gas volume is reduced to about $1/600^{th}$ of the volume needed for its vapor form. LNG is produced at different locations around the world. Its exact composition depends on the production sources (see table 6) and the undergone treatments ashore.

In addition, growing LNG demand coupled with globalization and decarbonation of the energy system favor mixtures and new players (shale gas, biogas, syngas, or even hydrogen through "Power-to-gas"). Mixing LNG with bio-LNG (from bio-gas) as a "drop-in" fuel, significantly reduces GHG emissions and, longer term, "power-to-gas" is perceived as a key technology with the potential to produce large volumes of renewable LNG with zero GHG emissions (see figure 3). Those trends are bluring the properties of tomorrow's natural gas as a fuel for ships [32][33][34].

The density of LNG is slightly less than half of water, thus it will float. The exact density is linked to the LNG composition. Figure 4 shows that:

- LNG density is significantly impacted by its composition;
- LNG with high fractions of complex alkanes (C_2+) have a higher density;
- LNG is weakly compressible but expands on heating.

Below 173 K, the vapor is heavier than air, so a vapor release from a tank will first hover close to the water surface, or deck. When the vapor warms above 173K, it becomes lighter than air and dissipates. The Low Heating Value (LHV) of natural gas is close to 49 MJ/kg (54 MJ/kg for the High Heating Value (HHV)). The properties of commercially available LNG varies significantly across the globe. To highlight this point, densities and LHVs have been computed for the LNG compositions in table 6 (see figure 5 and 6). Differences up to 6.4% for the densities and 7.5% for the LHVs are observed.

Origin	N_2	CH_4	C_2H_6	C_3H_8	C_4+	Total
Alaska	0.17	99.71	0.09	0.03	0.01	100
Algeria - Arzew	0.71	88.93	8.42	1.59	0.37	100
Algeria - Bethioua	0.64	89.55	8.20	1.30	0.31	100
Algeria - Skikda	0.63	91.40	7.35	0.57	0.05	100
Australia - Darwin	0.10	87.64	9.97	1.96	0.33	100
Australia - NWS	0.04	87.33	8.33	3.33	0.97	100
Brunei	0.04	90.12	5.34	3.02	1.48	100
Egypt - Damietta	0.02	97.25	2.49	0.12	0.12	100
Egypt - Idku	0.02	95.31	3.58	0.74	0.34	100
Equatorial Guinea	0.00	93.41	6.52	0.07	0.00	100
Indonesia - Arun	0.08	91.86	5.66	1.60	0.79	100
Indonesia - Badak	0.01	90.14	5.46	2.98	1.40	100
Indonesia - Tangguh	0.13	96.91	2.37	0.44	0.15	100
Libya	0.59	82.57	12.62	3.56	0.65	100
Malaysia	0.14	91.69	4.64	2.60	0.93	100
Nigeria	0.03	91.70	5.52	2.17	0.58	100
Norway	0.46	92.03	5.75	1.31	0.45	100
Oman	0.20	90.68	5.75	2.12	1.24	100
Peru	0.57	89.07	10.26	0.10	0.01	100
Qatar	0.27	90.91	6.43	1.66	0.74	100
Russia - Sakhalin	0.07	92.53	4.47	1.97	0.95	100
Trinidad	0.01	96.78	2.78	0.37	0.06	100
Yemen	0.02	93.17	5.93	0.77	0.12	100

Table 6: LNG average composition (% mass fraction) chosen as being representative among compositions reported by the different receiving terminals, from [12]

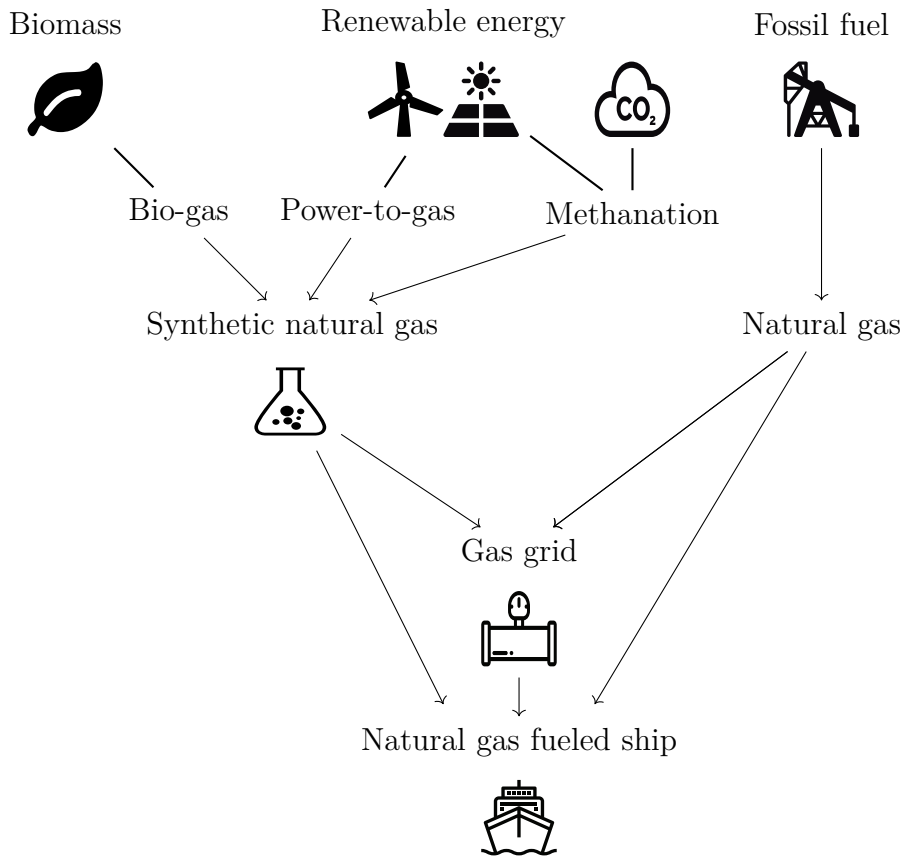

Figure 3: Diagram of the production sources for natural gas as a fuel for ships

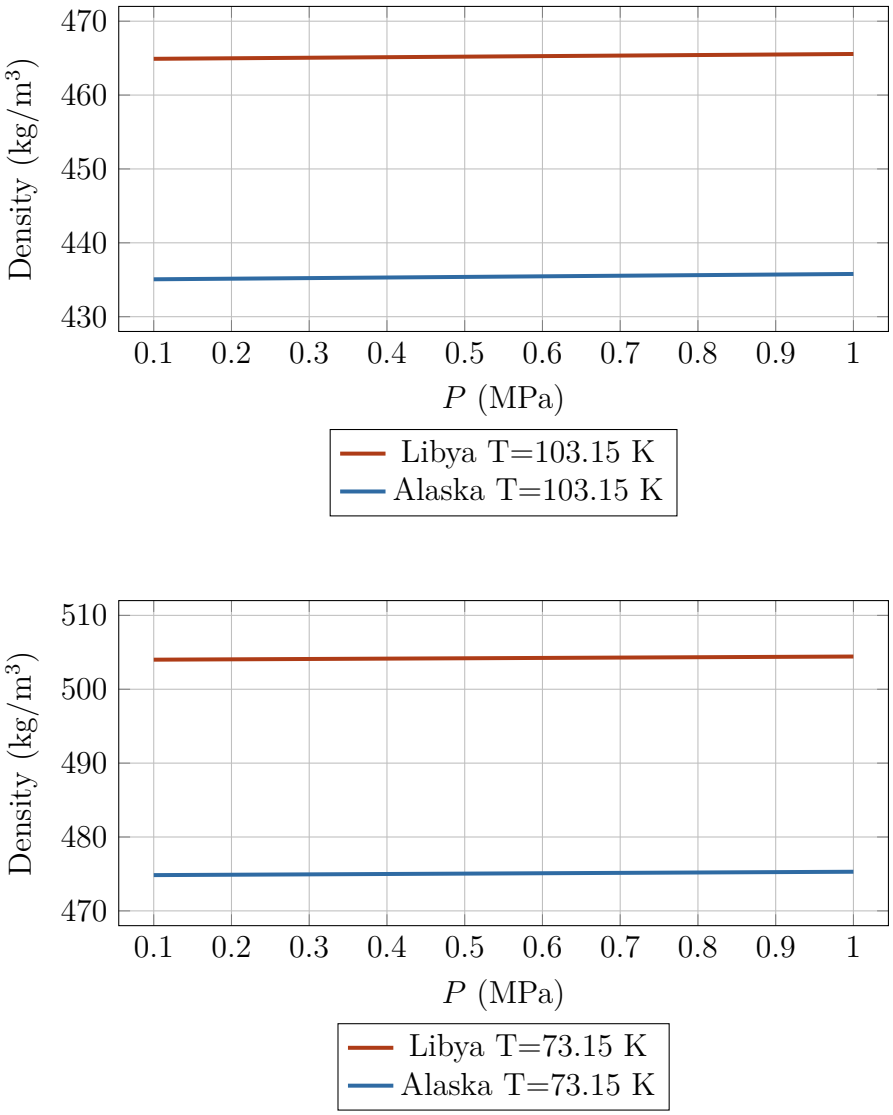

Figure 4: The LNG density for various pressures, temperatures and compositions, computed using [1]

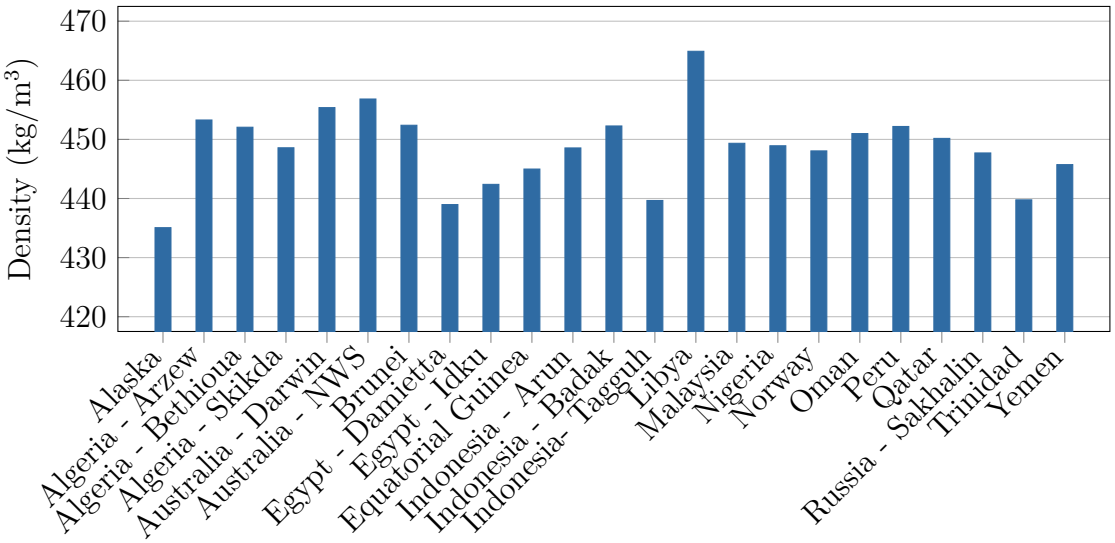

Figure 5: Density at P=0.1 MPa and T=103.15 K for various LNGs, computed using [1]

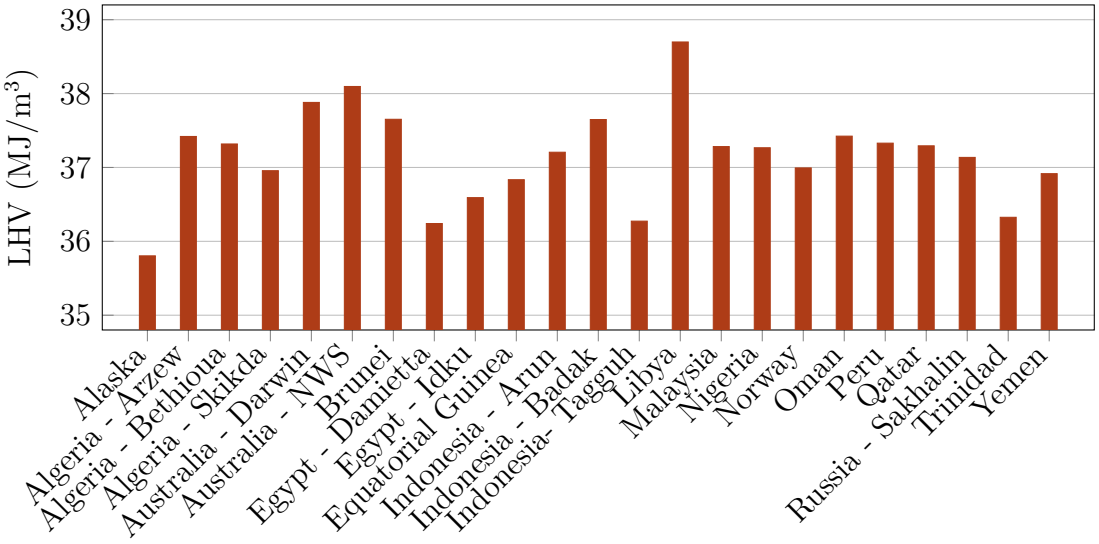

Figure 6: LHV (Ideal gas volume basis), at P=0.1 MPa and T=273.15 K for various LNGs, computed using [1]

Containment system The International code of safety for ships using Gases or other low-flashpoint Fuels (IGF) categorizes tanks into two main types:

- integral tanks;
- independent tanks.

The integral tanks are mainly of membrane type and the independent tanks can be further classified into three subcategories, which are referred to as type A, type B and type C (see figure 7).

Membrane tanks are non-self-supporting tanks which consist of a thin layer (membrane) supported through insulation by adjacent hull structure. The membrane is designed in such a way that thermal effects are compensated without significant stressing of the membrane. To control the effects on ship structure from the potential leakage of cryogenic liquids, a secondary barrier is required.

The type A tank has a full secondary barrier with the function of providing a redundancy to any possible leakage regardless if the leakage is caused by fatigue cracks or an over load of the tank causing a rupture of the tank primary barrier.

The type B tank is designed with a partial secondary barrier that provides redundancy to fatigue cracking only. The tank is designed for redundancy to fatigue damage but has no redundancy for a damage caused by extreme loads. The material utilization for extreme loading is therefore stricter as compared to a type A tank.

A type C tank has no redundancy to either fatigue damage or damage caused by extreme loading. The material utilization for a type C tank is therefore as strict as a type B tank for extreme loading but more strict with respect to fatigue loading. For a type C tank the fatigue safety is incorporated in the formulation of a minimum design pressure, i.e., designed for large static loads compared to the dynamic loads resulting in small dynamic stress amplitudes [35].

For a more detailed introduction to LNG storage systems on-board the reader is kindly referred to [36]. LNG containment systems for ships is a fertile field of innovations (see figure 8). For instance, one trend is the use of technologies and materials known from the aerospace industry such as lightweight composites. The technology aspires to provide weight savings up to 80% over current LNG tank designs. For Markus Rufer, Scorpius Space Launch Company President and CEO:

> *"Composite technology can make LNG a compelling choice for ship owners. The size and weight of existing technology reduces capacity and increases the need for additional horsepower. Composite tanks will remove these issues, offering significant improvement in vessels' OPEX and CAPEX, making LNG as a marine fuel viable for a wide range of marine applications."[37]*

Another promising technology is the use of internal lattice structures that enable a pressure vessel scalable in all directions with a box-like shape. For Keunoh Park, chief sales officer at Lattice Pressure Vessel company:

> *"With the flexibility of the Lattice Pressure Vessel in terms of scale and shape, the designer can fit the tank to the ship, – not the other way around. This way, we can fully utilize the available space in the hull, minimizing specific tank weight and cost while rendering valuable space for paying cargo. The technology enables volumes ranging from 0.5 m^3 to 50,000 m^3 and the Lattice Pressure Vessels can handle design pressures up to 50 bar."[38]*

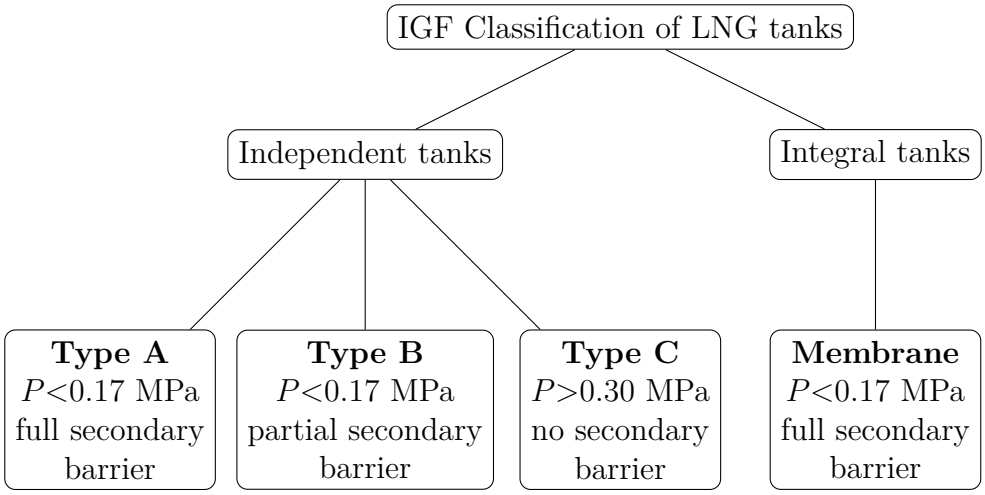

Figure 7: Categorization of LNG containment systems for ships

(a) Composite tanks, credit: ABS [39]

(b) Prototype of a box-shaped pressure tank, credit: KAIST [40]

Figure 8: Two innovative containment systems for LNG marine applications

Boil-off management and LNG ageing Despite a thermal insulation system, inevitable heat leaks from the environment into the cryogenic tank cause LNG heating and vaporization. The generated vapor is called Boil-Off Gas (BOG). This mass is expressed over a duration as the Boil-Off gas Rate (BOR). As a consequence, the pressure in the tank builds-up. To maintain the pressure below the tank's Maximum Allowable Working Pressure (MAWP), it is necessary to withdraw mass from the tank or re-liquefy some vapor. Removing 1 kg of vapor will cause a higher pressure drop than removing 1 kg of liquid. The removed fluid shall not be released directly to atmosphere (only allowed in emergency situations). Venting is not a suitable alternative for pressure control. Beside reliquefaction, the best possible end for BOG is thermal oxidation, i.e. combustion in the ship's consumers. However, if the energy need is lower than the BOR, the gas is "lost" through a burner, the Gas Combustion Unit (GCU). Conversely, when the energy need exceed the BOR, more fluid must be withdrawn from the tank.

During vaporization, as the different compounds' boiling point differ (see table 7), those who have a low boiling point such as nitrogen and methane escape first from the liquid phase into vapor, changing the LNG composition and properties. This phenomenon is called weathering or ageing. This phenomenon impacts the gas quality at engine inlet and thus the engine's behavior: its performances, emissions and operational profile. It is a key feature in the technical and economic assessment of the complete fuel system.

Compound	Normal boiling point (K)
N_2	77.4
CH_4	111.±2.
C_2H_6	184.6±0.6
C_3H_8	231.1±0.2
C_4H_{10}	272.7
Ref.: NIST WebBook of Chemistry	

Table 7: Normal boiling points of select LNG compounds

Methane number For Otto cycle engines, the Methane Number (MN) is comparable to the octane number used for gasoline. It's a dimensionless index to measure the detonating power of a gas. The references used are:

- Pure methane for the knock resistant. Its MN is 100.
- Pure hydrogen for the knock sensitive. Its MN is 0.

A marine engine can admit, within its design limits, a wide range of natural gas grade but, depending on its technology, variations in the MN can impact

its performances. For instance, the brake mean effective pressure can drop for too low MN: the engine is derated (see figure 9).

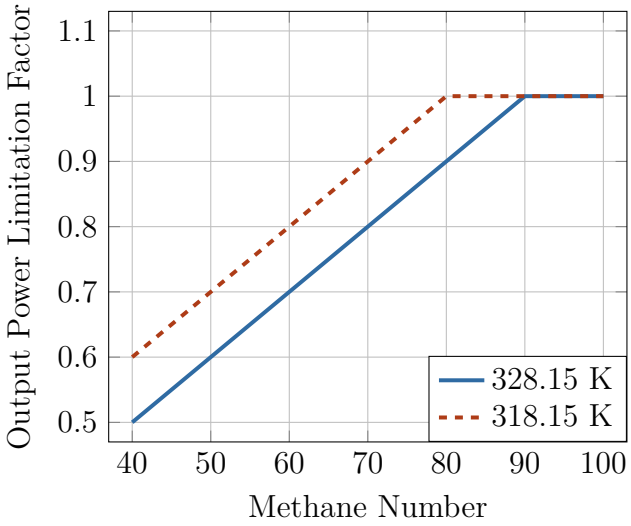

Figure 9: Output power limitation factor as a function of the methane number and the charge air receiver temperature, based on Wärtsilä 34DF product guide

Environmental impact The production process of LNG ensures that it is practically sulfur-free. Therefore, using LNG as a fuel generates almost no SO_x and PM. Low-pressure Otto-cycle gas engines burning natural gas comply with the IMO Tier III without exhaust gas treatments. Natural gas is primarily methane which has a great hydrogen to carbon ratio compared to other fossil fuels. It implies a higher energy content and a lower CO_2 generation. However the well-to-wake analysis of the use of LNG as marine fuel remains a controversial topic [41][42]. One of the issues that still needs to be addressed is natural gas leaks through:

- methane slip: unburned gas released during the combustion process;
- fugitive emissions: unwanted leaks along the fuel system and during bunkering operations.

Indeed, natural gas is a powerful greenhouse gas, some 20 times more potent than CO_2. Leaks need to be reduced further to minimize the environmental impact of LNG-as a fuel. Moreover, those leaks are also none-negligible shortfall regarding fuel OPEX.

Infrastructure and availability Bunkering infrastructures are still limited yet gaining momentum. Continuously updated maps giving detailed information on all LNG bunkering points in existence or under development are available online[6].

Liquefied natural gas fleet

Natural gas as a marine fuel has been used since the 40's. Indeed, in 1942, the natural gas powered Danish fishing boat, "Frank FN282" was launched. The vessel was equipped with a 2-cylinder, 90/100 hp, Alpha Diesel type 342 engine, customized for dual fuel operation, with oil injection as the pilot fuel igniting the gas charge [43]. In 1959, The "Methane Pioner" was the first ship to carry LNG internationally, on a voyage from Louisiana to the UK. Until then no one could be sure of the effectiveness of insulation systems and many possible designs have been developed and evaluated. "Methane Pioner" was a converted freighter, fitted with 5 tanks with balsa wood and glass fiber insulation. Her successful crossing of the Atlantic with 5,000 m^3 of LNG conclusively demonstrated the feasibility of internationally traded LNG and marked the start of the LNG era. The first two commercially viable methane carriers; "Methane Progress" and "Methane Princess", entered their service in 1964. Each of them carried 27,400 m^3 of gas [44]. The history of LNG-powered ships[7] began in 2000, with the "Glutra". The patriarch of LNG-fueled vessels is a double-ended car/passenger ferry with a capacity of 300 passengers and 100 cars. It was built at Langsten Yard in Norway, and put in operation in February 2000. The total cost was 30% higher compared to a similar diesel powered ferry. This was regarded as acceptable taking into account that it was the very first, requiring the introduction of new techniques for the yard and the ferry operator. From 2000 to 2010, 21 of such ships have been put into operation, and practically all of them operated only in the Norwegian waters. However, since 2010 this number skyrocketed (see figure 10). In April 2019, there were 154 LNG-fueled ships in operation and 146 on order. Moreover, 20 years after the first LNG-fueled ferry, LNG has become not only an option for smaller vessels operating in protected coastal areas but also for some of the world's biggest container ships (see figure 11). According to classification society experts, the uptake of LNG as a marine fuel will continue to advance as we head toward 2020, reaching the number of 1,000 vessels running on LNG in 2020 or shortly thereafter [45][46][31]. Despite these encouraging developments, LNG-fueled ships represent a small portion of the around 52,000 merchant ships contributing to international shipping of goods and passengers [28]. It is still a niche market.

[6] dnvgl.com/lngi

[7] In the rest of the thesis, unless specified, LNG carriers and inland waterway vessels are not considered.

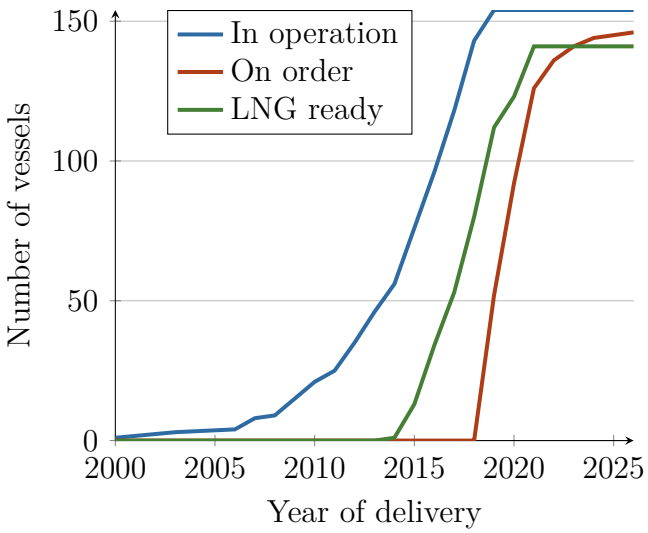

Figure 10: Yearly development of LNG-fueled fleet, data from [2]

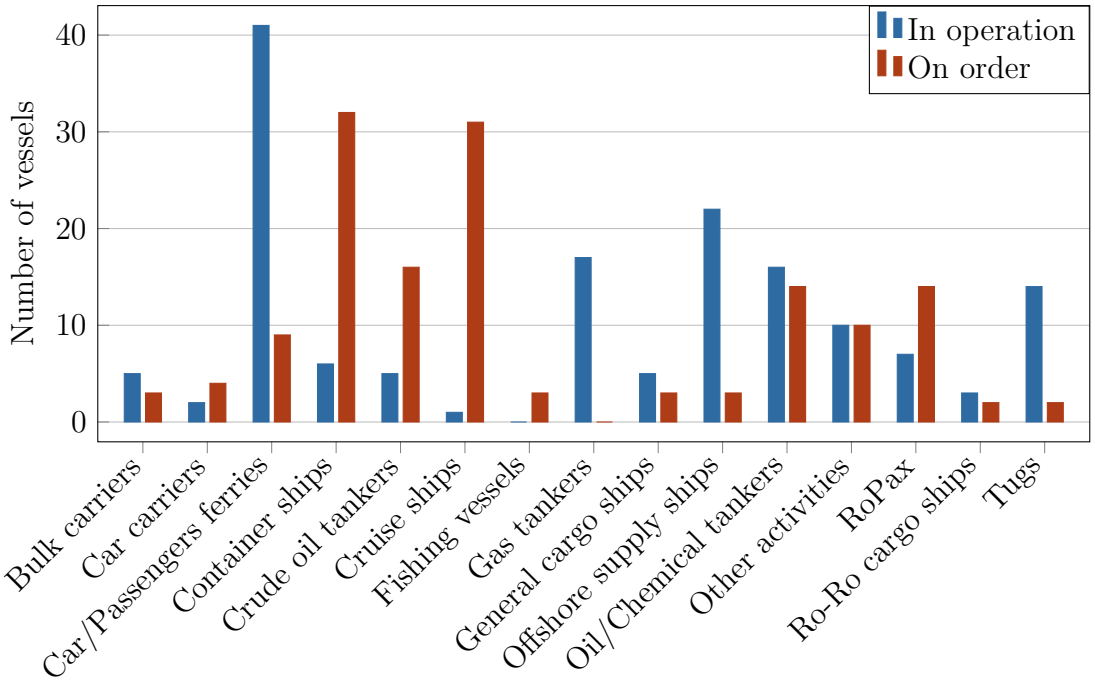

Figure 11: LNG-fueled fleet per segment, data from [2]

Remaining challenges

Commonly cited challenges in switching to LNG are:

- the high CAPEX;
- uncertainty of future LNG prices;
- the lack of LNG bunkering infrastructures.

Moreover, from interviews with French ship designers, LNG fuel system design requires more in-depth, thus costly, pre-feasibility and feasibility studies compared to a "business as usual" conventional fuel ship design process. The two main reasons are:

- it is a recent technology and designers often can not rely solely on their experience and extensive data base. This is especially true in medium size offices, designing vessels up to around 100 m in length, with limited resources and in-house activities;
- the handling of a cryogenic fuel is intrinsically more complex than conventional marine fuels.

At this stage, it is important to underline the feasibility and preliminary design phase stakes. The starting point for the feasibility project is the prospect's business plan or basic ship description. To win the bid, design offices need to develop an appealing yet realistic concept. It is critical, to quickly come up with a proposal establishing the credibility and competitive advantage of the bid. During this task, knowledge is still low (e.g. the amount of detailed information available) but major defining design decisions are made. The remaining freedom to adapt reduces and large amounts of the cost are locked (see figure 12). Misguided choices imply losing bids or unexpected larger costs in later stages when it turns out things need to change. Ultimately, it could prevent a project from achieving its objectives. It is our belief, the lack of appropriate tools and methods for LNG fuel systems technical feasibility assessment stalls its investigations, discarding it too quickly and slowing the transition to a low-carbon business.

To avoid this situation, the following applied research work proposes methods and tools to model a LNG fuel system at a concept design level. The thesis objectives are further detailed in the next section.

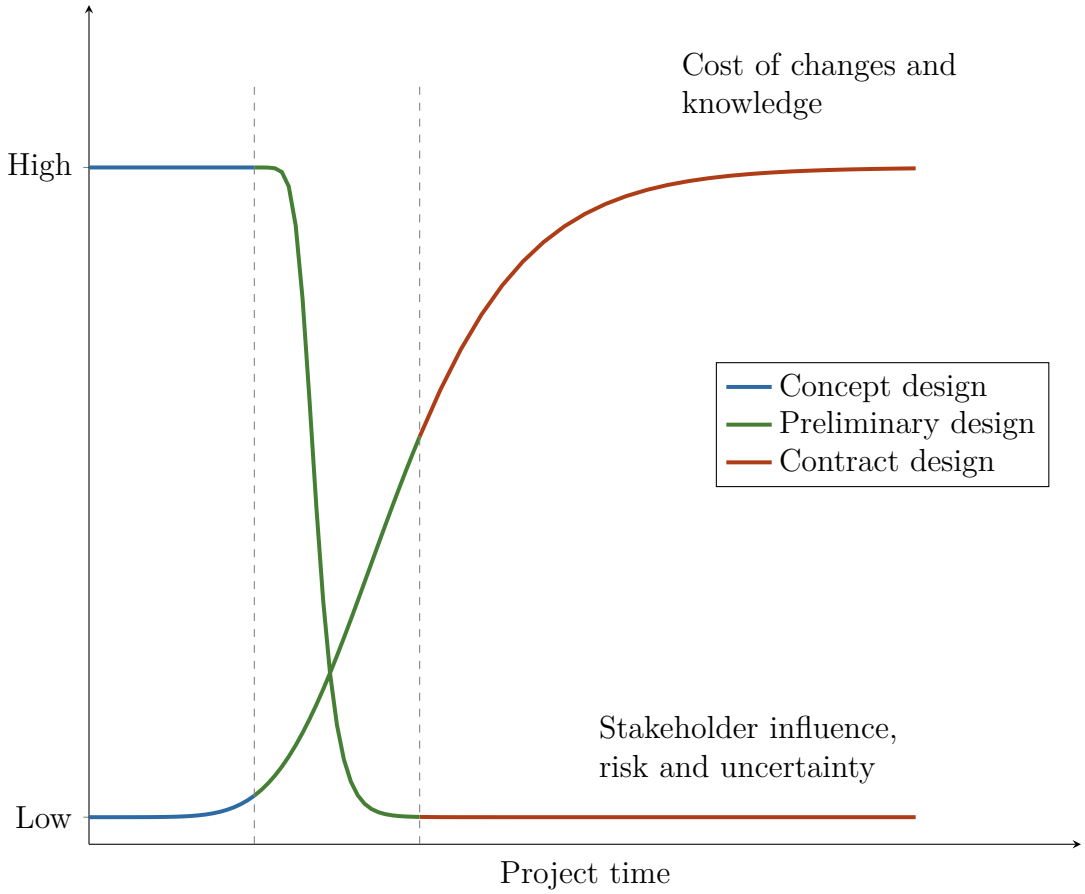

Figure 12: A generic design timeline, based on [3]

Objectives and literature review

Doctorate objectives

After discussions with marine engineering offices designing vessels up to around 100 m in length a set of practical value objectives have been defined. The goal of this PhD research is to develop a model to predict the:

1. tank pressure evolution;
2. natural gas quality evolution at engine inlet.

More precisely, the aim is to:

1. assess the impact of fuel quality on the bunkered energy content and thus the ship's autonomy;
2. detect mismatches between the operational profile and the consumption required to avoid tank over-pressure or unwanted pressure reduction strategies (through the GCU or re-liquefaction);
3. quantify ageing in the storage tank and thus, methane number and heating value at engine inlet over a journey.

Ideally, the methods and tools proposed will assist the decision maker efficiently, using the minimum amount of time, resources, and effort to provide just enough details for confidence in the final LNG fuel system design proposals. Hence, the model should:

- run in few minutes on a basic laptop enabling fast and easy-to-iterate parametric studies;
- as much as possible rely on common software/programming language for small and medium-sized ship design companies. This requirement is to ensure ease-of-use and maintainability.

According to Eduardo Perez Orue, shipping consultant at Small-LNG.com, in 2000, 23.09% of the small LNG carriers (less than 40,000 m^3) were equipped with type C tanks. In 2021, type C tanks should equip 67% of the fleet. There is a trend to move towards type C tanks in the smaller ships [47]. From membrane provider's own admission, the type C tanks are also planned to equip most of the LNG as a fuel market for small capacities (below 1,000 m^3). It is a well known fact that four-stroke engines are much more prominent than two-strokes but the ships concerned are with a few notable exceptions such as multi-engined cruise

ships, much smaller and include craft such as tugs, workboats and similar. This is usually the core activity for small and medium sized ship design offices. Hence, in this study we will focus on LNG fuel systems made of type C tanks feeding 4 strokes engines. It's our belief this will be the dominant technology for strong value-added small/medium-sized ships.

Modeling and simulation of fuel systems for LNG-fueled ships is a growing topic. Yet, it suffers from a limited open academic literature. To that extend, this thesis constitutes an original contribution.

Literature review

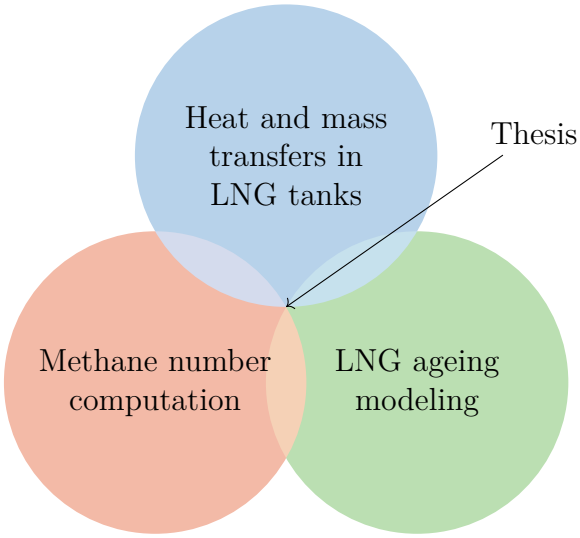

Figure 13: Scope of work and relevant fields for literature review

As illustrated by the above figure, this thesis is at the crossroad of several disciplines (mainly heat and mass transfers in LNG tanks, methane number computation methods and LNG ageing modeling). In this section, relevant literature from each field will be presented. A special attention will be given to literature at the intersection of fields with marine applications.

heat and mass transfers in LNG tanks Most of the literature deals with LNG tanks on onshore facilities or for LNG carriers. Chen and al., 2004 [48] investigated the effects of tank storage capacity, insulation material and tank pressure on the capital cost of a truck refueling station. A thermodynamic model was developed to analyze different mechanisms of heat leak into the tank. The paper compared two options: a double wall vacuum option and a polyurethane insulation with a

liquefier. The latter was presented as a more economical option. Hasan and al., 2009 [49] identified several factors that affect the BOR on LNG carriers:

- sea conditions through sloshing;
- grade of LNG;
- ambient temperature;
- overall thermal transmittance;
- tank pressure;
- the procedure at loading/unloading.

In 2010, Adom and al. [50] focused on the effect of pressure and heat leakages on BOR for large stationary tanks. Results showed a direct correlation between BOR and operating pressure. The study also found that larger LNG tanks have less BOR; however as the operation pressure is increased the differences in BOR among tanks is decreased. In 2011, R. J. Bossier [51] presented numerical solutions to some examples of LNG systems:

- First, for an open two-tank system with only a lower pipe connection, a single-component fluid and constant temperature;
- Then, the same situation for a closed system;
- In the next part, an upper pipe was added to the closed two-tank system;
- Then, a model was proposed for a one-tank system with an external heat flux, allowing temperature variations, together with vaporization and condensation;
- The same study was then proposed for a two-tank system;
- Last, the study was extended in the case of multi-component fluids.

Between 2015 and 2018, Grotle and al. discussed several issues related to the LNG fuel system on-board including pressure control in the tank [52][53][54]. He particularly investigated the pressure response to sloshing. Y. Shao and al. focused on the optimal time limit of ship-to-ship LNG bunkering by dynamic simulation, highlighting the link between the total BOG and the bunkering time limit [55]. In 2017, Hulsbosch-Dam and al., proposed a model for the behavior of LNG tanks under extreme heat load (tanks in fire) [4]. The analytical results were compared to an experiment performed with liquid nitrogen. T. Wlodek showed that BOR

is higher for LNG composition which contains nitrogen [56]. E. Lisowski and al. used a Finite Element Method (FEM) method to quantify heat leaks through containerized tanks [57]. In his master thesis, Singstad Paulsen investigated the relationship between ambient conditions (notably temperature and sea state) and the BOR of LNG carriers using a data driven approach [58]. A linear relationship between the ambient temperature and the BOR was uncovered, in agreement with Hasan et al. [49]. LNG is also used as a fuel for trucks in smaller tanks. Their technical reports for market approval include many tests and validation programs [7]. Last but not least, the behavior of cryogenics fuel is a well known research topic in the spatial industry [59][60].

LNG ageing modeling In 1995, Shah and al. proposed a mathematical model to predict ageing in a typical flat-bottom above-ground LNG tank and during a 125,000 m^3 LNG carrier voyage [61]. In 1998, the company Gaz de France developed a semi-empirical and physical model to assess cargo ageing on LNG carriers [62]. In 1999, Kountz presented the results of a test program on the weathering of LNG storage tanks for vehicles. Several compositions were weathered in an instrumented tank. Close correlation was found between test results and the predictions from a model based on equilibrium between liquid and vapor phases [8]. In 2008, G. G. Dimopoulos and al. proposed a detailed model for LNG operation during marine transportation which accounts for the variation of BOR, composition and thermodynamic properties during the voyage [63]. The study indicated that the BOR and its quality vary significantly during a voyage and therefore should be taken into account in the thermo-economic assessment of the marine energy systems. Faou and al. associated LNG to a binary mixture (CH_4 and N_2) and considered ageing in their holistic ship energy model [64]. M. Miana and al. published in 2009 two models for LNG ageing during ship transportation: a physical algorithm and an "intelligent" model based on historical data and a neural network. The physical model was based on a constant BOR approach [65]. In 2014, L. A. Pellegrini and al. published a model to predict ageing in LNG above-ground tanks for an assigned value of BOR as a well as when the heat flow to the tank is assigned and the BOR must be computed. The paper showed, by comparison with experimental data, the misleading results obtained using a mean value of the BOR instead of calculating it from the heat exchanged with the surroundings [66]. In 2016, Miana and al. compared two models: an ageing by heat flow versus by evaporation rate. The two models were compared with published results and 558 real LNG voyages. The comparison between the different ageing models revealed that, globally, the approaches defined by the evaporation rate show better predictions than those of constant heat flow [67]. However, the selection of an accurate BOR value remains an open issue. In 2015, C. Migliore and al.

published a model removing a number of constraints in the precedent literature, namely:

- heat ingress is calculated based on the outside temperature and LNG composition, allowing for daily or seasonal variation;
- BOR is not an input parameter, but is calculated as part of the simulation;
- the LNG density is estimated using an accurate experimentally based correlation.

The model was tested using measured data from LNG properties after marine transportation (voyage ranging from 98 h to 390 h at sea) showing satisfactory agreement [68]. Later, C. Migliore and al. called into question the thermal equilibrium assumption between the liquid and the vapor phase and published a non-isothermal model [69]. Recently, C. Huerta and al. also developed a non-isothermal model [70]. K. Arrhenius and al. investigated the LNG variations at refueling stations for trucks [71] and A. Benito in receiving terminals [72].

Methane number computation To ensure that the engines to be used match the expected variations in fuel composition, the MN must be determined unambiguously. Although it is linked to the composition, the MN is not a standard thermophysical property since it also depends on the engine technology. Setting a standard method to compute the MN is a burning issue. In 2015, the International Council on Combustion Engines (CIMAC) published a position paper asking for: *"a standard calculation method for MN"* and a MN *"close to 80 or higher for highest efficiency, economy and lowest GHG emissions"* [73]. This implies more processing for LNG providers. The latter replied:

> *"A methane number of 80, as recommended by some organizations in Europe, would endanger the LNG supply to the market, limiting acceptable LNG sources, or would require expensive gas treatment just for the benefit the natural gas vehicles - a small, albeit growing, sector of the market."[74]*

This situation is a long-standing opposition. In 2012, another association representing the natural gas industry wrote as a conclusion:

> *"A Methane Number of 80 as recommended by Euromot*[8] *would endanger the Security of natural gas supply to the European market, limiting acceptable gas sources, especially LNG but also some pipeline supplies, or would require expensive gas treatment just for the benefit of a few gas consumers (...)*

[8]European Association for Internal Combustion Engine Manufacturers

- *Gas quality adjustment for Methane Number is complex and prohibitively expensive and would benefit only a very small percentage of gas consumers and impact less than 0.02% of European gas demand;*
- *It is not economic to remove residual natural gas liquids*[9] *for gas imported into Europe. This will add quality adjustment cost to the gas system that, in the end, would be paid by end-users, reducing the benefit of gas quality harmonization;*
- *Limiting or preventing the addition of Hydrogen into the gas grid goes against the desires of the European Commission to diversify supplies and promote renewable energy sources.*

The Methane Number can't directly be used to optimise engine operation as there is no guarantee that the Methane Number at the point of measurement will correspond to the gas quality at the engine. Automation of engine emissions monitoring and automatic optimisation is the best method of ensuring optimum operation over a range of gas qualities further making the inclusion of Methane Number unnecessary."[75]

From a classification society perspective, variability in MN induce reductions in power or an increased fuel consumption and is not a safety issue [76]. In the meantime, methods to compute the MN from the natural gas composition flourish:

- **the Gas Research Institute (GRI) method**: It is described in the UK implementation of ISO/TR 22302:2014 [77];
- **the AVL method**: The exact algorithm is confidential and property of AVL Inc.;
- **the MWM Euromot method**: The code is available online and distributed under the Apache license;
- **the Wärstilä method**: Wärtsilä offers an online tool[10] for ship owners and operators to calculate the MN. The calculation result indicates whether or not the given gas quality is suitable for use in Wärtsilä dual-fuel engines;
- **the Cummins Westport method**: According to the engine manufacturer:

[9] naturally occurring components found in natural gas - include ethane, propane and butane, among others

[10] https://www.wartsila.com/marine/build/gas-solutions/methane-number-calculator

> *"The Cummins proprietary methane number calculation is a numerical, regression-analysis based method using an extensive set of experimental test data. While neither this data or the resulting calculation can be shared, this fuel quality calculator can be used to determine methane number for a given fuel composition."*[11]

- **the Det Norske Veritas and Germanischer Lloyd (DNV-GL) method:** In 2016, the classification society DNV-GL launched an online methane number calculator. According to Johan Knijp, head of gas quality and energy transition, DNV GL Oil & Gas:

  > *"Together with an international industrial consortium, the calculator is currently being extended to cover a full range of engines. Market analyses using the tool can be used by the entire supply chain - by engine manufacturers, ship and truck owners, by traders and by international policy makers on LNG."*[12]

From the literature review, it is clear that models exist to:

- asses a cryogenic fluid's behavior during heat and mass transfers in a tank with sufficient confidence for concept design studies;
- predict mixture composition variations due to ageing;
- compute the methane number from a known composition;

However, each topic has been mostly studied independently and very rarely linked in the context of global LNG fuel system concept design studies. If we disregard the literature dealing with LNG carriers consuming their cargo, the remaining work is very scarce. In that respect, to the best of the author's knowledge, this thesis is a novel and original contribution.

[11] https://www.cumminswestport.com/fuel-quality-calculator
[12] https://www.motorship.com/news101/lng/dnv-gl-launches-lng-methane-number-calculator

Part 1

Modeling part

Highlights

- The vapor-liquid equilibrium assumption holds for rough estimations and requires few details about the tank which is convenient at a concept design level.
- The ageing model shows heating value variations of up to 6%: ageing impacts significantly energy balance.
- Using massive queries and a neural network interpolation method an online proprietary methane number calculator has been mapped.

Contents

In this part, first, the assumptions are listed. Then, the energy and mass balance equations in the system are set. The equation of state software used to compute the fluid thermophysical properties is presented. The heat inflow computation method is also explained. An explicit numerical scheme is implemented.

Then, a model to simulate self-pressurization is compared to experimental data. Enhancements are implemented. Although they do improve the model accuracy they are not retained because their require tuning coefficients unknown at a basic design level.

After, an ageing model is introduced and compared with experimental data. The results are thoroughly discussed.

In the last section, a meta-model to compute dynamically the methane number is developed. It is based on a reverse engineering approach.

Assumptions

All the assumptions made in this research work are listed in this section. For the sake of clarity, they will also be introduced at their first occurrence.
Assumptions are:

1. The fluid in the tank evolves through vapor-liquid equilibrium states and components do not react with each other;
2. Heat transfer through the tank occurs by conduction only and the apparent thermal conductivity is assumed constant unless specified;
3. Heat fluxes are well below the nucleate boiling limit and will not greatly perturb the vapor-liquid interface;
4. The vessel is assumed even keel (no trim nor list) and still;
5. The thermal contraction or expansion of the tank is ignored;
6. Inside the tank, the volume occupied by devices, for instance sensors, is neglected;
7. The tank outer surface temperature is the ambient temperature (T_{amb}).

An oft-quoted remark in the world of modeling made in the 70's by the statistician George Box remains a useful rule of thumb:

> *"All models are wrong, but some are useful."*

The problem appropriate level of detail is set when the behavior of the system can be predicted within acceptable bounds. It means assumptions hold if the model accuracy allows to assess the fuel system technical and economical feasibility.

Energy and mass balance in the tank

The system is the fluid enclosed in the tank. It is an open system. Despite the various fuel system solutions, a common feature is that mass and heat flow through the tank boundaries. The first law of thermodynamics for open systems states that a system internal energy (U) increase is equal to the amount of energy added to the system by matter flowing in and by heat (δQ), minus the amount lost by matter flowing out and in the form of work (δW) done by the system. The internal energy variations can be written:

$$dU = \delta Q + dU_{in} - dU_{out} - \delta W \tag{1.1}$$

where U_{in} is the average internal energy entering the system, and U_{out} is the average internal energy leaving the system. In our case, the work is solely pressure-volume work to push matter in/out the system boundaries:

$$\delta W = d(P_{out} \cdot V_{out}) - d(P_{in} \cdot V_{in}) \tag{1.2}$$

Substitution into the above equations leads to:

$$dU = \delta Q + dU_{in} - dU_{out} - d(P_{out} \cdot V_{out}) + d(P_{in} \cdot V_{in}) \tag{1.3}$$

By definition of the enthalpy (H) [78]:

$$dU = \delta Q + dH_{in} - dH_{out} \tag{1.4}$$

The inlet and outlet mass flow (respectively $\dot{m}_{in}$ and $\dot{m}_{out}$) can be natural gas under its liquid or vapor form (respectively $\dot{m}_L$ and $\dot{m}_V$). Assuming the specific enthalpy (h) variations are small over a set time step ($\dot{H} = h \cdot \dot{m} + \dot{h} \cdot m \approx h \cdot \dot{m}$) leads to:

$$\dot{U} = \delta\dot{Q} + \dot{m}_{L_{in}} \cdot h_L + \dot{m}_{V_{in}} \cdot h_V - \dot{m}_{L_{out}} \cdot h_L - \dot{m}_{V_{out}} \cdot h_V \tag{1.5}$$

Also, the mass in the system obeys the law of conservation:

$$\dot{m} = \dot{m}_{L_{in}} + \dot{m}_{V_{in}} - \dot{m}_{L_{out}} - \dot{m}_{V_{out}} \tag{1.6}$$

Equations of state

It is assumed that the fluid in the tank evolves through vapor-liquid equilibrium states and that the components do not react with each other. The number of degrees of freedom (F), i.e. the number of independent intensive variables, can be computed using the Gibbs phase rule:

$$F = 2 + C - Ph \tag{1.7}$$

C is the minimum number of fixed-composition mixtures that could be used to prepare each phase individually and Ph is the number of different phases. Duhem's theorem is another rule which is similar to the phase rule, but less celebrated. It applies to closed systems at equilibrium for which the extensive state as well as the intensive state of the system is fixed. The theorem states that for any closed system of a given composition and mass, the equilibrium state is completely determined when any two independent properties are fixed. The two independent properties may be either intensive or extensive; however, the maximum number of independent intensive properties that can be specified is given by the Gibbs phase rule.

For a pure fluid in vapor-liquid equilibrium ($C = 1$ and $Ph = 2$), the number of degree of freedom is one ($F = 1$) so at least one of the two variables must be extensive. Indeed, vaporization at a given pressure is isotherm so two intensive variables (such as pressure (P) and temperature (T)) do not allow to define the fluid state (see figure 1.1).

For a mixture in vapor-liquid equilibrium ($C = 2$ and $Ph = 2$), the number of degree of freedom is two ($F = 2$) so the two variables can be extensive. The vaporization at a given pressure is not isotherm so the couple (P; T) is sufficient to define the fluid state (see figure 1.2).

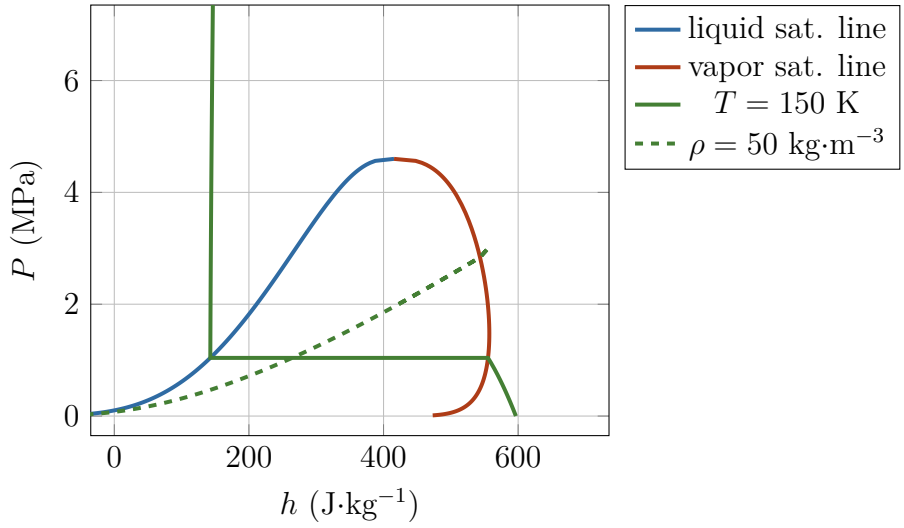

Figure 1.1: Pressure enthalpy diagram for pure methane, computed using [1]

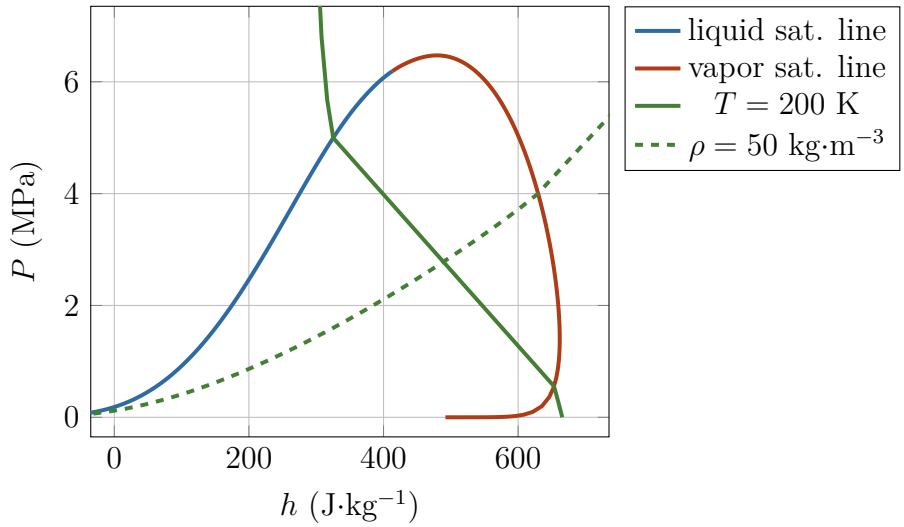

Figure 1.2: Pressure enthalpy diagram for LNG Libya, computed using [1]

From the mass and energy balance, if the fluid density and its specific internal energy are specified, all the other properties, can be determined using an Equations Of State (EOS). EOS are thermodynamic equations relating state variables. They are not deduced from the laws of thermodynamics but drawn from experiments or "imported" from other scientific fields such as chemistry. A number of software packages with preset equations of state dedicated to a class of applications exist. In 2008, the European Gas Research Group (GERG) developed a wide-range EOS for natural gases and other mixtures: the GERG-2008 EOS. It is valid in the homogeneous gas, liquid and super-critical regions, and for vapor-liquid equilibrium states. It can be applied to mixtures consisting of an arbitrary combination of the 21 compounds listed below:

- methane;
- nitrogen;
- carbon dioxide;
- ethane;
- propane;
- n-butane;
- isobutane;
- n-pentane;
- isopentane;
- n-hexane;
- n-heptane;
- n-octane;
- n-nonane;
- n-decane;
- hydrogen;
- hydrogen sulfide;
- carbon monoxide;
- water;
- oxygen;
- argon;
- helium.

The normal range of validity covers temperatures of:

$$90 \text{ K} \leq T \leq 450 \text{ K}$$

and pressures of:

$$P \leq 35 \text{ MPa}$$

This range corresponds to the use of the equation in both standard and advanced technical applications using natural gases and similar mixtures, e.g. pipeline transport, natural-gas storage and processes with liquefied natural gas [79]. Details regarding the EOS structure is beyond the scope of this research work and can be found in [80][81].

It is recognized that, equations of state of the cubic, virial and "molecular-based" families are well-known and have been used widely in the oil and gas in-

dustry, as well as in the academia. However, it has been shown that using the GERG-2008 EOS leads to more accurate results to design cryogenic LNG systems [82]. Hence, despite its higher mathematical complexity, as long as the computational requirements remain acceptable, the GERG-2008 EOS is used. The EOS software, containing the GERG-2008 will now be presented.

In 1989, while MS Windows was in its infancy, the National Institute Standards and Technology (NIST) released the very first version of REFPROP. Back then, it standed for "REFrigerant PROPerties" and customers received a 3.5-inch floppy disk containing an executable program, a source code in FORTRAN and a small binder containing the Users' Guide (see figure 1.3). Based upon the pioneering work of Morrison and McLinden published in NIST Techical Note 1226, "Application of a Hard Sphere Equation of State to Refrigerants and Refrigerant Mixtures" [83], the code contained data for 15 pure fluids, only binary mixtures. Although REFPROP was referred to as a "database" throughout its history it has been a data system allowing a user to calculate data according to specific needs. Over the years, the program became more and more complete and the acronym REFPROP was reborn in REFerence fluid PROPerties. The code has been progressively enhanced to include more EOS (notably the GERG-2008 EOS) for many pure fluids and mixture, transport equations, a GUI, wrappers and DLLs enabling calls from various languages (Matlab, Python, C/C++, C#, VB, VB.NET, "G" the graphical programming language used in LabVIEW). In this thesis, the latest version of REFPROP is used [1]. It has been judged user-friendly and affordable (the license costs 325.0 $) and therefore suitable for use at a concept design level.

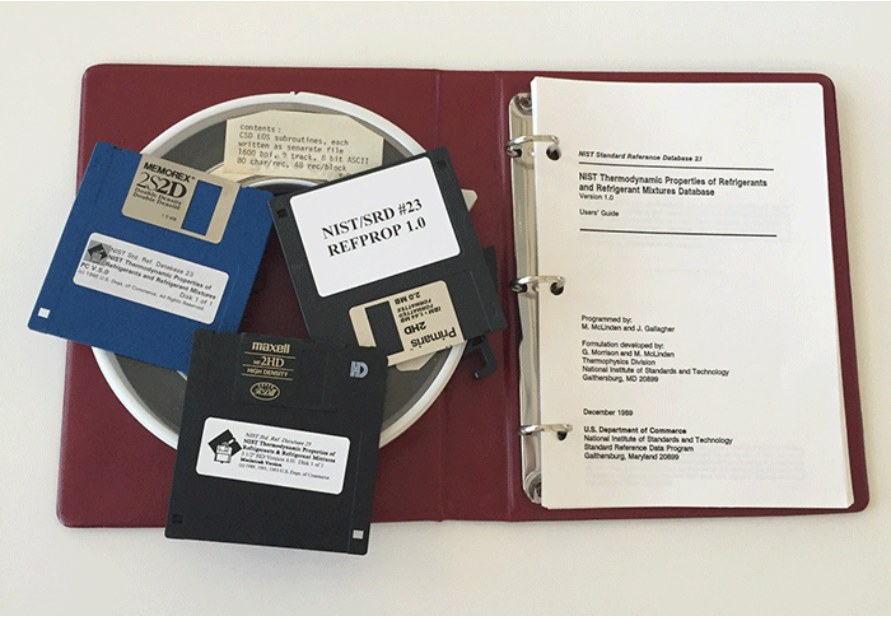

Figure 1.3: Original REFPROP distribution, version 1.0, credit: Mark McLinden, NIST

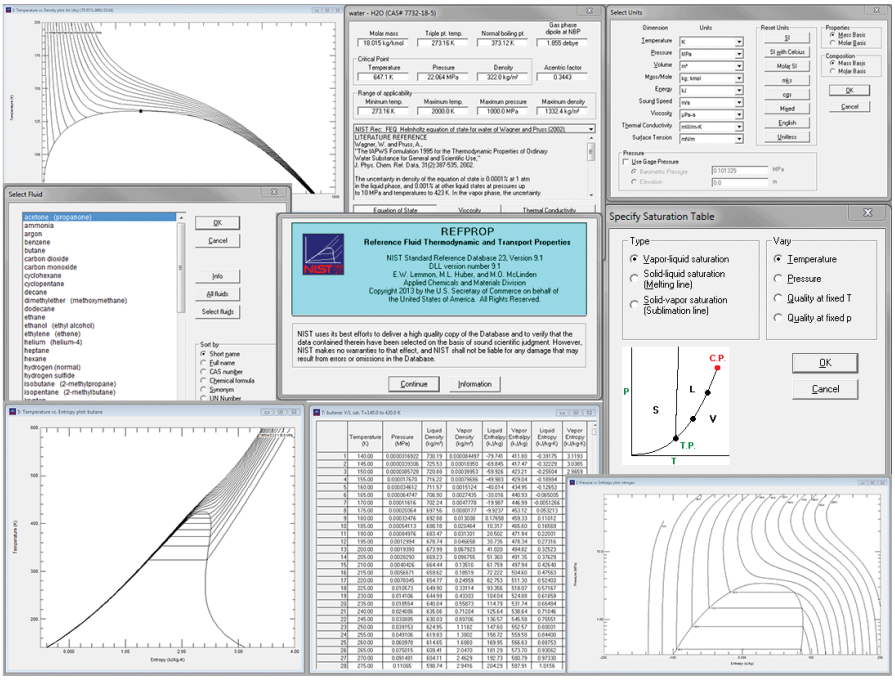

Figure 1.4: A collage of REFPROP screens

Heat inflow

Because LNG is a cryogenic liquid, naturally, heat from ambient flows in the tank and warms the fluid. The heat flux through the wall ($\vec{q}$) is modeled by Fourier's law:

$$\vec{q} = -\kappa \cdot \nabla T \tag{1.8}$$

where κ is the apparent thermal conductivity, which is supposed to be constant and ∇T the temperature gradient. In a first approach, the thermal resistance of a warped surface whose local radius of curvature is always much higher than its thickness can be approached by that of a same thickness and same surface flat wall. The heat flux then becomes uniform:

$$q = -k \cdot (T - T_{amb}) \tag{1.9}$$

The (positive) coefficient k denotes the heat flux per unit area per unit temperature. T is the fluid temperature and T_{amb} is the ambient temperature. If $T_{amb} > T$, then $q > 0$ and if $T_{amb} < T$, then $q < 0$. If we assume k to be constant and uniform over the walls of the tank, we can write the total heat transfer rate $\delta\dot{Q}$ as:

$$\delta\dot{Q} = -\frac{\kappa \cdot S}{e} \cdot (T - T_{amb}) \tag{1.10}$$

where S is the internal tank surface and e is the tank thickness.
This heat causes an evaporation of the liquid phase: the Boil-Off Gas (BOG). The produced vapor rate (the Boil-Off gas Rate (BOR)) such that:

$$BOR = \delta\dot{Q}/\tilde{L} \tag{1.11}$$

where $\tilde{L}$ is the specific heat of vaporization. Tank manufacturers usually express the BOR as the fraction of the initial liquid volume in the tank that evaporates daily. With $m_{l_{init}}$ the initial liquid mass, it comes:

$$BOR = \frac{24 \cdot 3.6 \cdot 10^3 \cdot \delta\dot{Q}}{\tilde{L} \cdot m_{l_{init}}} \tag{1.12}$$

Mixing equation (1.10) and (1.12) leads to:

$$BOR = -\frac{24 \cdot 3.6 \cdot 10^3 \cdot \kappa \cdot S \cdot (T - T_{amb})}{\tilde{L} \cdot m_{l_{init}} \cdot e} \tag{1.13}$$

Numerical methods

Numerical methods to solve first-order initial value problems[1] can be divided between explicit and implicit methods. Explicit methods calculate the state of a system at a later time from the state of the system at the current time, while implicit methods find a solution by solving an equation involving both the current state of the system and the later one. Among the explicit methods, the Euler's method is the most basic one and is the simplest Runge–Kutta method. It writes:

$$U^{t+\Delta t} = U^t + \Delta t \cdot \dot{U}^t \tag{1.14}$$

$$m^{t+\Delta t} = m^t + \Delta t \cdot \dot{m}^t \tag{1.15}$$

The Euler explicit scheme is easy to implement in a spreadsheet. At a concept design level, ease-of-use is a key feature. Therefor this numerical scheme is retained. To ensure convergence, the time step (Δt) is reduced until the results are independent from it.

For the sake of clarity, in this thesis, a parameter is defined as a constant set before launching the simulation whereas a variable is initialized and can change during the simulation.

All the simulations run on a basic laptop (see table 1.1) within a reasonable time (few minutes). Consequently, computation time issues are not considered.

The next section presents the models and their validation with experimental data.

Type	HP EliteBook 840 G3 – PC x64
CPU	Intel® Core™ i5-6300U CPU at 2.4GHz, 2401 MHz, 2 cores
RAM	8 Gb

Table 1.1: Computer details

[1] In this context, a 1^{st} order initial value problem is an evolution equation specifying how, given initial conditions, the system will evolve with time. The models have no spatial dependency, they are only time dependent: they are 0D models.

Models and experimental data

No experimental work has been done during this thesis. All experimental data have been extracted from literature plots using Plot Digitizer. Plot Digitizer[2] is a Java free program used to digitize plots.

Pressurization test 1

In 2017, the Netherlands Organization for Applied Scientific Research (TNO) performed experimental tests to assess the thermodynamic behavior of a LNG tank engulfed in flames (see figure 1.5)[4][6]. The objective was to predict the pressurization rate of a cryogenic tank under extreme heat load. The application is a safety concern. If the duration of the tank exposure to fire is known, the time before the internal pressure reaches the opening pressure of the Pressure Relief Valve (PRV) can be estimated based on thermodynamic calculations. Opening of the PRV might cause escalation of the fire, causing difficulty for the fire response team. The time before the PRV opens can be used by the fire response team to approach safely the accident. It is a safe time window and its prediction is of the utmost importance. Even though the heat inflow in fire is faster than the natural heat inflow, the underlying physics are similar. This is why this experiment is retained to validate the models.

Figure 1.5: Double walled tank containing cryogenic liquid engulfed in fire during the experiment, from [4]

[2]plotdigitizerourceforge.net

The tank is a double-walled tank with an inner volume (V) of 3 m^3. The inner and outer tanks are separated by 20 cm of vacuumed perlite, which is the insulation material chosen for the experiment. Figure 1.6 shows a vacuumed space with perlite filling.

Figure 1.6: Vacuum space with perlite filling, from [5]

The volume filled with perlite was vacuumed to 200 mbar. The inner and outer tanks are modeled as cylinders with flat end caps. This is an approximation of the exact geometry presented in figure 1.16 and 1.17. The inner tank diameter (R) is 1.2 m and its length (L) is 2 m. The internal tank surface (S) is given by:

$$S = 2 \cdot \pi \cdot R^2 + 2 \cdot \pi \cdot R \cdot L \tag{1.16}$$

The tank is partially filled with Liquefied Nitrogen (LIN). The fluid in the tank is assumed in vapor-liquid equilibrium. The PRV is set at 0.76 MPa. No mass leaves the tank (closed system) and the volume of the tank is constant. Consequently, the heating process of the tank can be described by a constant density line in a pressure-enthalpy diagram. To assess the model, a linear interpolation is performed on the model results at the experimental time coordinates and the relative error is computed. The relative error is defined, for a variable X at time t', as:

$$error^{t'} = \left| \frac{X^{t'}_{experimental\ value} - X^{t'}_{model\ value}}{X^{t'}_{model\ value}} \right| \tag{1.17}$$

Model 1

Description The workflow is detailed in figure 1.10. Calls to the EOS software REFerence fluid PROPerties (REFPROP) are expressed as an "f" function such that:

$$outputs = f(inputs)$$

The initial values and parameters are given in table 1.2. The final pressure is computed for various time steps (see figure 1.7). The time step is successively reduced until the difference is acceptably small. A time step of 1 minute (Δt=1 min) is selected.

Variable	**Initial value**	**Unit**
P	0.2013	MPa
Parameter	**Value**	**Unit**
m	1,400	kg
κ	120	$mW{\cdot}m^{-1}{\cdot}K^{-1}$
T_{amb}	900	K
V	3	m^3
S	15	m^2
e	0.2	m
Δt	60	s

Table 1.2: Model 1 - Initial values and parameters for pressurization test 1

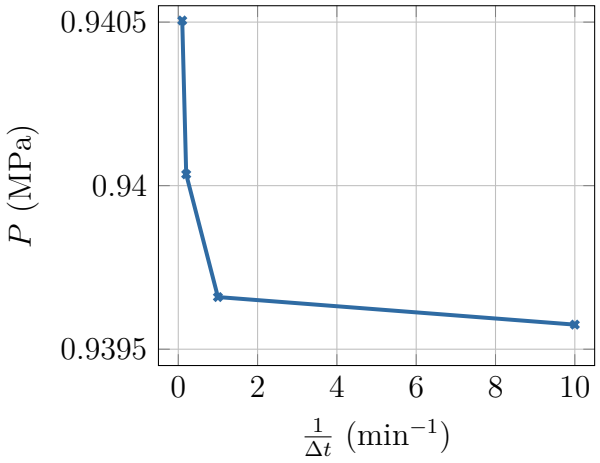

Δt	P	variation (%)
10	0.9405	+ 0.099
5	0.9400	+ 0.049
1	0.9397	+ 0.009
0.1	0.9396	ref.

Figure 1.7: Final pressure (at t=140 min) for various time steps

Results Figure 1.8 shows:

- the experiment pressure evolution (orange line);
- the model pressure evolution (blue line) named "model 1";
- the TNO models pressure evolution (dashed green and orange lines).

The TNO equilibrium model (dashed green line) assumes the fluid evolves through liquid-vapor-equilibrium states. The TNO non-equilibrium model (dashed orange line) removes this assumption and considers the vapor and liquid zones separately. In this plot, $t = 0$ min corresponds to the start of the fire. First, the pressure slowly increases and after 40 minutes it starts to rise faster. After 120 minutes the pressure reaches 7.6 bars and the PRV opens. For a very short time the pressure remains constant then the fire is switched off and the pressure decreases again. The non-equilibrium model captures better the pressure evolution. However, the solution is dependent on non-physical "tuning coefficients". It is not easily scalable to an arbitrary tank hence not suitable for basic design phase and will not be further considered. TNO equilibrium model is very similar to the model 1 so the pressure curves are close. The only difference is that the TNO model switches to an open isobaric heating process once the PRV opens (after t=120 min). Globally, model 1 overestimates the pressure. Figure 1.9 shows the maximum error is 33% (for t=56 min). The error after opening of the PRV is meaningless since the model does not consider this event.

An explanation for the slow pressure increase at the start of the fire could be that a heating of the wall and insulation occurs before an effective heat transfer to the fluid starts. The tank has a thermal inertia causing thermal lag and damping. TNO shared this opinion:

> *"The slow increase in pressure and temperature of the fluid directly at the start of the fire is caused by the heating of the wall and insulation before an effective heat transfer to the fluid starts. This delays the increase in temperature of the fluid, as is shown by the small slope at the start of the test. In the equilibrium model, the heating of the walls and the insulation are not included. For this reason the increase of temperature and pressure is nearly constant over time and doesn't show a speed up."[4]*

However, thermal inertia does not explain the pressurization rate increase after one hour. In [6], it is said that:

> *"It is furthermore (conservatively) assumed that vacuum of the annular volume is lost at the moment the fire is ignited. The actual moment at*

which vacuum was lost could not be determined. However the fact that at 1:49 hrs after ignition a vacuum disc was broken was evidence that vacuum was lost at some point during the experiment."

TNO proposed ways to improve the model:

> *"The model can be improved by using the time dependent tank temperature and temperature dependent heat conductivity."[4]*

This proposal is investigated in the next model.

Plots

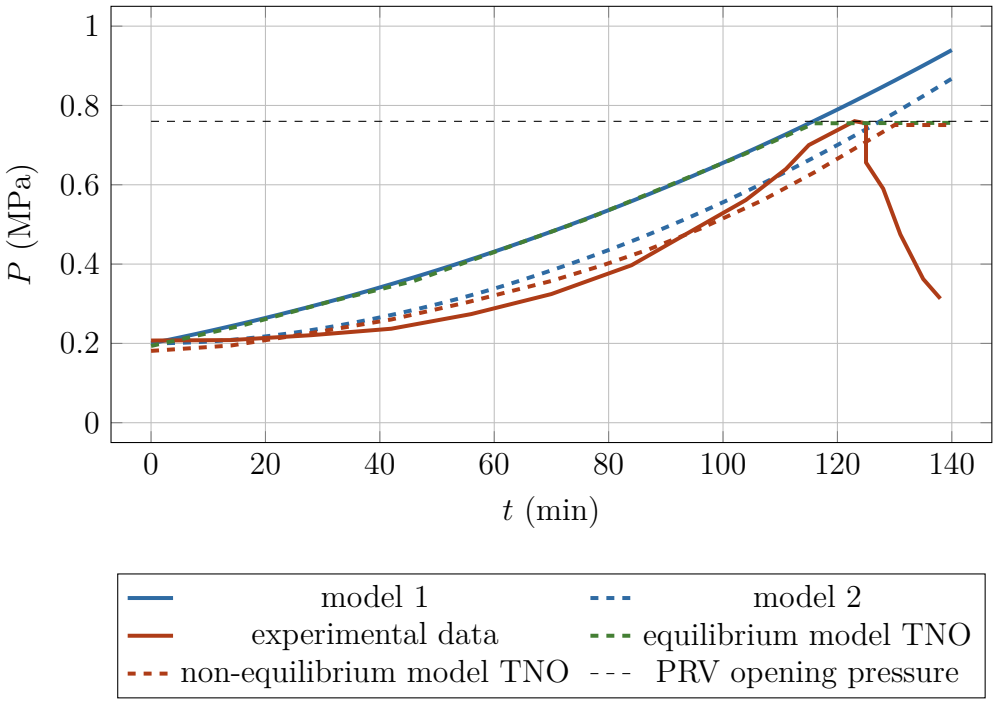

Figure 1.8: Pressure evolution

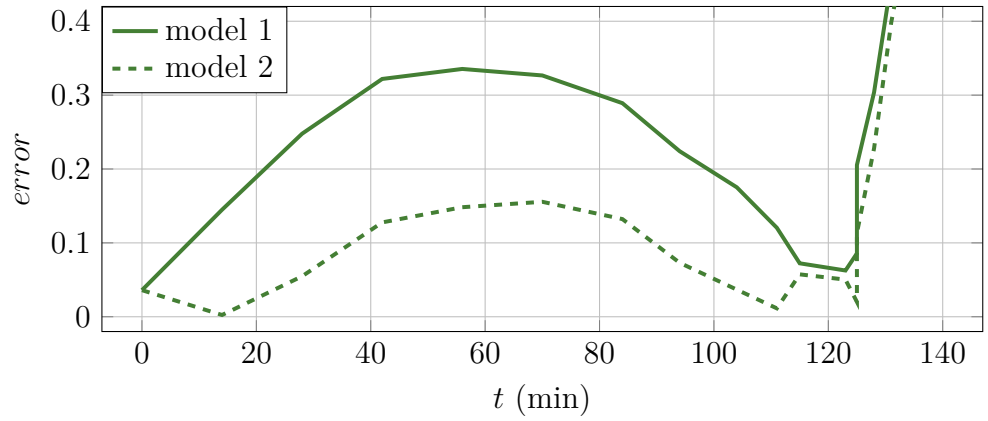

	model 1	model 2
mean error	26%	16%
standard deviation	0.18	0.19

Figure 1.9: Error evolution

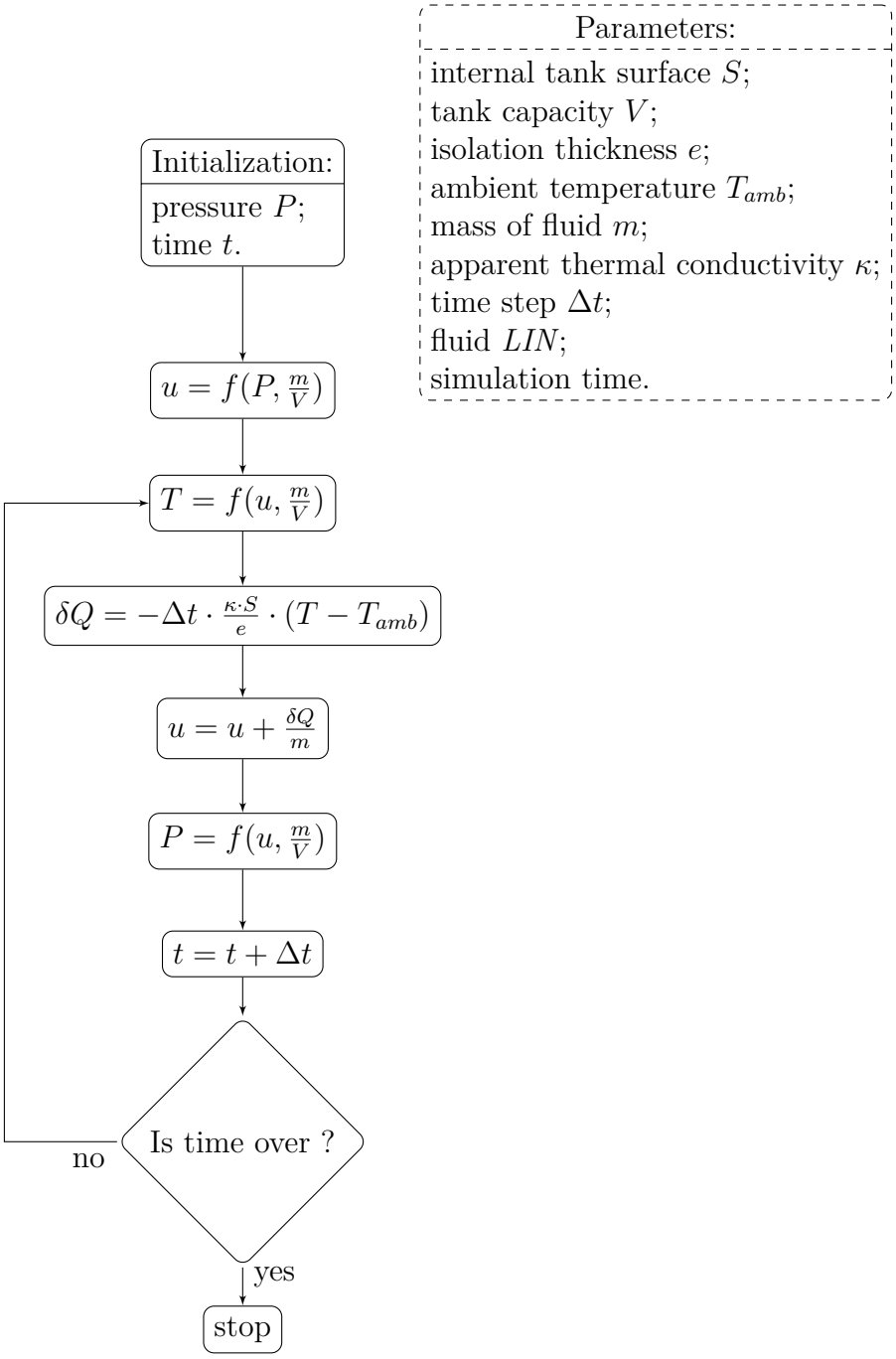

Figure 1.10: Model 1 - Pressurization flow chart

Model 2

Description In this second model (called "model 2"), two modifications are made compared to "model 1". First, the outer tank surface temperature (T_{amb}) is not constant. It is modeled based on typical fire temperature curves [84] (see equation 1.18 and figure 1.11).

$$T_{amb} = 800 \cdot (1 - e^{-0.05 \cdot t}) + 293.15 \tag{1.18}$$

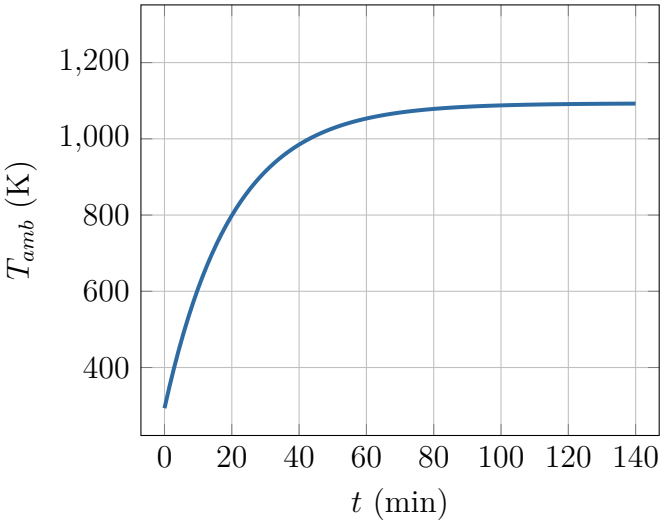

Figure 1.11: Model 2 - Tank outer surface temperature evolution

Secondly, the tank apparent thermal conductivity is interpolated as a function of two variables:

- the tank average temperature (T_t) defined as:

$$T_t = \frac{T_{amb} + T}{2} \tag{1.19}$$

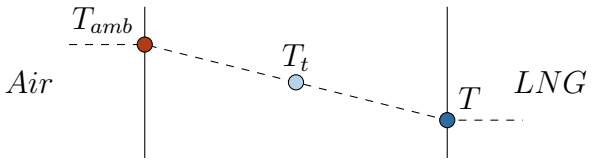

Figure 1.12: Schematic of the temperature distribution through the tank

- the tank vacuum pressure (P_{vac}). Vacuum is lost during the experiment since the vacuum discs are broken. To model this event, P_{vac} follows an "S-shaped" curve or sigmoid curve raising from the initial vacuum level (0.02 MPa) to atmospheric pressure (0.1 MPa). The pressure profile is shown in figure 1.13.

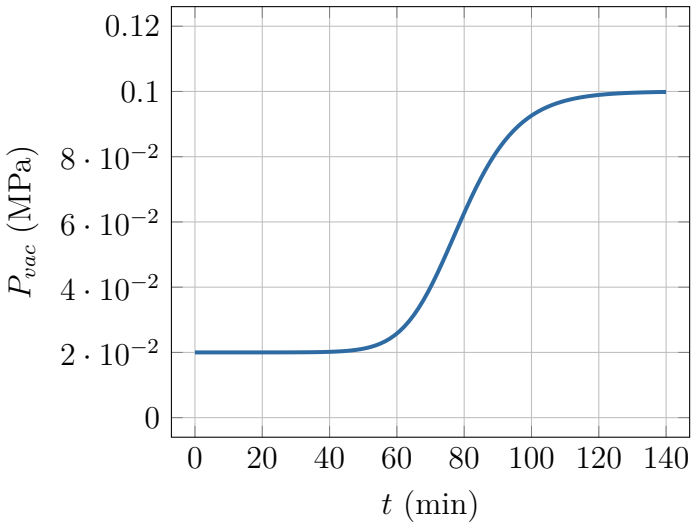

Figure 1.13: Model 2 - Vacuum pressure evolution

The values of κ as a function of the tank vacuum pressure (P_{vac}) and temperature (T_t) are given in [6]. Bilinear interpolation is then used, at each time step to set κ (see figure 1.14). During the first 2 minutes, because T_t is out of bounds, κ is set to 30 mW$\cdot$ m$^{-1}\cdot$ K^{-1}. The workflow is detailed in figure 1.15. Like in "model 1", calls to the EOS software are expressed as an "f" function such that:

$$outputs = f(inputs)$$

Calls to compute T_{amb} and P_{vac} are expressed as an "f'" function of time (t) and calls to compute κ are expressed as an "f''" function of T, T_{amb} and P_{vac}. The initial values and parameters are given in table 1.3.

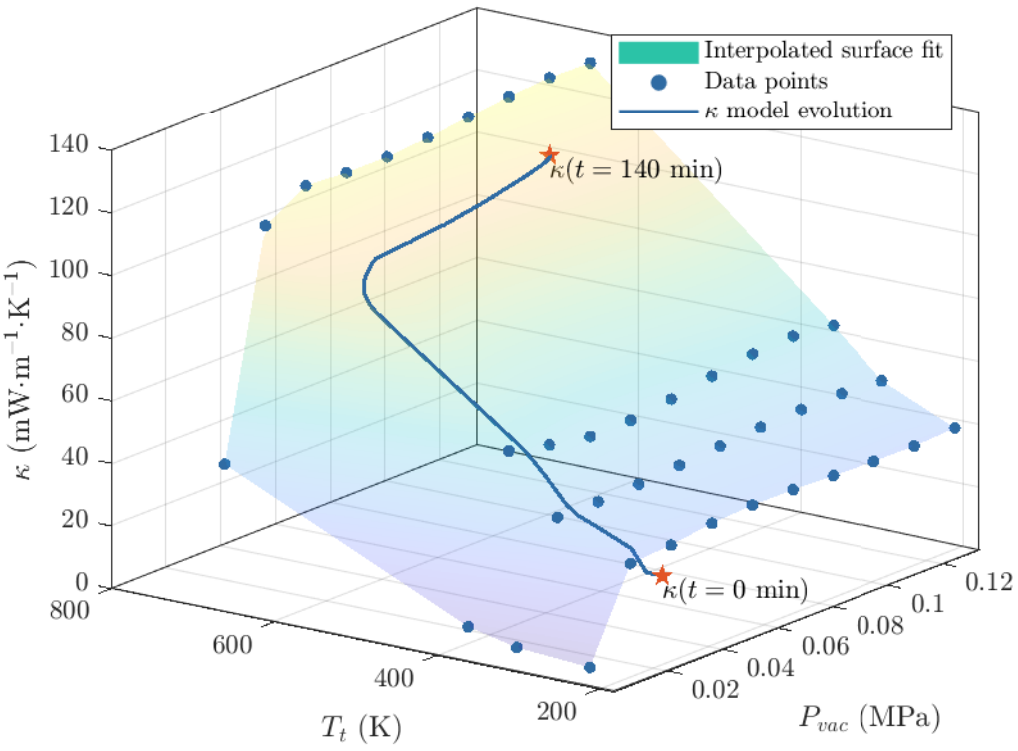

Figure 1.14: The apparent thermal conductivity (κ) as a function of the tank average temperature (T_t) and its vacuum pressure (P_{vac})

Variable	**Initial value**	**Unit**
P	0.2013	MPa
κ	30	$mW{\cdot}m^{-1}{\cdot}K^{-1}$
T_{amb}	293.15	K
Parameter	**Value**	**Unit**
m	1,400	kg
V	3	m^3
S	15	m^2
e	0.2	m
Δt	60	s

Table 1.3: Model 2 - Initial values and parameters for pressurization test 1

Results The model 2 pressure increase over time is shown in figure 1.8 with the dashed blue line. Figure 1.9 shows the maximum error is 14% (for t=70 min). Globally, the error is reduced with model 2. However:

- the tank outer surface temperature and the vacuum pressure are realistic values but their evolution has been slightly tuned to reduce the relative error profile;
- for the intended applications, the tank will not be engulfed in fire. The ambient temperature and the heat inflow should be lower. Consequently , the tank apparent thermal conductivity and its vacuum pressure should be almost constants.

To be more conclusive, a second experimental test has been considered and is presented in the following section.

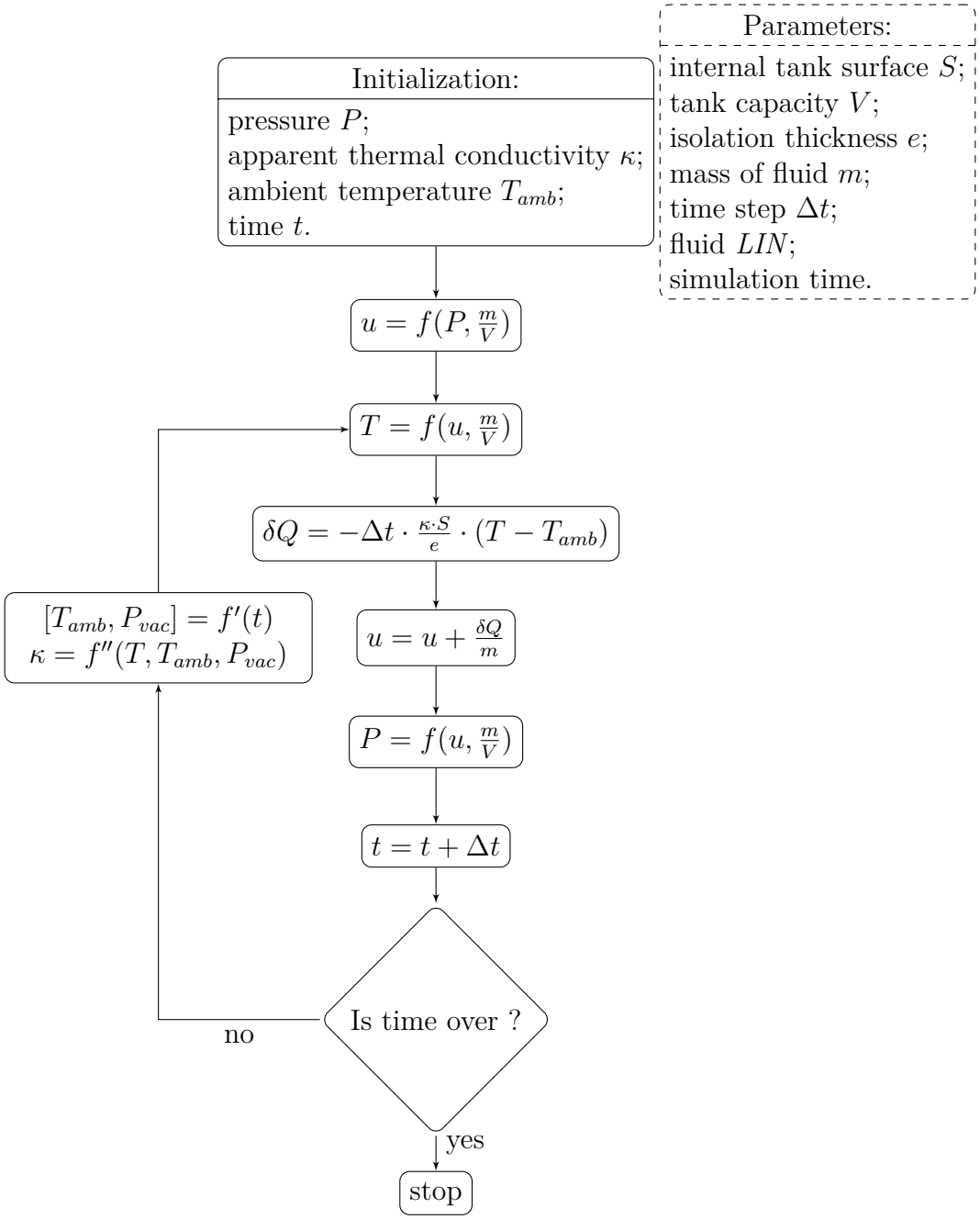

Figure 1.15: Model 2 - Pressurization flow chart

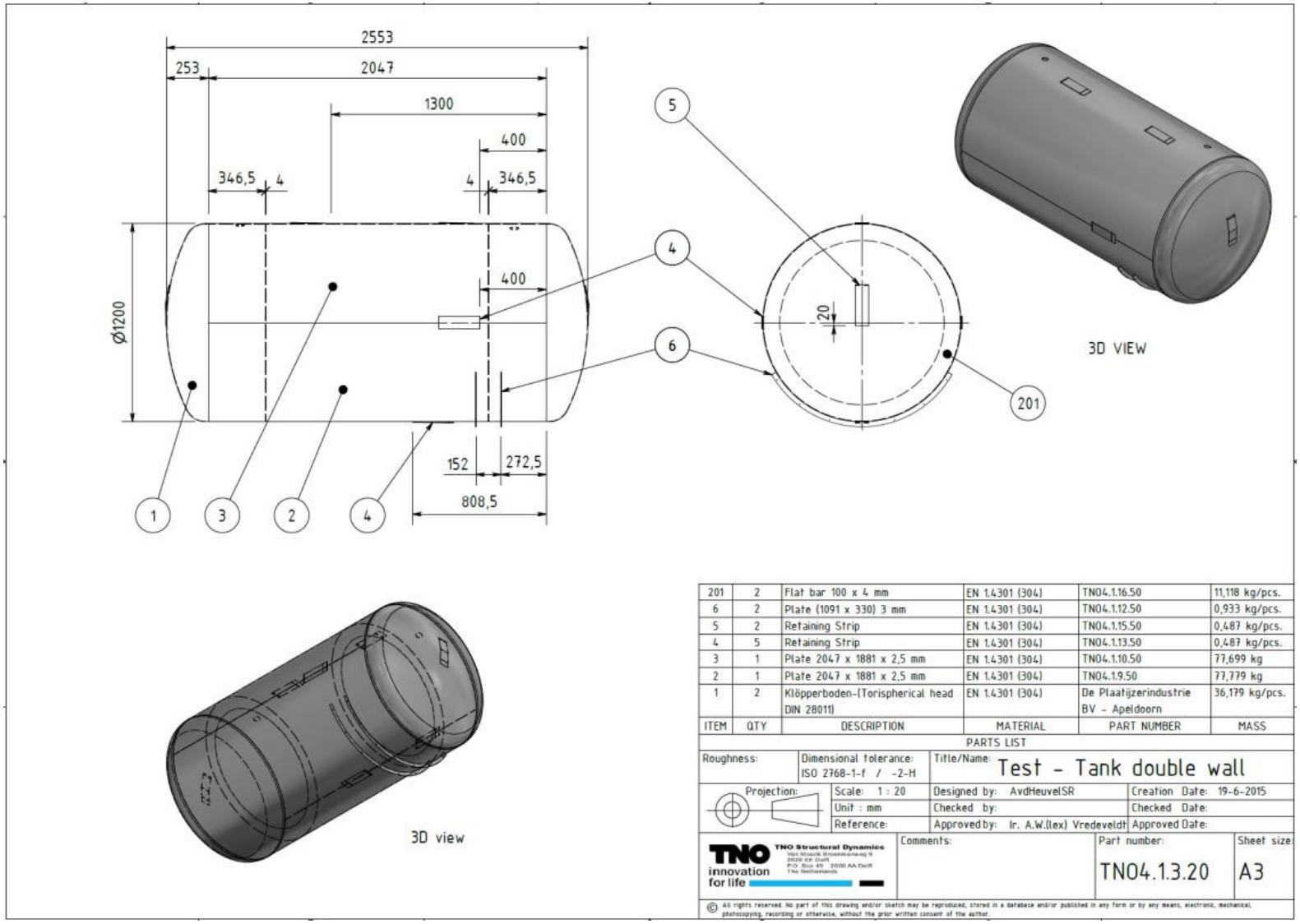

ITEM	QTY	DESCRIPTION	MATERIAL	PART NUMBER	MASS
201	2	Flat bar 100 x 4 mm	EN 1.4301 (304)	TN04.1.16.50	11,118 kg/pcs.
6	2	Plate (1091 x 330) 3 mm	EN 1.4301 (304)	TN04.1.12.50	0,933 kg/pcs.
5	2	Retaining Strip	EN 1.4301 (304)	TN04.1.15.50	0,487 kg/pcs.
4	5	Retaining Strip	EN 1.4301 (304)	TN04.1.13.50	0,487 kg/pcs.
3	1	Plate 2047 x 1881 x 2,5 mm	EN 1.4301 (304)	TN04.1.10.50	77,699 kg
2	1	Plate 2047 x 1881 x 2,5 mm	EN 1.4301 (304)	TN04.1.9.50	77,779 kg
1	2	Klöpperboden-(Torispherical head DIN 28011)	EN 1.4301 (304)	De Plaatijzerindustrie BV - Apeldoorn	36,179 kg/pcs.

PARTS LIST

Roughness: | Dimensional tolerance: ISO 2768-1-f / -2-H | Title/Name: Test - Tank double wall

Projection: | Scale: 1 : 20 | Designed by: AvdHeuvelSR | Creation Date: 19-6-2015

Unit : mm | Checked by: | Checked Date:

Reference: | Approved by: Ir. A.W.(Iex) Vredeveldt | Approved Date:

TNO innovation for life — TNO Structural Dynamics, Van Mourik Broekmanweg 6, 2628 XE Delft, P.O. Box 49, 2600 AA Delft, The Netherlands

Comments:

Part number: TN04.1.3.20

Sheet size: A3

Figure 1.16: Cryogenic vacuum inner test tank, from [6]

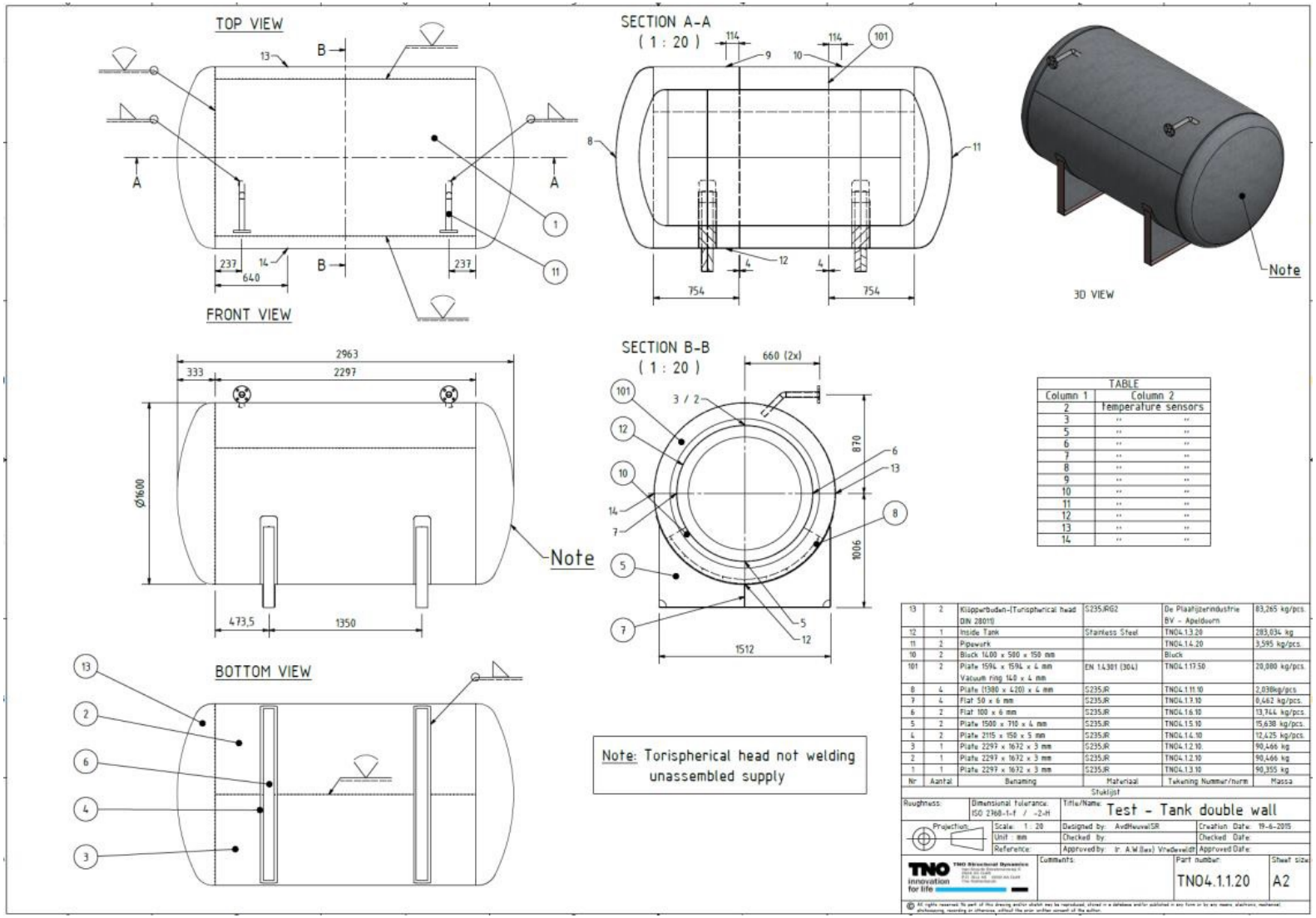

Figure 1.17: Cryogenic vacuum outer test tank, from [6]

Pressurization test 2

In 2003, Cummins Westport Incorporated has designed and developed a LNG vehicle fuel system for trucks. This system was tested and analyzed under the U.S. Department Of Energy (DOE) Advanced LNG Onboard Storage System (ALOSS) program. One test was a holding time test (defined as the time until the pressure reaches the PRV opening pressure). The tank is a double-walled tank with an inner volume (V) of 0.257 m^3. The insulation thickness is 3 cm. The internal tank surface (S) is 2.279 m^2. The inner tank and the outer tank are modeled as cylinders with flat end caps. This is an approximation of the exact geometry (see figure 1.18). The inner tank diameter (R) is 0.6 m and its length (L) is 0.909 m. The tank is partially filled with LNG. The fluid in the tank is assumed in vapor-liquid equilibrium. The PRV opening pressure is set at 1.585 MPa.

Figure 1.18: ALOSS test tank, from [7]

Model 1

Description This model is exactly the same as "model 1" for pressurization test 1. The workflow is detailed in figure 1.10. The initial values and parameters are given in table 1.4.

Results The pressure increase over time is shown in figure 1.21 with the orange line. The blue line represents the pressure curve obtained by the model. The pressure increases non linearly over time. Globally, model 1 overestimates the pressure rise. Figure 1.22 shows the maximum error is 26% (for t=138 hours). In [85], the authors suggested:

> *"Thermodynamic models with zero thermal mass for storage tanks underestimate the LNG holding time and overestimate the average daily BOG generation rate."*

Considering the tank thermal mass is further investigated in the next model.

Model 2'

Description The second model (called "model 2' ") describes the heat flow through the wall using a single thermal mass model. It is analogous to an electrical circuit constituted of two resistances (R) and a capacitance (C), as illustrated in figure 1.20. Parameters of the model are: the lumped thermal mass (C), its initial temperature ($T_t^{t=0}$) and two thermal resistances (R). The measured quantities are: the internal (T) and external (T_{amb}) temperatures. Heat may be stored by or released from the thermal mass, creating a time shift in the response of the measured heat flux to changes in internal temperature. Thermal resistances are defined as:

$$R = \left| \frac{\Delta T}{\delta Q} \right| \tag{1.20}$$

$$R = \frac{e \cdot \Delta t}{2 \cdot S \cdot \kappa} \tag{1.21}$$

The thermal mass is modeled by a capacitance, which reflects the ability of the tank to store internal energy. It is characterized by the insulation mass (m_t) and its specific heat (c_p). The thermal mass behavior is described by the following equation:

$$\dot{\delta Q} = m_t \cdot c_p \cdot \frac{dT_t}{dt} \tag{1.22}$$

The initial tank temperature is unknown ($T_t^{t=0}$). It is set to match experimental data to 160 K. The model is implemented in the Simulink environment (see figure 1.19).

Results The pressure increase over time is shown in figure 1.21 with the orange line. The dashed blue line represents the pressure curve obtained by model 2'. The pressure increases non linearly over time. Globally, model 2' fits better experimental data compared to model 1. However, the tank initial temperature ($T_t^{t=0}$) is tuned at 160 K (between T_{amb} and $T^{t=0}$) to reduce the relative error (see figure 1.22).

In the models presented so far, κ is known. However, LNG tank data-sheet usually do not provide values for κ. Instead, results of a holding time test are provided. In the next section, a method is proposed to deduce a value for κ from the holding time test results.

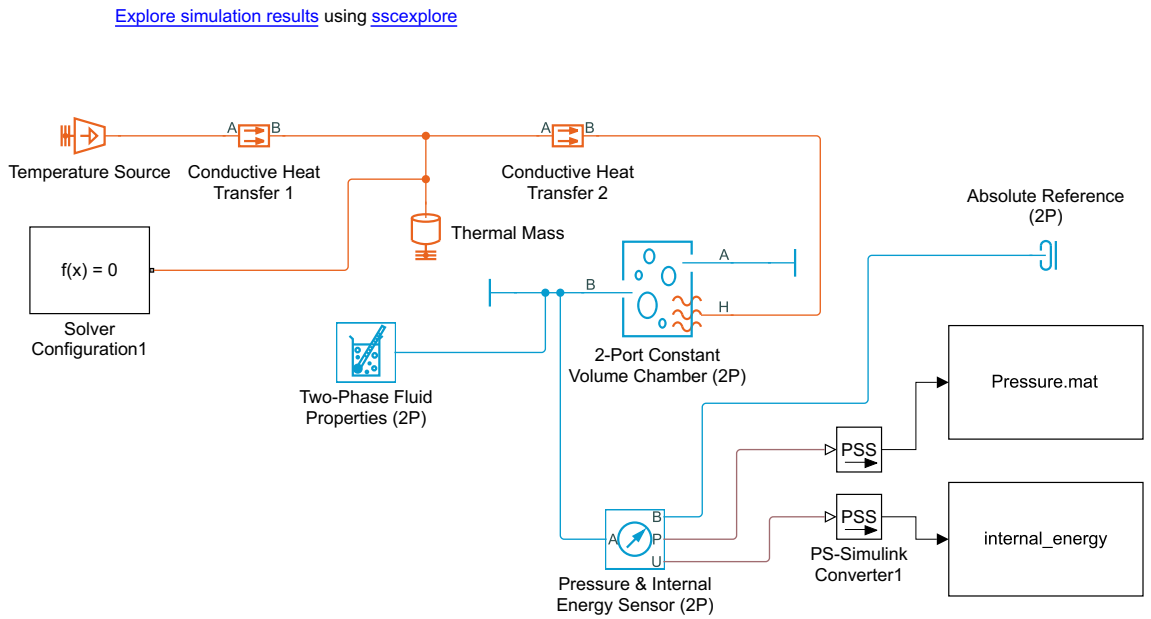

Figure 1.19: Model 2' - Caption of the thermal model in the Simulink environment

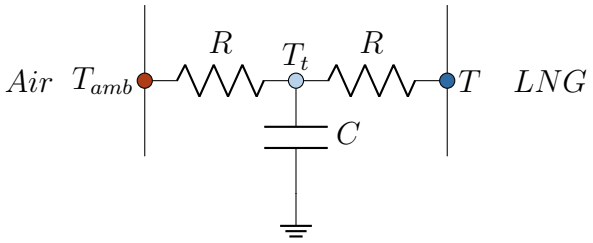

Figure 1.20: Model 2' - Schematic diagram of the single thermal mass model showing the electrical equivalent circuit for the heat transfer through the wall

Variable	**Initial value**	**Unit**
P	0.2013	MPa
T_t	160	K
Parameter	**Value**	**Unit**
m	77.3	kg
κ	2.158	$\mathrm{mW{\cdot}m^{-1}{\cdot}K^{-1}}$
T_{amb}	298.15	K
V	0.257	$\mathrm{m^3}$
S	2.279	$\mathrm{m^2}$
e	0.03	m
Δt	60	s
m_t	175	kg
c_p	477	$\mathrm{J{\cdot}kg^{-1}{\cdot}K^{-1}}$

Table 1.4: Model 2' - Initial values and parameters for pressurization test 2

Plots

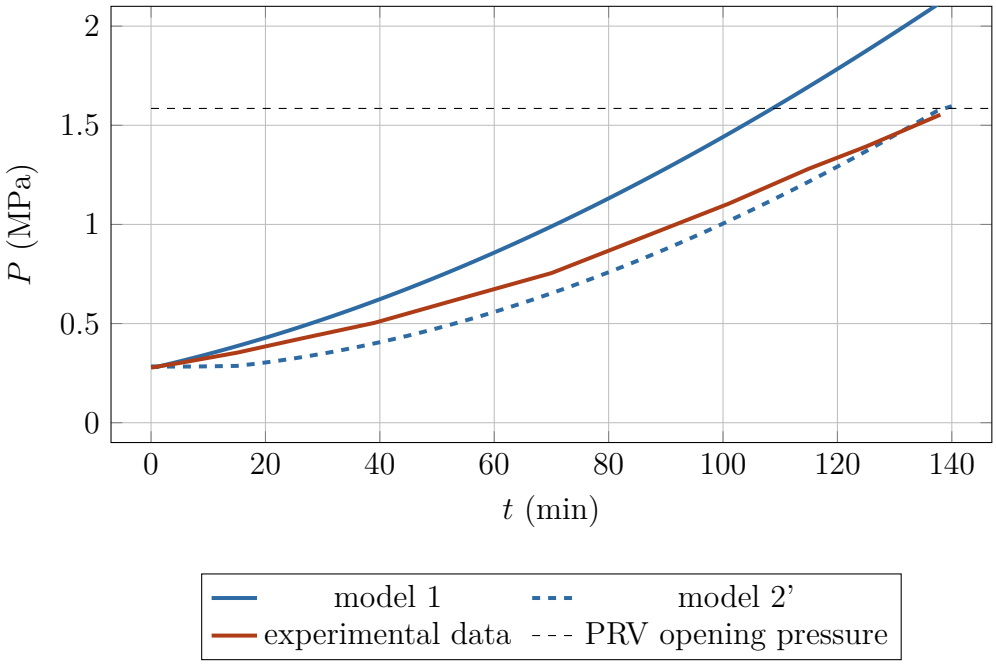

Figure 1.21: Pressure evolution

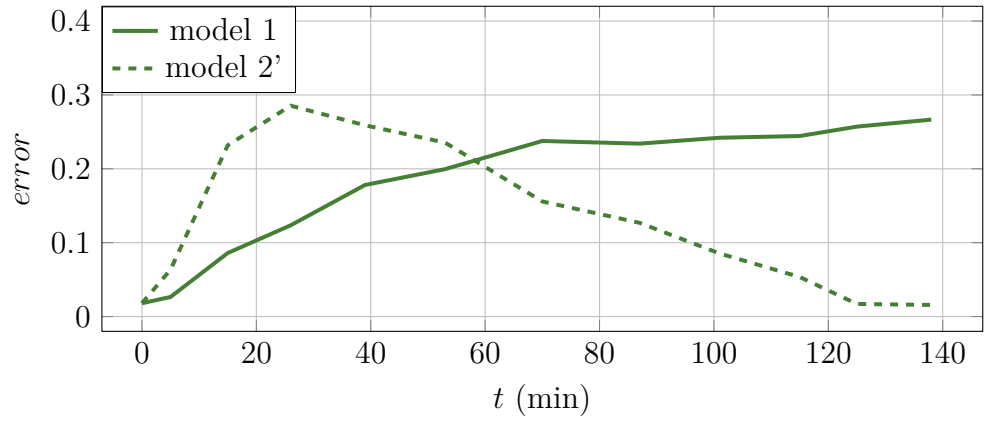

	model 1	model 2'
mean error	18%	13%
standard deviation	0.09	0.10

Figure 1.22: Error evolution

LNG ISO 40 ft tank - thermal insulation data-sheet

A common piece of information embedded in tank data-sheet is the holding time. In this section, it is shown how, from the holding time, it is possible to define the constant apparent thermal conductivity (κ) used in the previous models. The tank is a horizontal 40 ft. cryogenic tank container (see figure 1.23). It's vacuumed with multi-layer thermal insulation. It is modeled as a cylinder with two concentric oblate ellipsoidal heads. Its main characteristics are presented in figure 1.24 and table 1.25. Assuming a realistic ellipsoid aspect ratio of 0.5, the insulation thickness, supposed uniform, is deduced from equation 1.23. The internal surface of the tank is computed with equation 1.24. The tank is meant to be operated between 1 atm and a Maximum Allowable Working Pressure (MAWP) of 10 bars with a service pressure of 7 bars.

The tank holding time is given for various products (see table 1.5). The fluids considered are:

- Liquefied Nitrogen (LIN);
- Liquefied Oxygen (LOX);
- Liquefied Argon (LAR);
- Liquefied methane (LCH_4);
- Liquefied ethane (LC_2H_6);
- Liquefied ethylene (LC_2H_4).

Knowing the holding time allows to run a pressurization simulation using model 1 with κ such that the pressure at the end of the holding time ($P^{t=holding\,time}$) is 10 bars. The value of κ is found using a Generalized Reduced Gradient (GRG) solver. This process is repeated for various ambient temperatures (T_{amb}). If the model 1 is valid, considering the different fluids should result in close values for κ. Furthermore, κ should be similar to reported values in the literature for vacuumed multi-layer insulation. The result are presented in figure 1.26. For liquefied methane, the apparent thermal conductivity minimizing the squared pressure difference (equation 1.25) over an extended ambient temperature range (see table 1.6) is 1.84 $mW \cdot m^{-1} \cdot K^{-1}$. This is in good agreement with reported values in the literature for vacuumed multi-layer thermal insulation [5].

$$V = \frac{4 \cdot \pi \cdot (r - e) \cdot (R - e)^2}{3} + \pi \cdot (R - e)^2 \cdot L \tag{1.23}$$

$$\begin{aligned} S &= 2 \cdot \pi \cdot (R - e)^2 \cdot \left(1 + tanh^{-1}(c) \cdot \frac{1 - c^2}{c}\right) + 2 \cdot \pi \cdot (R - e) \cdot L \\ c^2 &= 1 - \frac{(r - e)^2}{(R - e)^2} \end{aligned} \tag{1.24}$$

$$\begin{aligned} error_{T_{amb}} &= \left(P^{t=holding\ time} - MAWP\right)^2 \\ \overline{error} &= \frac{\sum_{i=1}^{N} error_i}{N} \end{aligned} \tag{1.25}$$

Figure 1.23: LNG Trifleet 40 ft. ISO tank, courtesy of Trifleet

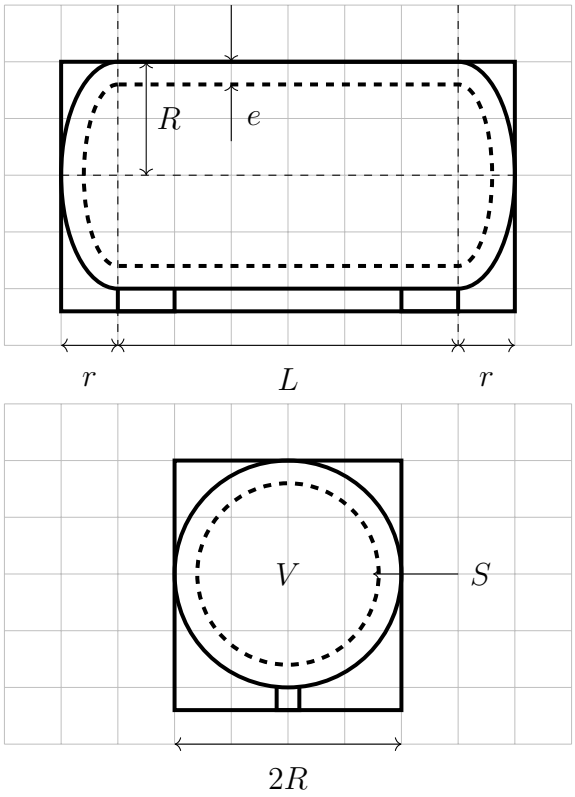

Figure 1.24: Trifleet LNG tank diagram

	Description	**Value**	**Unit**
Manufacturer specifications			
$L + 2R$	Length	12.192	m
$2R$	Width	2.438	m
V	Nominal capacity	46	m^3
Assumption regarding the geometry			
r/R	Ellipsoid aspect ratio	0.5	–
Computed data			
e	Insulation thickness	0.0981	m
S	Internal surface	87.8	m^2
κ	Apparent thermal conductivity	0.0018	$W{\cdot}m^{-1}{\cdot}K^{-1}$

Figure 1.25: Trifleet LNG tank data

Product	Holding time (days)	Payload (10 bar) at max. holding time (kg)	Initial Filling Pressure (bar)
LIN	54	24,400	1
LOX	56	24,400	1
LAR	39	24,400	1
LCH_4	100	16,000	1
LC_2H_6	230	20,600	1
LC_2H_4	187	21,500	1

Table 1.5: Trifleet LNG tank thermal performance, data from [13]

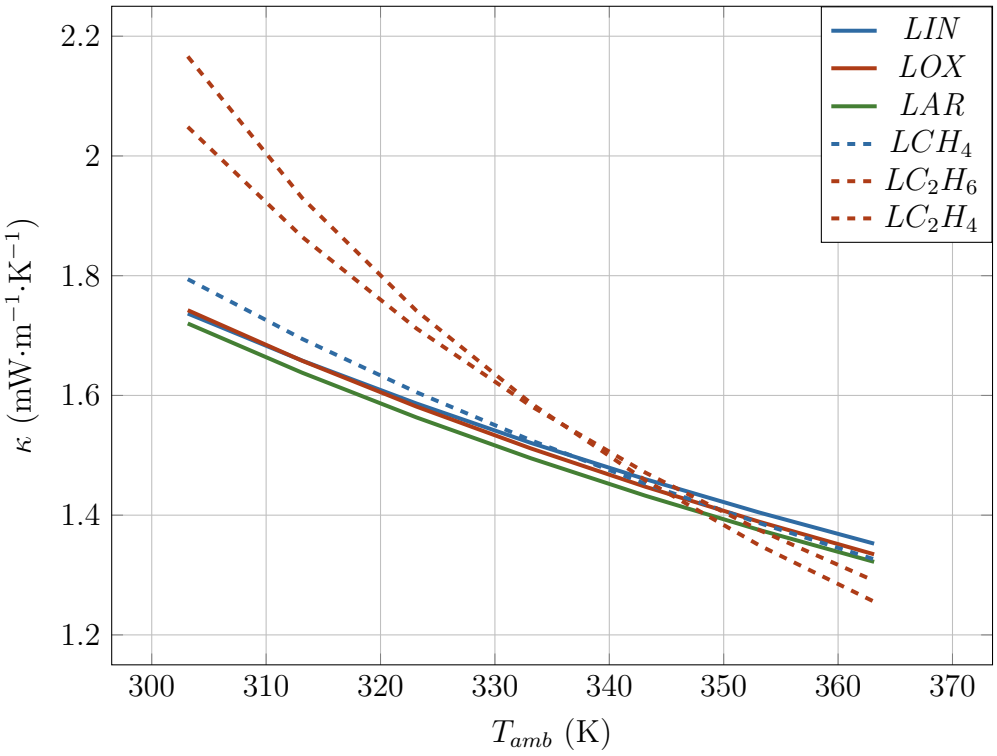

Figure 1.26: Values of κ such that the pressure at the end of the holding time is 10 bars

T_{amb} (K)	κ (mW$\cdot$ m$^{-1}\cdot$ K^{-1}) such that $P^{t=holding\ time}$=10 bar	error for κ=1.9	error for κ=1.84	error for κ=1.8
263.15	2.35	0.07992	0.10081	0.11580
268.15	2.26	0.05770	0.07695	0.09108
273.15	2.18	0.03849	0.05565	0.06859
278.15	2.10	0.02271	0.03725	0.04871
283.15	2.03	0.01077	0.02214	0.03176
288.15	1.97	0.00307	0.01063	0.01804
293.15	1.91	0.00003	0.00314	0.00794
298.15	1.85	0.00213	0.00006	0.00181
303.15	1.79	0.00984	0.00180	0.00003
308.15	1.74	0.02365	0.00882	0.00300
313.15	1.69	3.18373	0.02155	0.01113
$\overline{\text{error}}$		0.31200	0.03080	0.03617

Table 1.6: Liquefied methane - error considering κ equals 1.9, 1.84 and 1.8 mW$\cdot$ m$^{-1}\cdot$ K^{-1} for various ambient temperatures

Conclusions on pressurization tests

The fluid self-pressurization by natural heat leaks has been assessed using several models:

- Model 1: Assuming the tank has no thermal mass and a constant apparent thermal conductivity. The fluid evolves through vapor-liquid equilibrium states and the ambient temperature is constant;
- Model 2: Assuming the tank has no thermal mass but a variable apparent thermal conductivity. The apparent thermal conductivity depends on the ambient temperature, the fluid temperature and the insulation vacuum pressure. The fluid evolves through vapor-liquid equilibrium states and the ambient temperature evolves through time;
- Model 2': Assuming the tank has a thermal mass and a constant apparent thermal conductivity. The fluid evolves through vapor-liquid equilibrium states and the ambient temperature is constant.

In the two experimental cases, model 1 tends to overestimate the pressurization rate. Ways of improvement, suggested in the literature, are implemented. In the first experimental case, because the tank is engulfed in flames, the model has been enhanced (model 2) considering:

- an apparent thermal conductivity based on the tank temperature and vacuum pressure;
- an ambient temperature matching typical fire temperature curves.

In the second experimental case, the model has been enhanced (model 2') considering the tank thermal inertia. In both cases, the enhancements did reduce the model relative error. However, some parameters has been slightly tuned to match experimental data:

- In model 2: the ambient temperature (T_{amb}) and vacuumed pressure curves (P_{vac});
- In model 2': the initial temperature value of the thermal mass ($T_t^{t=0}$).

Model 1, since it overestimates the pressurization rate, is a conservative assumption. To err by the side of caution, at a feasibility design stage, model 1 is retained. Then, it has been shown how thermal performances, as commonly reported in product data-sheet, can be used to determine an apparent tank thermal conductivity.

It is to note, other studies claim the vapor-liquid equilibrium assumption is misleading [86][70]. In reality, the temperature change exhibits a thermal stratification phenomenon characterized by a non-homogeneous state. This phenomenon exhibits very different results from those predicted by homogeneous models. Notably, thermal stratification leads to a reduced holding time. However, the sloshing on-board tends to break thermal stratification. It has been shown, that sloshing induces pressure drops. The pressure drop stops when the mixing of the liquid in the sloshing area is completed, namely when a steady state has been reached [87][88]. At a concept design level, this issue can be left open: the vapor-liquid equilibrium assumption remains convenient for rough estimations. However, it should be further investigated once moving to more detailed engineering.

In the next section, a model will be proposed to assess LNG ageing in the tank.

Ageing model

The experimental program run by K. J. Kountz for the Gas Technology Institute (GTI) in 1999, included six weathering tests with various initial LNG compositions. Due to dissemination policy issue, this thesis presents the test facility and results for one test case [8].

A 0.19 m^3 tank is fitted with a pressure sensor, a temperature sensor, a pressure relief valve and a liquid sampling line connected to a gas chromatograph. The compositions are expressed as vectors. Each component of the vector is a mole fraction: the number of moles of one chemical compound over the total number of moles in the fluid. The experimental test report contains different initial compositions of methane, ethane, propane and nitrogen. Detected traces of higher hydrocarbons have been lumped into the propane molar fraction. The following table lists the molar percentage of the four LNG components in the selected test case:

Component	Molar fraction
x_{CH_4}	0.968
$x_{C_2H_6}$	0.020
$x_{C_3H_8}$	0.006
x_{N_2}	0.006

Table 1.7: LNG ageing model - charged LNG composition in the tank

So, in the model, the composition is expressed as:

$$\vec{x} = \begin{bmatrix} 0.968 \\ 0.020 \\ 0.006 \\ 0.006 \end{bmatrix} \tag{1.26}$$

The tank is on an electronic weight scale (see figure 1.27). The pressure relief valve is set to vent vapor at 10.96 bar. The experimental data give no information regarding the tank material. In Kountz's report, it is noted that, to accelerate the LNG ageing, heat was added to the exterior of the tank containing the inlet valve sections, by means of a catalytic heater. The initial values are given in table 1.8.

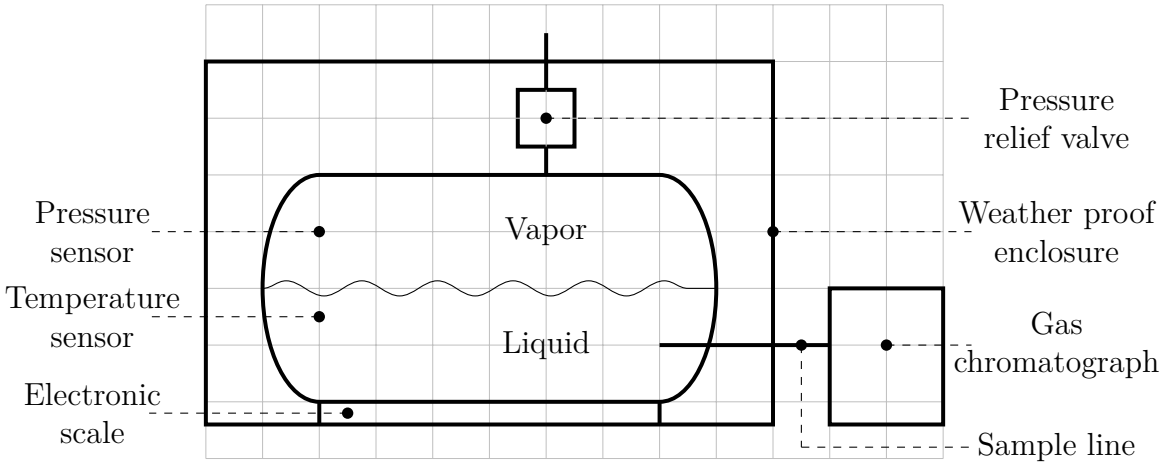

Figure 1.27: LNG ageing test facility, based on [8]

Variable	**Initial value**	**Unit**
m	60.7	kg
Parameter	**Value**	**Unit**
P	10.96	bar
V	0.19	m^3
Δt	0.1	day
T_{amb}	293.15	K

Table 1.8: LNG ageing model - Initial values and parameters

As part of the test program, a non-disclosed physical model was developed and it assumes a constant heat leakage of 50 Btu/hr ($\approx$ 14.6 W). The tank is loaded with 60.7 kg of fluid. Here, the self-pressurization phase (before the pressure reaches the relief valve pressure) is ignored. The simulation starts at the opening of the pressure relief valve (at t=3.26 days). From the fluid mass (m), its composition ($\vec{x}$), the tank capacity (V), the relief pressure and assuming vapor-liquid equilibrium, other values are computed:

- the temperature (T);
- the specific enthalpy (h);
- the vapor mass fraction (χ);
- the vapor density (ρ_V);
- the liquid density (ρ_L);

- the liquid LHV (LHV_L);
- the vapor LHV (LHV_V);
- the liquid MN (MN_L);
- the vapor MN (MN_V).

Using the initial fluid temperature ($T^{t=3.26}$), the apparent thermal conductivity times the internal surface over the insulation thickness is computed according to equation 1.27.

$$\begin{cases} \frac{\kappa \cdot S}{e} = -\frac{\delta\dot{Q}}{T_{amb} - T^{t=3.26}} \\ \delta\dot{Q} = 14.6 \end{cases} \tag{1.27}$$

Then, during the simulation, the heat leak isn't constant; it's weighted by the temperature difference (see equation 1.9). The system is considered closed and redefined at each time step, removing the BOG. The weathering process is modeled considering iteratively the following steps:

1. From the fluid temperature, the heat leak is computed. It is associated to an isobaric enthalpy increase. The fluid (liquid+vapor) volume increases (it is higher than V).
2. A (P, h) flash computation is performed to define the new composition in each phase;
3. The volume is redefined (as equal to V). The excess of vapor is considered as BOG. The total mass and composition left in the tank are updated accordingly.
4. The new fluid temperature and specific enthalpy are computed with REFPROP using the new density (m/V), composition ($\vec{x}$) and the constant relief pressure (P):

$$(T, h) = f(\frac{m}{V}, P, \vec{x}) \tag{1.28}$$

The workflow is detailed in figure 1.28. Again, calls to REFPROP are expressed as an "f" function. For conversion, the molar mass ($\vec{M}$) is introduced. Each component of $\vec{M}$ is the molar mass of the corresponding compound in $\vec{x}$.

In the flow chart, calls to the MN computation method are expressed as an "f'" function. The methane number is computed using the GRI method [77]:

- First, the Motor Octane Number (MON) is computed using two different equations (equation 1.29 and 1.30). HC is the hydrogen to carbon ratio.

$$\begin{aligned} MON\,1 = {} & 137.78 \cdot x_{CH_4} + 29.948 \cdot x_{C_2H_6} \\ & - 18.193 \cdot x_{C_3H_8} - 167.062 \cdot x_{C_4H_10} \\ & + 181.233 \cdot x_{CO_2} + 26.994 \cdot x_{N_2} \end{aligned} \tag{1.29}$$

$$MON\,2 = -406.14 + 508.04 \cdot HC - 173.55 \cdot HC^2 + 20.17 \cdot HC^3 \tag{1.30}$$

- Then, the MN is computed using equation 1.31 for each MON;

$$MN = 1.445 \cdot MON - 103.42 \tag{1.31}$$

The method states that if the difference between the two MNs is more than 6, another method should be employed. Furthermore, the method specifies a concentration limit for each component (see table 1.9). In the model, if the composition is out of bounds, the MN is not computed and the code proceeds to the next time step.

Component	Limit (molar fraction)
x_{CH_4}	$\geq$0.75
$x_{C_2H_6}$	$\leq$0.14
$x_{C_3H_8}$	$\leq$0.25
x_{C_4+}	$\leq$0.01
x_{CO_2}	$\leq$0.018
x_{N_2}	$\leq$0.035

Table 1.9: MN calculation GRI method - The concentration limit for each component

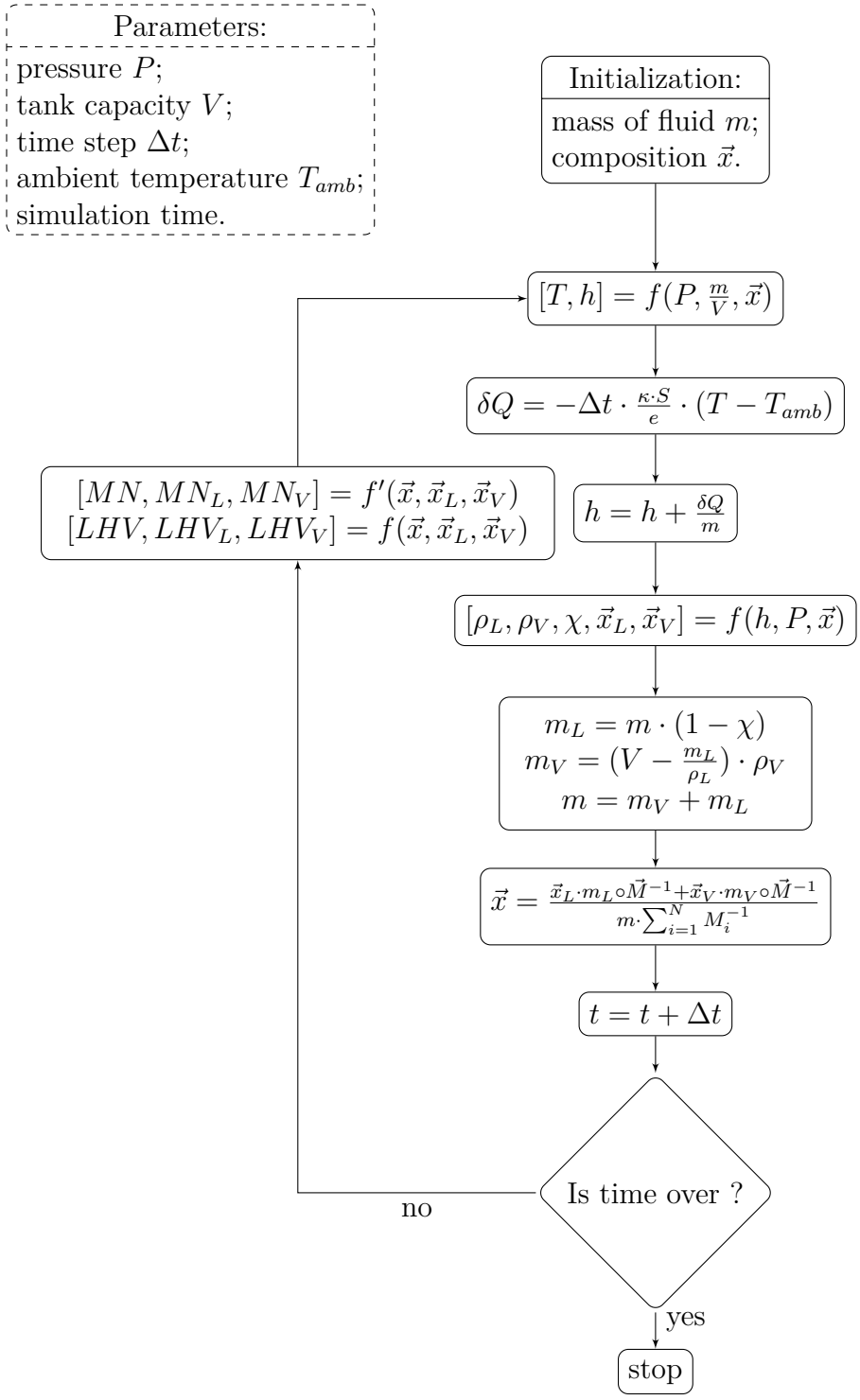

Figure 1.28: LNG ageing - flow chart

Results According to figure 1.29, the mass evolution follows a quasi linear slope. The experimental results match this development until around day 18. After this period, the model tends to overestimate the mass reduction rate. The model mass reduction rate slows down after day 22 mainly due to the liquid temperature increase which diminishes the heat flow. Consequently, the BOG is almost constant (2.7 kg/day) until day 22 where it drops to 1 kg/day.

From figure 1.30, the pressure is constant during the test and this is a key hypothesis for the model (allowing $\Delta(PV) = P\Delta V$). This is why the transient initial phase (the tank pressurization) is not considered. Self-pressurization has been considered in the previous section. At the end of the weathering period, the temperature rise is due to the composition change in the liquid toward greater percentages of the higher boiling point components as the methane composition decreases. However, the model lags to predict the recorded temperature increase. Two hypothesis are proposed to explain this discrepancy:

1. The temperature sensor was located near the pressure relief valve, a local thermal bridge;

2. Thermal stratification occurs in the vapor phase and the temperature is not homogeneous. It's higher at the top of the tank, where the sensor is located, than at the interface.

A potential way to enhance the model could be to reconsider the vapor-liquid hypothesis and discretize spatially the tank, moving to a zonal model as in [89, 90, 91, 92]. Once again, at a concept design level, the vapor-liquid equilibrium assumption is satisfactory.

The model predictions regarding LNG composition during the weathering process are reasonably well verified by the experimental results (see figure 1.31). The methane molar fraction decrease and the increase of the ethane and propane molar fraction in the liquid are due to the continuous removal of the vapor charged with methane.

At day 24, half the mass is in the vapor phase (the vapor mass fraction, χ, is 0.5) (figure 1.32). At that time, ethane starts to evaporate (boiling point around 184 K), rising the density of the vapour phase. The liquid density rises while methane is leaving the liquid phase. Liquid is left with propane which is not evaporating but expands due to temperature increase. This causes the liquid density to slightly decrease during the last day of the simulation (see figure 1.33). The evolution of the LHV (see figure 1.34) can be divided into three steps:

1. First, the LHV increases in both phases (up to day 7). This is due to the nitrogen evaporation in the boil-off. As nitrogen is an inert gas, removing it enhances the LHV;

2. Then, methane leaves the liquid phase towards the vapor phase. As it has the highest heating value on a molar basis, its departure lowers the liquid LHV while rising the vapor LHV (from day 7 to day 20);

3. Methane is released in the BOG, and ethane evaporates so the vapor LHV also drops.

The LHV variation amplitude in the liquid phase is of 5.5% and 6.4% in the vapor phase. Due to the method limitations, the MN is not computed over the whole period (see figure 1.35). Nevertheless, on the valid portion, the tendencies corroborate the previous analysis. Primarily, nitrogen is removed, rising the fraction of methane and so the MN increases in both phases. After that, the methane transfer leads to a MN increase in the vapor phase, and conversely, a drop in the liquid phase. The final stage is a serious drop due to high hydrocarbons in the vapor phase. Globally, for a given percentage of methane, higher hydrocarbons (and hydrogen) lower the MN whereas inert gases raise it.The MN variation amplitude is of 4.3% in the liquid phase and 9.6% in the vapor phase.

Figures 1.36 and 1.37 show the relative error evolution (as defined by equation 1.17) for the fluid mass in the tank, the temperature, the pressure and the liquid phase composition. Pressure and temperature errors are below 20 %. The mass error is also below 20% before day 20. The error then skyrockets since it's a relative error and the level is low. For the composition, the error is high for C_2H_6 and C_3H_8. However, since for C_2H_6 and C_3H_8 the molar fraction is low and the graph molar fraction range is broad (from 0 to 1), a slight inaccuracy of the digitized plot would generate large error value. Globally, the model is judged satisfactory. It does provide correct trends regarding the LNG behavior during ageing which is the aim at a concept design level.

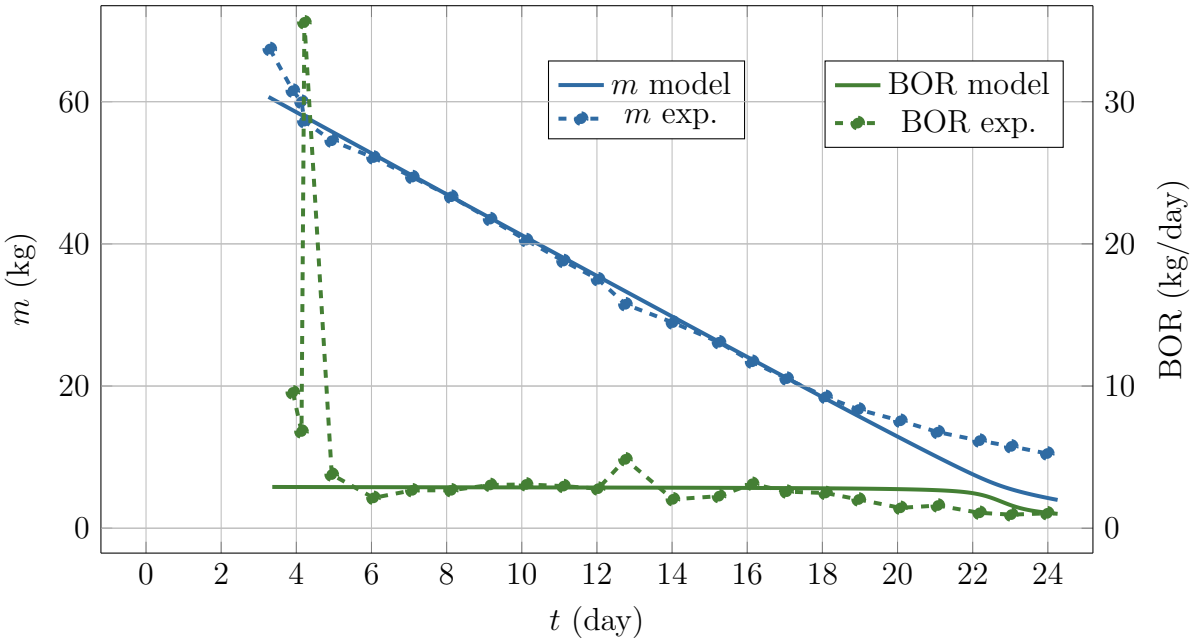

Figure 1.29: Model vs. experiment: scale weight evolution

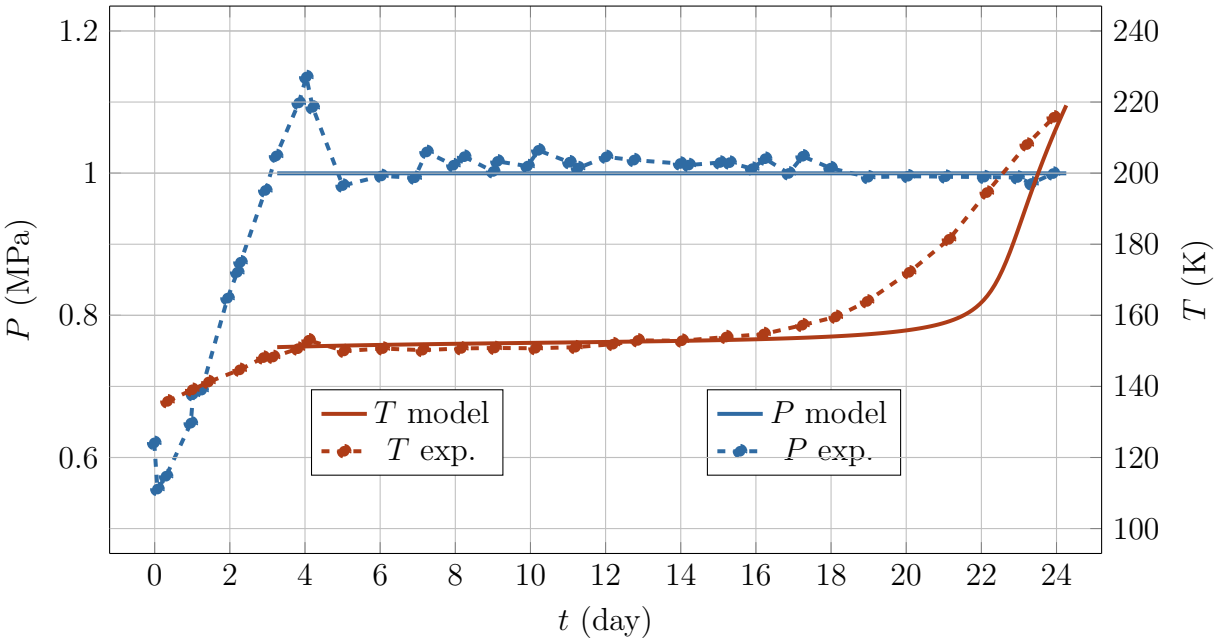

Figure 1.30: Model vs. experiment: pressure and liquid temperature evolution

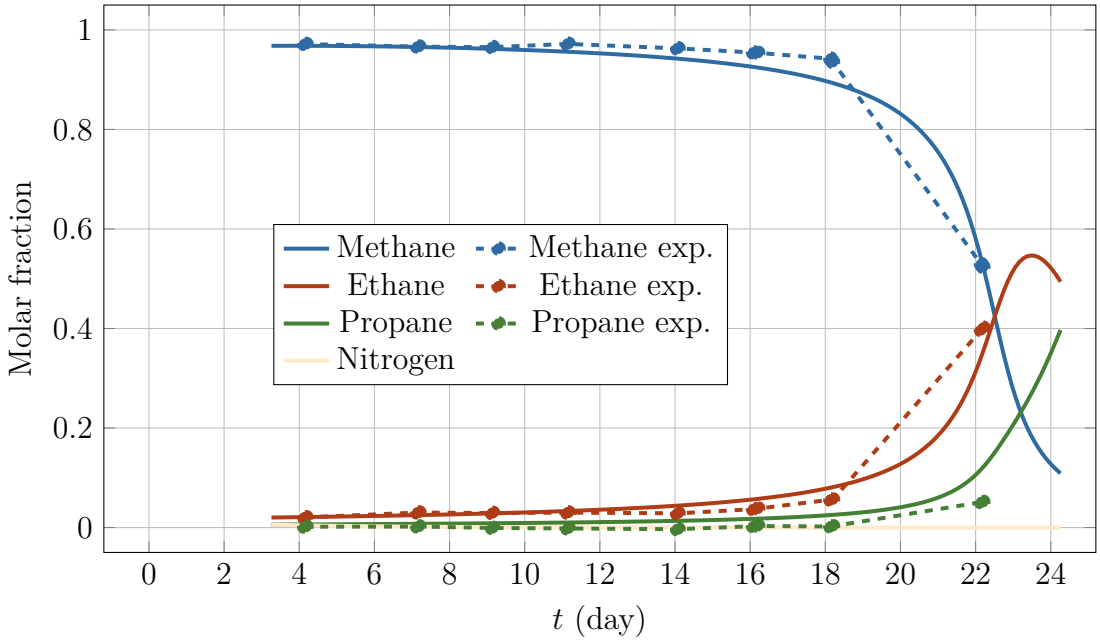

Figure 1.31: Model vs. experiment: liquid composition evolution

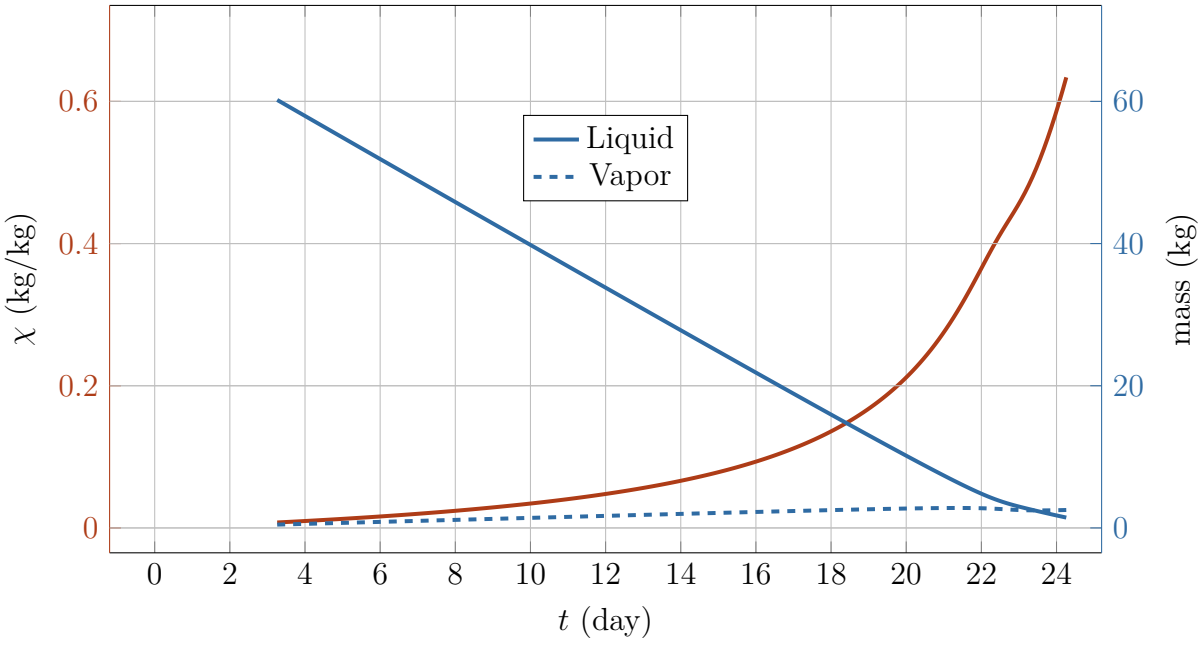

Figure 1.32: Model: mass and vapor mass fraction evolution

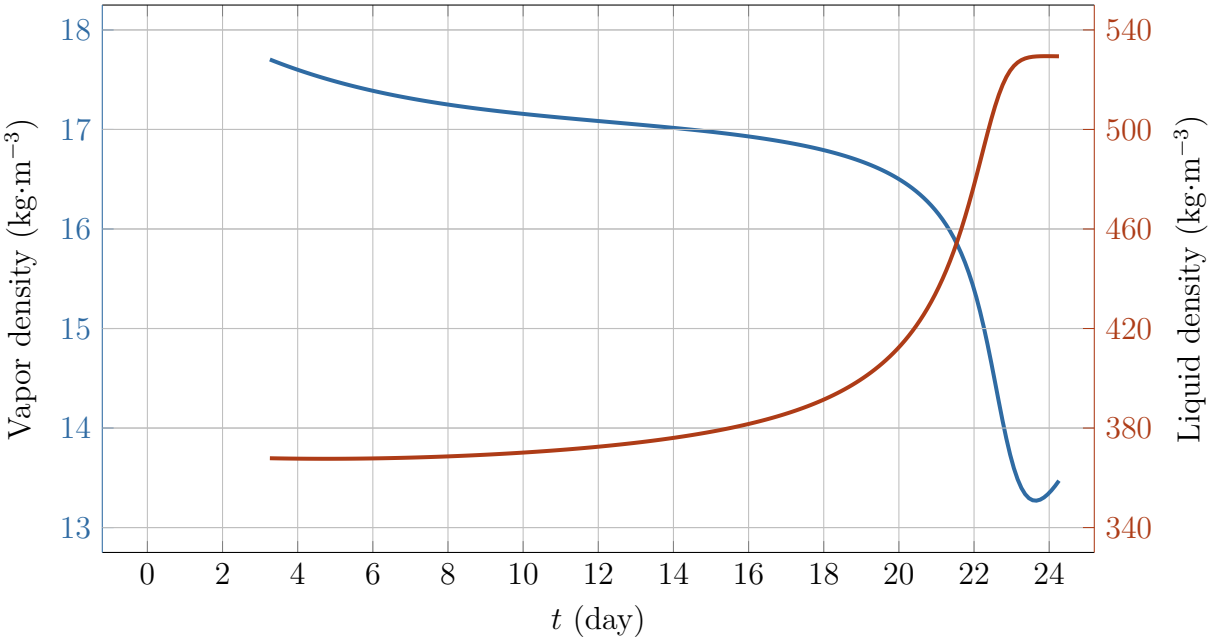

Figure 1.33: Model: densities evolution

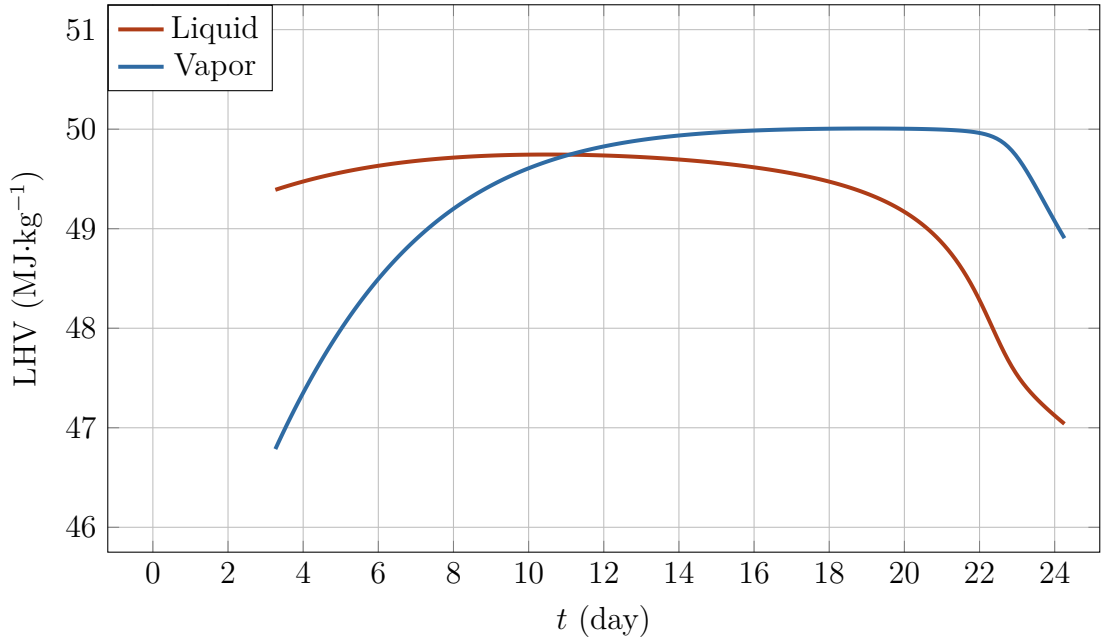

Figure 1.34: Model: low heating values evolution

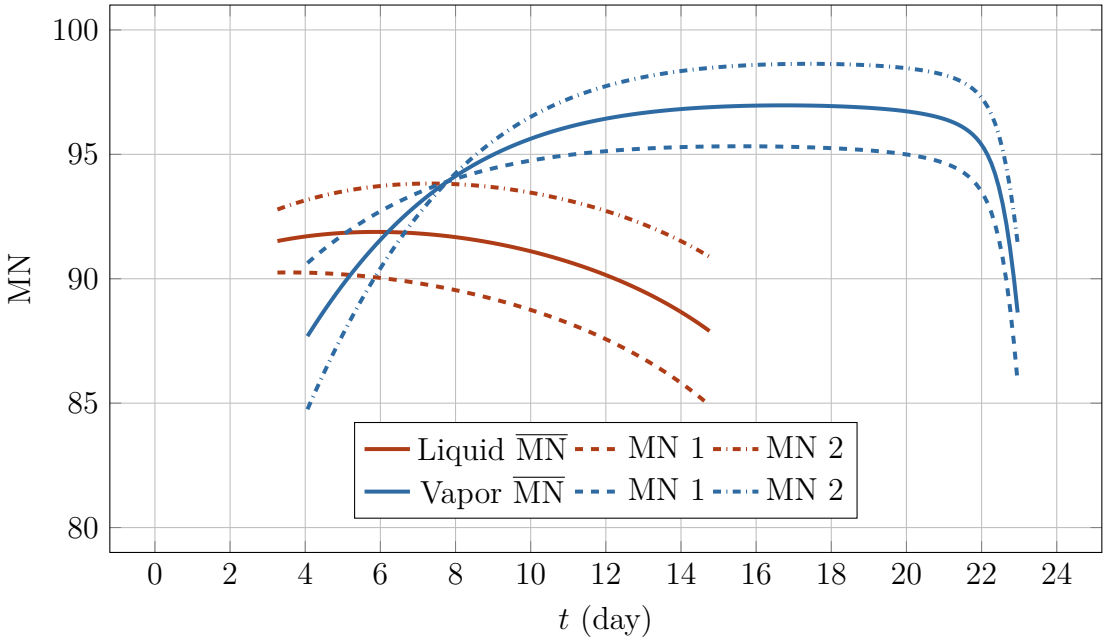

Figure 1.35: Model: methane number evolution

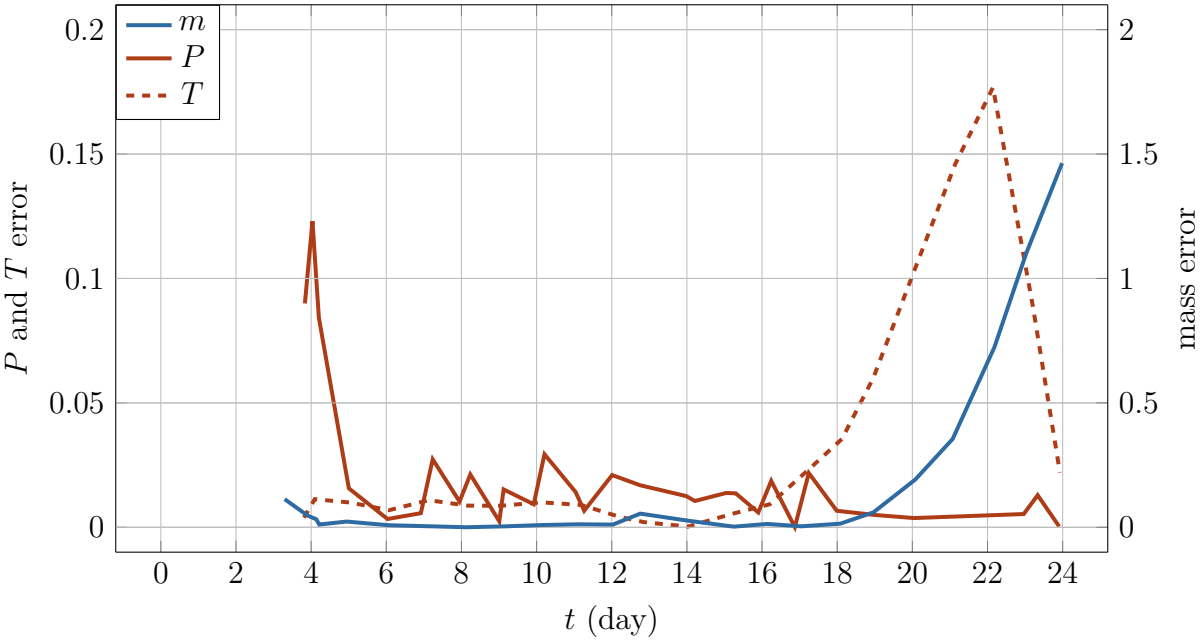

Figure 1.36: Error evolution 1

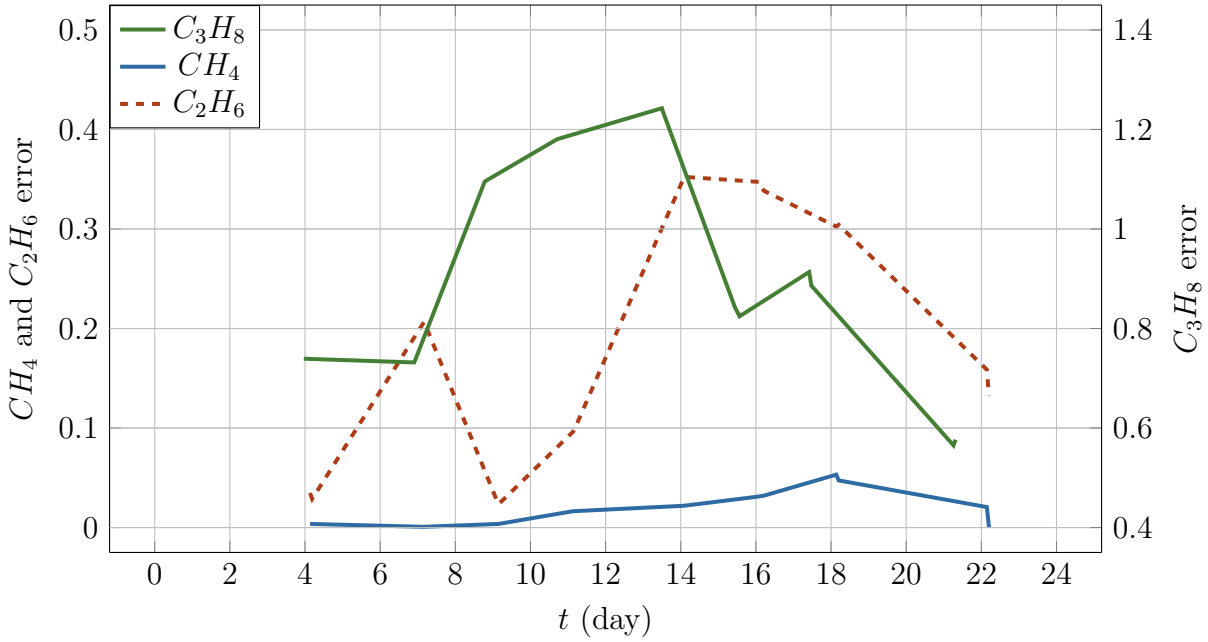

Figure 1.37: Error evolution 2

Methane number calculator

While the development of LNG as a fuel is gaining momentum, the lack of a commonly agreed method to characterize LNGs in term of the Methane Number (MN) is impedimental for its progress [93]. In the previous section, the MN has been computed using the GRI method as described in ISO/TR 22302:2014. However, different MN computation methods lead to different results (see figure 1.39). It is to note that between 2017 and 2018, the International Group of Liquefied Natural Gas Importers (GIIGNL) removed Libya from their list of receiving terminals [12][94]. LNG from Libya will therefor no longer be considered in this thesis. Figure 1.40 shows that:

- The MN of commercially available LNGs varies between 80 and 100;
- The MN difference between calculation methods varies from 0.5 (Nigeria) to 5.7 (Alaska).

It has been shown that during the ship's journey, the LNG composition varies due to ageing. The MN should hence be computed at each time step using the method prescribed by the engine manufacturer. From literature review, easily available MN computation methods are online black-box models: they take a sequence of query inputs (natural gas composition) and return corresponding output (the MN). The algorithm isn't explicitly open. To implement a MN dynamic calculation tool a meta-model has been developed. First, from a sequence of queries, a data-set is collected. Then two multivariate interpolation methods have been compared. One has been retained. The overall approach (see figure 1.38) is detailed below.

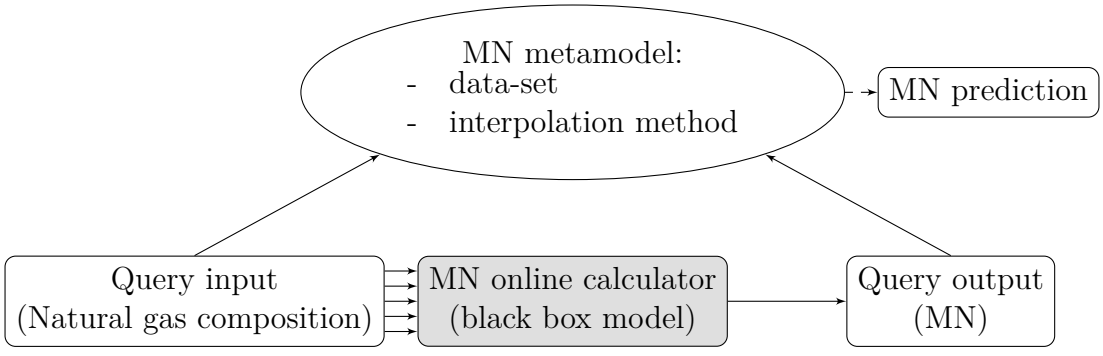

Figure 1.38: Overview of the MN metamodel approach

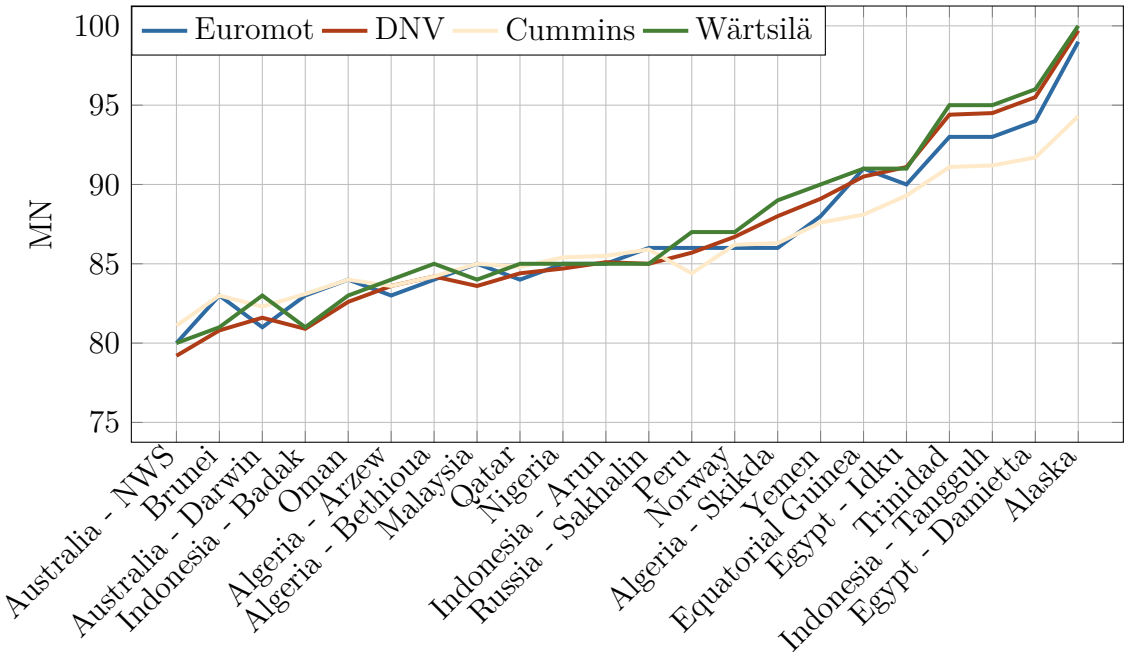

Figure 1.39: The MN for various compositions and different computation methods (C_4+ treated as C_4H_{10})

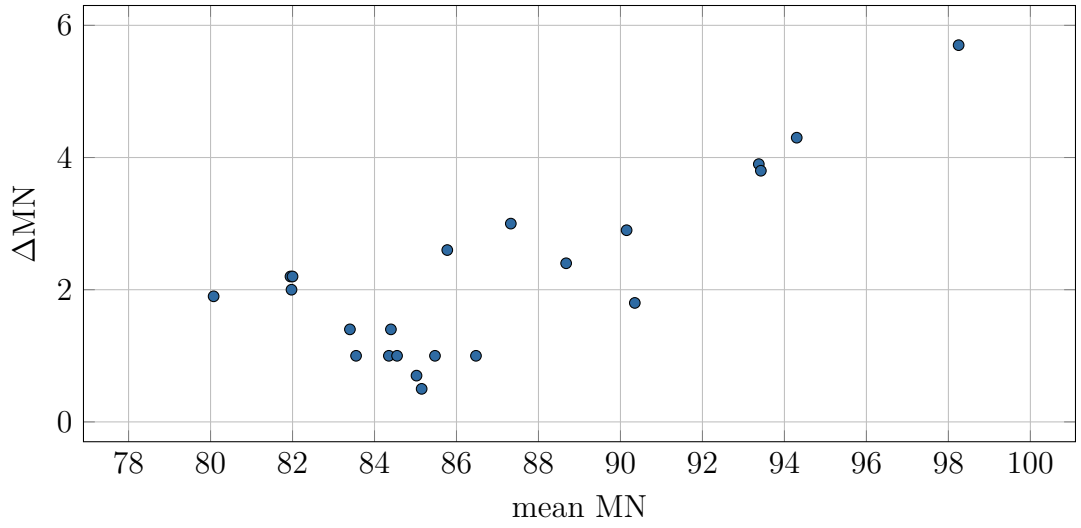

Figure 1.40: The mean MN for each composition vs. the MN maximum difference between computation methods

Arbitrarily, the DNV-GL calculation method has been selected but the approach could be used on any black box MN calculator.

The first step is to generate a discrete set of known data points. The compositions are expressed as vectors. Each components of the vector is a mole fraction. The online calculator sets a concentration limit for each component (see table 1.11 and figure 1.41). The range of validity of each component is divided by steps of 2% (see table 1.10). The step is chosen as a trade-off between the number of computation points and the data-set generation time. Indeed, a sufficient number of computation points are required to map correctly the response surface but the mapping process time rises significantly with finer meshes. Among the number of combinations N (see equation 1.32), only combinations with a sum equal to one are considered.

$$N = 11 \cdot 16 \cdot 11 \cdot 11 \cdot 11 \cdot 3 = 63,888 \tag{1.32}$$

Component	min.	max.	step	number of values
x_{CH_4}	0.70	1	0.02	16
$x_{C_2H_6}$	0.00	0.20	0.02	11
$x_{C_3H_8}$	0.00	0.20	0.02	11
$x_{C_4H_{10}}$	0.00	0.05	2	3
x_{N_2}	0	0.20	0.02	11

Table 1.10: The range of the data-set for MN mapping

This criterion reduces the number of valid combinations to 1 595. Even though the composition range is respected, some cases are returned as "out of range" (see figure 1.42). The reason is unknown. They are neglected and the final number of computed points is 1 179. For each composition, the script performs the following actions:

1. read the composition;
2. field the website form accordingly and ask for the MN;
3. if the computation succeeds, store the ouput (MN).

Each loop lasts approximately 10 seconds so the total time is 4h30. To automate the process in the browser, an open-source tool written in java is used: Kantu[3].

The second step is to select an interpolation method. In numerical analysis, multivariate interpolation is interpolation on functions of more than one variable. In this study, the unknown function contains five variables, the five components

[3]https://ui.vision/

of the composition. Interpolation methods differ in such properties as: accuracy, cost, number of data points needed and smoothness of the resulting interpolation function. In this thesis, two multivariate interpolation methods are investigated: the Inverse Distance Weighting (IDW) method and the Neural Network (NNET) method.

Component	Limit (molar fraction)
x_{CH_4}	$\geq$0.70
$x_{C_2H_6}$	$\leq$0.20
$x_{C_3H_8}$	$\leq$0.20
$x_{C_4H_{10}}$	$\leq$0.05
x_{N_2}	$\leq$0.20

Table 1.11: MN calculation DNV-GL method - The concentration limit for each component

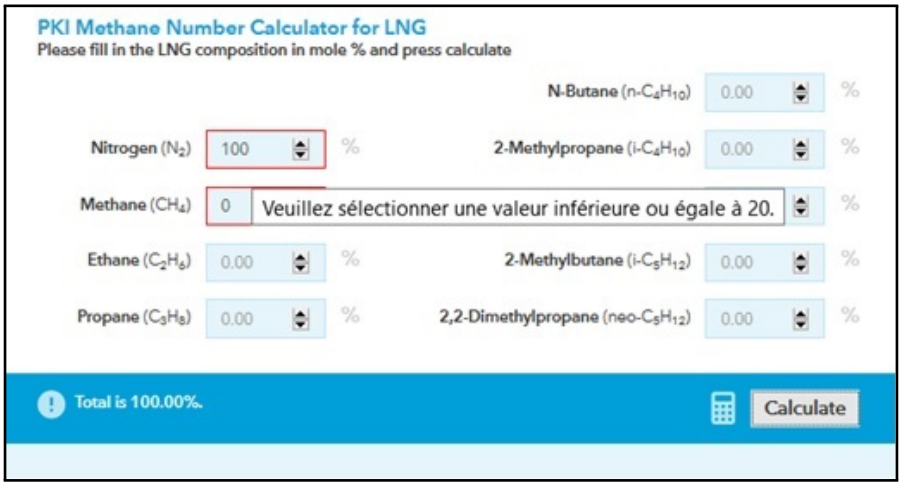

Figure 1.41: Screenshot of the MN online calculator - requirements regarding the molar fraction of nitrogen

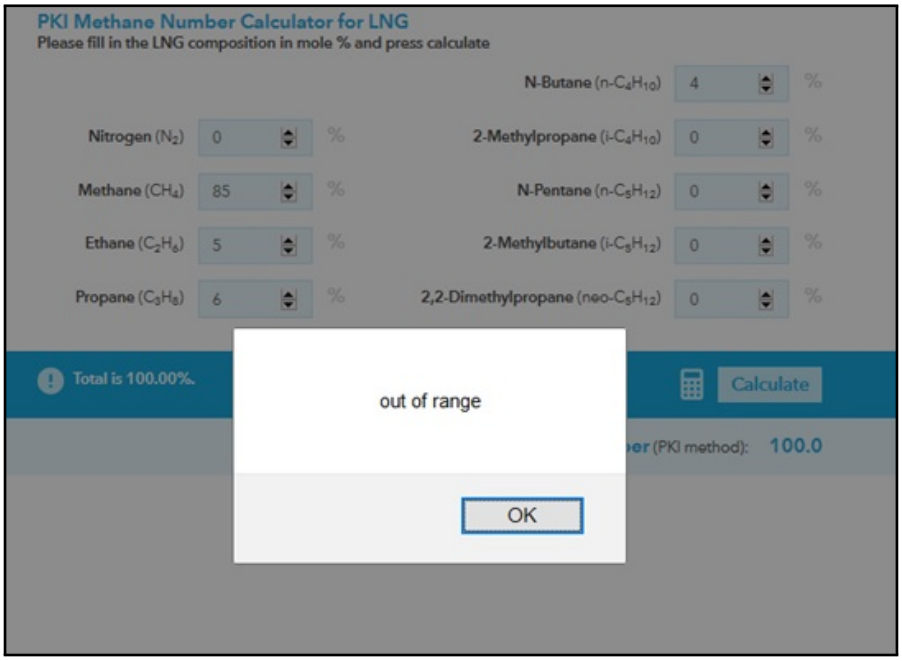

Figure 1.42: Screenshot of the MN online calculator - pop up message when the composition is considered “out of range”

Inverse Distance Weighting (IDW) method IDW is a type of deterministic method for multivariate interpolation with a known scattered set of points. The assigned values to unknown points are calculated with a weighted average of the values available at the known points. Basically, IDW explicitly makes the hypothesis that compositions that are "near" to one another are more MN alike than those that are farther apart. For a composition $\vec{x}$ interpolated in a data-set of N samples:

$$MN(\vec{x}) = \begin{cases} \frac{\sum_{i=0}^{N} MN_i/|\vec{x}-\vec{x_i}|^p}{\sum_{i=0}^{N} 1/|\vec{x}-\vec{x_i}|^p} & \text{if } |\vec{x}-\vec{x_i}| \neq 0 \\ MN_i & \text{if } |\vec{x}-\vec{x_i}| = 0 \end{cases} \tag{1.33}$$

p is a positive real number, called the power parameter. Greater values of p assign greater influence to values closest to the interpolated point (At p= 2, increasing the distance by a factor of 2 means reducing the weight by a factor of 4. At p= 3, increasing distance by a factor of 2 means reducing the weight by a factor of 8.).

To gauge this interpolation method, part of the data-set is dedicated for evaluation. It is referred to as the test set. The Root Mean Square Error (RMSE) for a test set of N samples is computed as:

$$RMSE = \sqrt{\frac{\sum_{i=0}^{N} |MN_{i_{online\ calculator}} - MN_{i_{IDW prediction}}|^2}{N}} \tag{1.34}$$

Figure 1.43 shows the impact of the power parameter on the RMSE. Raising the power parameter above 10, does not reduce the RMSE established around 1.

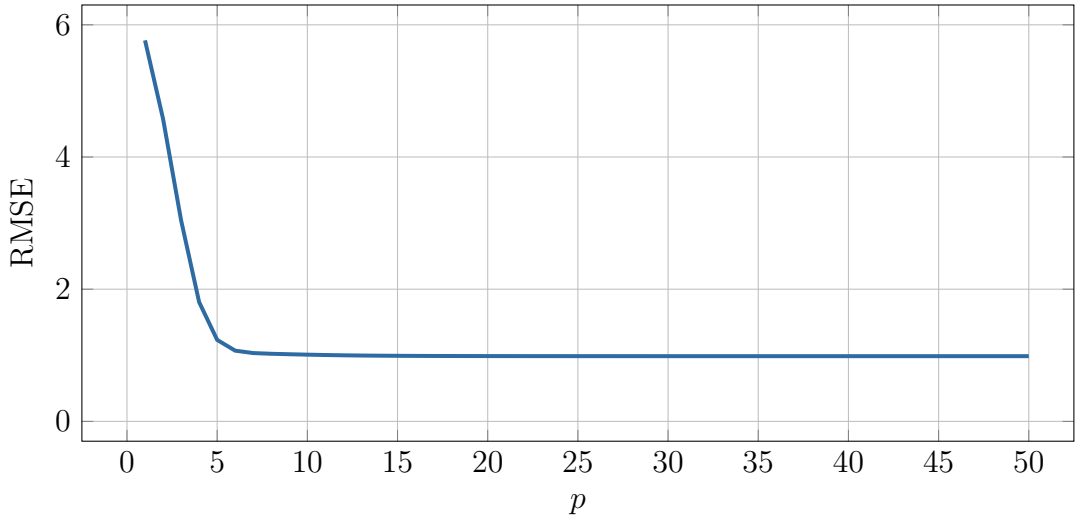

Figure 1.43: The RMSE of the IDW interpolation method for various power factors

Neural Network (NNET) method Since trained NNETs derive relationships from data samples, they are suitable for function approximation and can be used as a multivariate interpolation technique [95]. The network that is used for function fitting is a two-layer feed-forward network, with a sigmoid activation function in the hidden layer and a linear activation function in the output layer. The number of hidden neurons is set to 10 (see figure 1.44 and 1.45). The data set is divided into three subsets. The first subset is the training set (70% of the data-set), which is used for computing the gradient and updating the network weights (w) and biases (b). The second subset is the validation set (15% of the data-set). The error on the validation set is monitored during the training process. The validation error normally decreases during the initial phase of training, as does the training set error. However, if the network begins to over-fit the data, the error on the validation set typically begins to rise. The network weights and biases are saved at the minimum of the validation set error [96]. The test set (15% of the data-set) is not used during training, but it is used for evaluation. The generated function for deployment in the spreadsheet is compared to the IDW method using the same test data-set. Its RMSE is 0.018 (see figure 1.46).

To further compare the two methods, 57 random compositions (within the validity range) are generated. Their MNs are compared first using the online calculator, then using the interpolation methods (IDW and NNET method). The errors is defined as:

$$error = |\frac{MN_{online\ calculator} - MN_{interpolated}}{MN_{online\ calculator}}| \tag{1.35}$$

Figure 1.47 shows the error for each of the 57 composition. The error is lower for the NNET method.

To sump up, first a discrete set of data points, within a validity domain, have been computed from an online calculator, a black box model. Then, two interpolation methods (IDW and NNET) have been tested with 57 random inputs. The NNET method has a lower error and standard deviation compared to the IDW method and is retained.

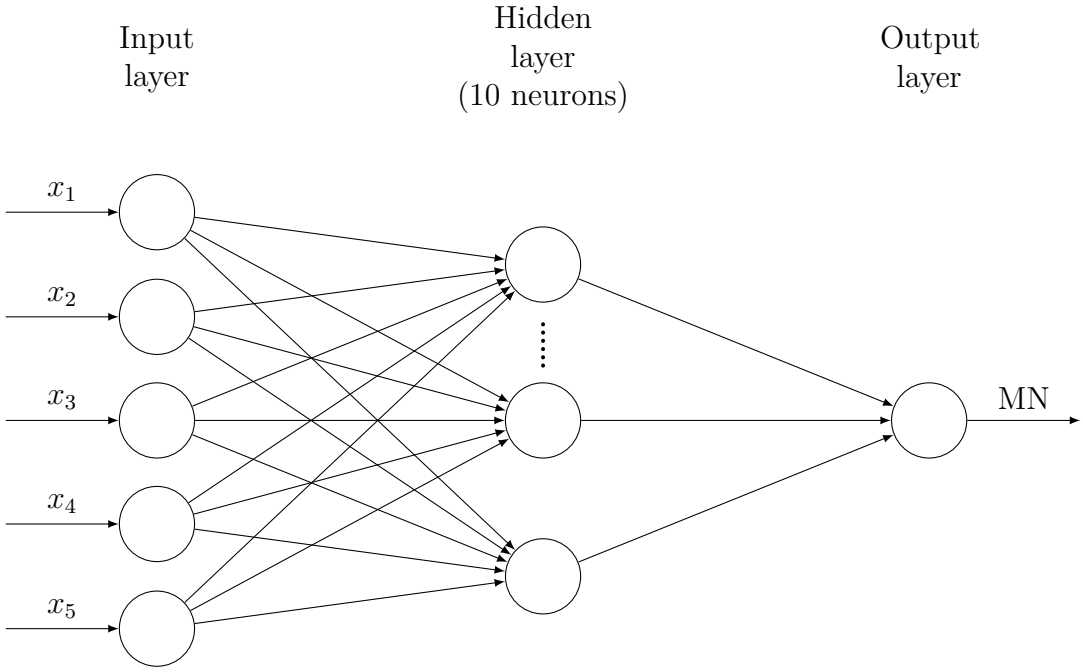

Figure 1.44: Architecture of the artificial neural network

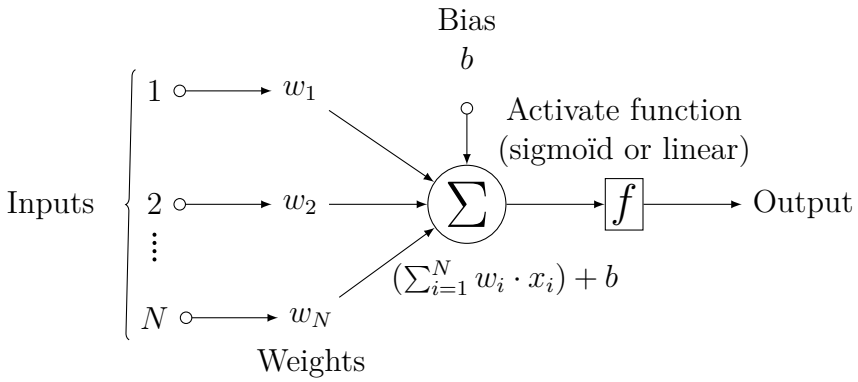

Figure 1.45: Architecture of one neuron in the hidden or output layer

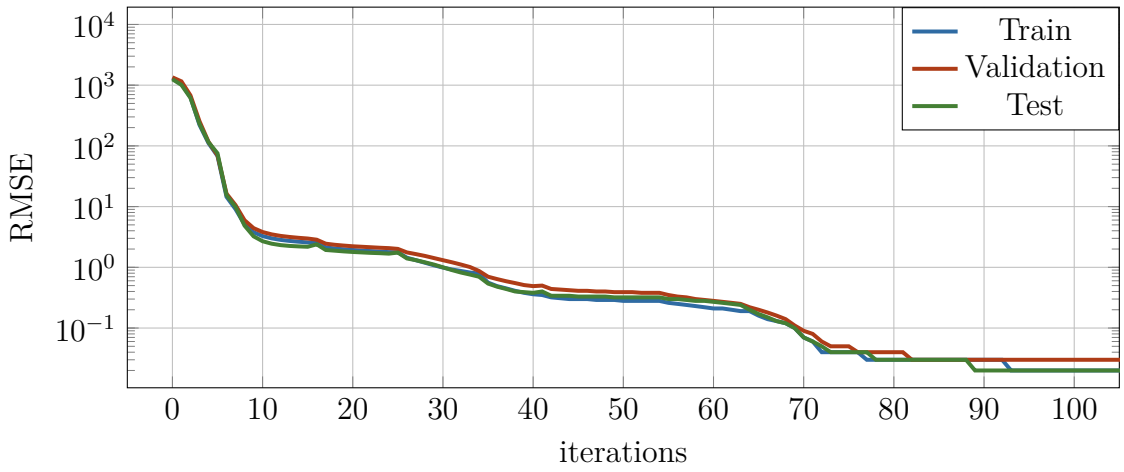

Figure 1.46: The RMSE of the validation, train and test data-set over NNET training.

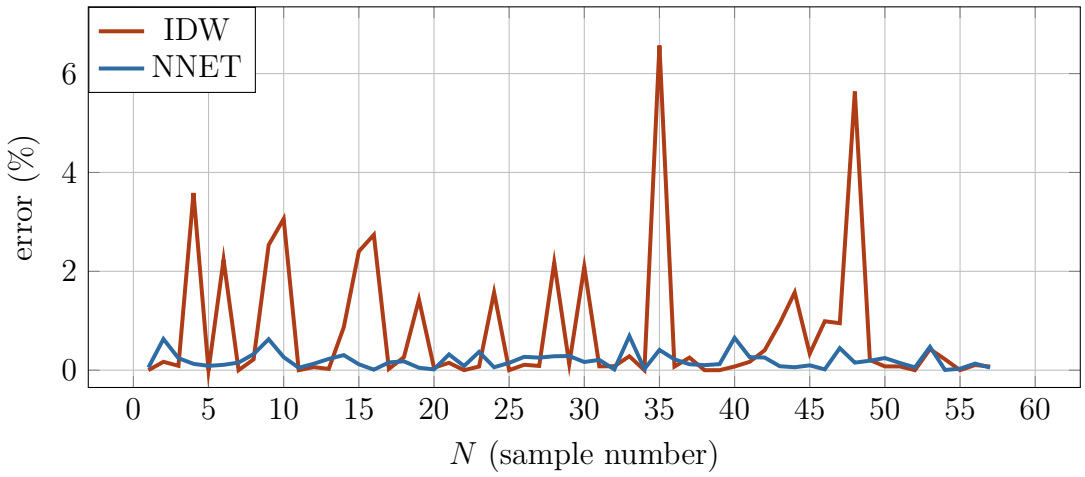

	IDW	**NNET**
mean error (%)	0.8	0.18
standard deviation	0.137	0.0022

Figure 1.47: Interpolation methods error over 57 random compositions

Part 2

Practical application part

Highlights

- Modular fuel systems allow LNG loading with no bunkering operations.
- Fuel cost savings are planned to be negligible.
- The models are used to monitor the tank pressure, its liquid level and the methane number at engine inlet. No "off-spec" events are detected and feasibility is confirmed.
- The method proposed in this part, can easily be adapted to a large range of profiles. The underlying models contain just enough relevant details to allow quick feasibility studies leading to significant development cost savings for shipowners.

Contents

In this part, first, the case study is presented. The operational profile is the starting point. The ambient temperature is modeled using a global measurements database. Then, the fuel system is detailed. It is a modular fuel system made of containerized LNG tanks. The driving equations are explicitly set. The control strategy is briefly presented.

After, based on fuel price quotes, fuel operational expenditures are compared for various bunkering scenarios. One scenario is retained for further investigations.

Conditions to fulfill are set before simulation. The results are presented through one figure and discussed. By trials and errors, settings fulfilling all conditions are found.

The company

Zéphyr&Borée is a French small company based in Nantes. They promote the comeback of traditional sailing freight. They believe a modern freight that combines cutting-edge technologies and wind energy is the best way to reach cost effective and sustainable transport solutions. In 2018, Zéphyr&Borée investigated the use of LNG combined with wind energy for propulsion. The concept is further developed below.

The ship

The ship design is meant for a niche market: it offers transportation of rolling and out of gauge freight in ports apart from the competition with the main lines which benefit from a large scale effect. In 2021, the ship will sail between few ports in Europe and French Guiana. A ship illustration and her main dimensions are provided below (see figure 2.1).

Length	125	m
Breadth	23	m
Draft	5	m
Loaded displacement	11,500	t
Service speed	12	kt

Figure 2.1: Ship concept design illustration and main dimensions, courtesy of Zéphyr&Borée

The operational profile

Due to confidentiality issues, some data have been slightly modified and some results are voluntarily not presented. For more details the reader is kindly invited to contact the author.

A common way to define an operational profile is to define the power consumption over various navigation modes. Three navigation modes are defined:

- **maneuvering mode:** This mode will usually "speed up" the response of the engines, so that power becomes more "instant". It is used to maneuver and during channeling. The average consumption is 12 t of MDO per day.
- **open sea mode:** It is the mode at which all the different factors combined makes it the most economic. The average consumption is 24 t of MDO per day.
- **stand-by mode:** It is the mode at berth or at anchorage. The energy consumption is only linked to the hotel load or to the commercial operations. The average consumption is 3 t of MDO per day.

Ports are defined by their UN/LOCODE. The rotation is:

- Rotterdam (NLWAL);
- Le Havre (FRLEH);
- Bordeaux (FRBOD);
- Dégrad-des-Cannes (GFDDC);
- Bremen (DEBRE).

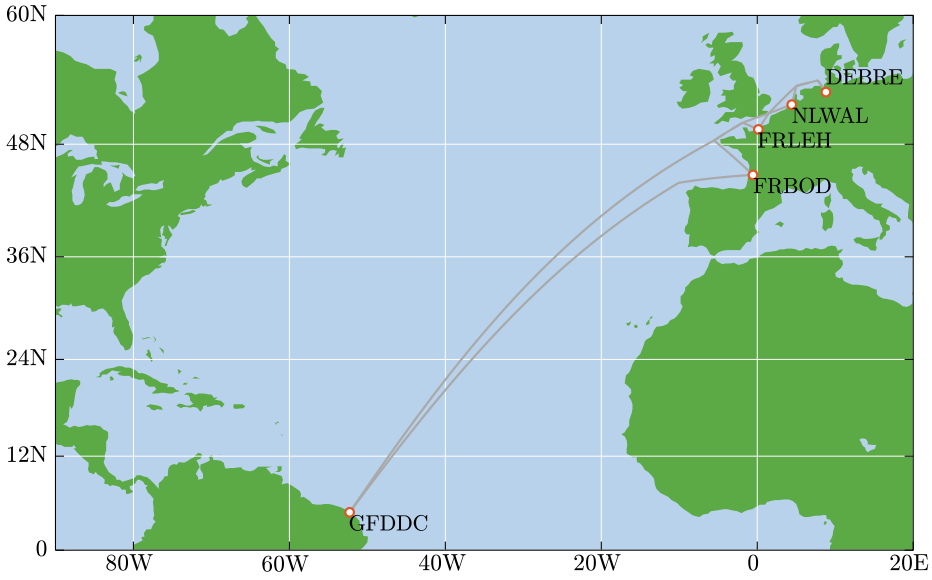

Figure 2.2: Map of the rotation

The duration of each leg is given below:

Port of departure	Port of call	Duration (hours)				Total
		Channeling out	Voyage at sea	Channeling in	At berth	
NLWAL	FRLEH	3	14	3	6	26
FRLEH	FRBOD	16	30	6	20	72
FRBOD	GFDDC	65	220	1.5	72	358.5
GFDDC	DEBRE	7	254	7	6	274
DEBRE	NLWAL	7	14	3	6	30

Table 2.1: Duration of each leg of the rotation

The MDO consumption on each leg is given below:

Port of departure	Port of call	MDO consumption (t)				Total
		Channeling out	Voyage at sea	Channeling in	At berth	
NLWAL	FRLEH	1.5	13.9	1.5	0.75	17.7
FRLEH	FRBOD	1.5	30	3	2.5	37
FRBOD	GFDDC	3	220.1	1.5	9	232.8
GFDDC	DEBRE	0.8	253.9	3.5	0.75	259
DEBRE	NLWAL	3.5	13.9	1.5	0.75	19.7

Table 2.2: MDO consumption on each leg of the rotation

According to [97], the MDO LHV is 42.7 MJ/kg so the energy need on each leg of the rotation is computed. The results are given below:

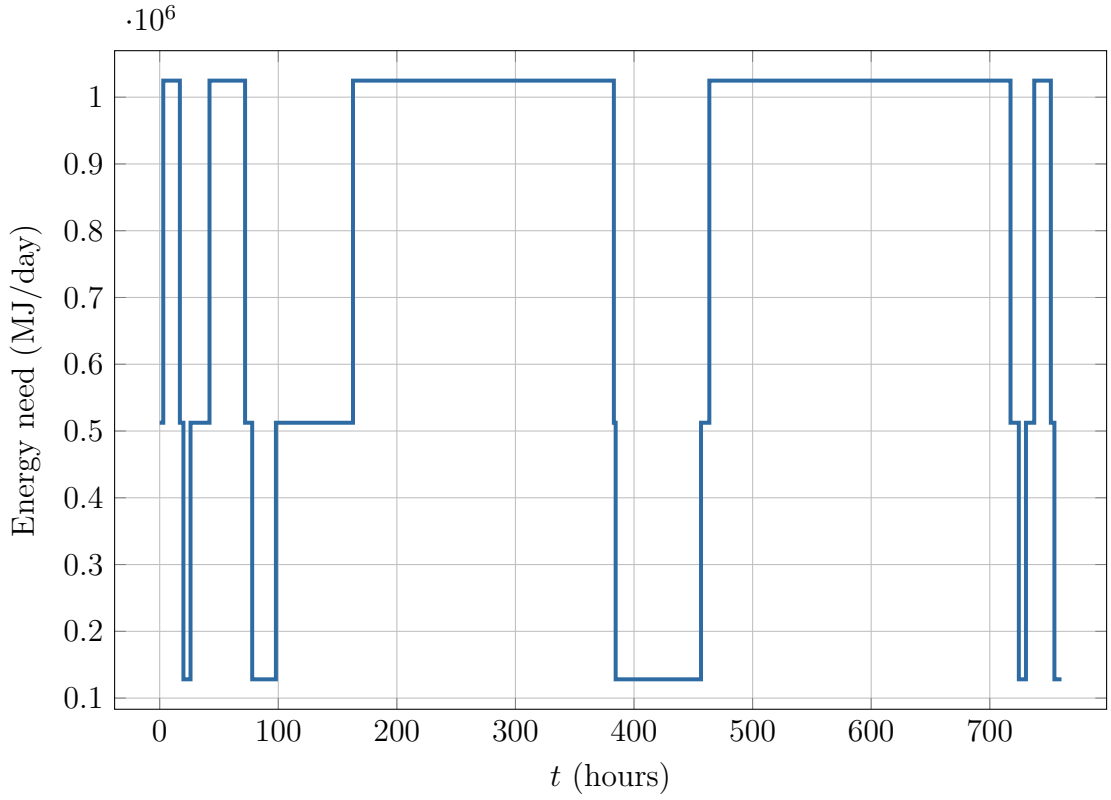

Figure 2.3: Ship's energy profile

Environmental conditions

It has been shown, in the previous part, that the ambient temperature impacts significantly the BOR and should be carefully considered. In the case study, the ambient temperature is not constant. For each navigation mode (maneuvering mode, open sea mode, stand-by mode) an ambient temperature is set. Average annual temperature profiles near each port of call are available online[1]. During maneuvering and stand-by modes, using a worst-case-design approach, the highest average annual temperature is retained (see figure 2.4). In open sea mode, an ambient temperature of 293.15 K is retained which is an offshore realistic temperature.

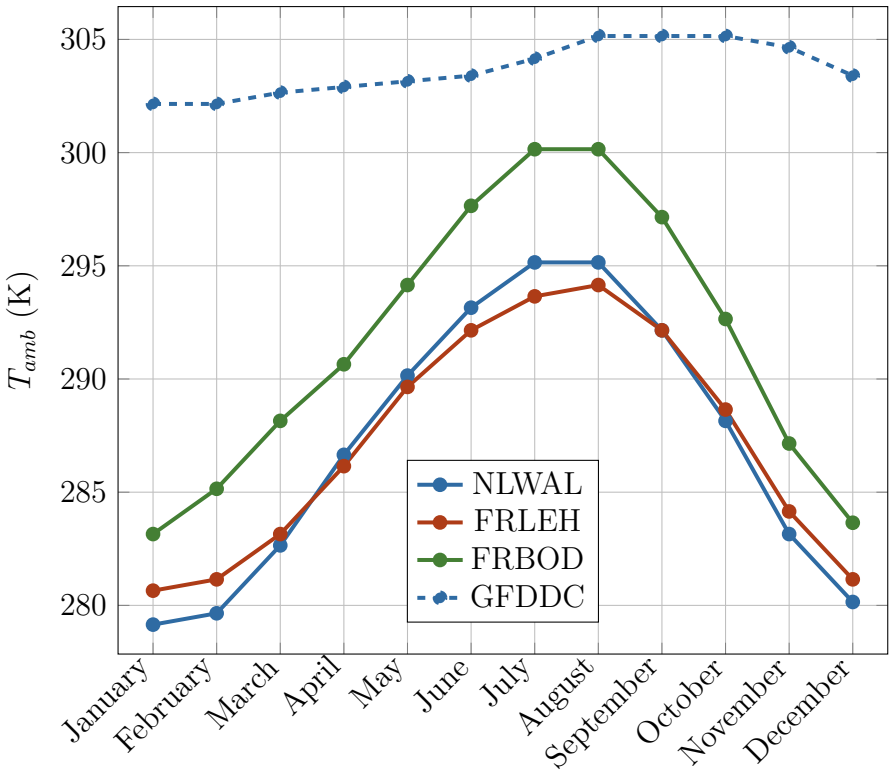

Figure 2.4: Average annual temperature evolution in each port of call

[1]https://www.noaa.gov/

The fuel system

Since LNG bunkering facilities are not available yet in French Guiana, a fuel gas handling system utilizing multiple removable LNG fuel tank containers is being investigated. The containers can be transported by road to the nearest LNG terminal for refilling. Therefore, the loading on-board requires no bunkering procedure. This "plug-and-play" skid-based approach makes the system installation fast and cost competitive. This is not a novel concept (see figure 2.6 and 2.7). The ship is fitted with dual fuel 4 strokes low pressure admission engines. The fuel system is made of the following main elements:

- **The tank**. The one investigated in this study is designed to withstand pressure. It is defined by the IGF code, entered into force in 2017, as a type C tank [98]. This type of tank allows a MAWP of 1.1 MPa with a service pressure around 0.7 MPa. Maintaining the service pressure above 0.6 MPa allows conventional low-pressure gas feed with no further apparatus. Framed in a 40 ft. container, the tank main characteristics are given in table 1.25.

- **The Pressure Build-up Unit (PBU)**. It is a heat exchanger using water glycol to vaporize LNG. In the pressure build-up process, cold LNG is drained from the tank bottom to the PBU where it is vaporized and sent back to the top tank to maintain the service pressure roughly above 0.6 MPa. The PBU is activated when liquid or gas is withdrawn from the tank and pressure is decreasing. When there is no liquid or gas removal, the PBU unit is stopped.

- **The vaporizer (VAP)**. It is also a water glycol heat exchanger. Its function is to vaporize the fuel before the engine inlet.

- **The three-way-valve**. The piping allows mixing the vapor and liquid phase outflow (respectively $\dot{m}_{V_{out}}$ and $\dot{m}_{L_{out}}$) before the vaporizer using a three-way-valve.

More details on this fuel system solution and others are given in [99]. Figure 2.5 is a diagram of the fuel system.

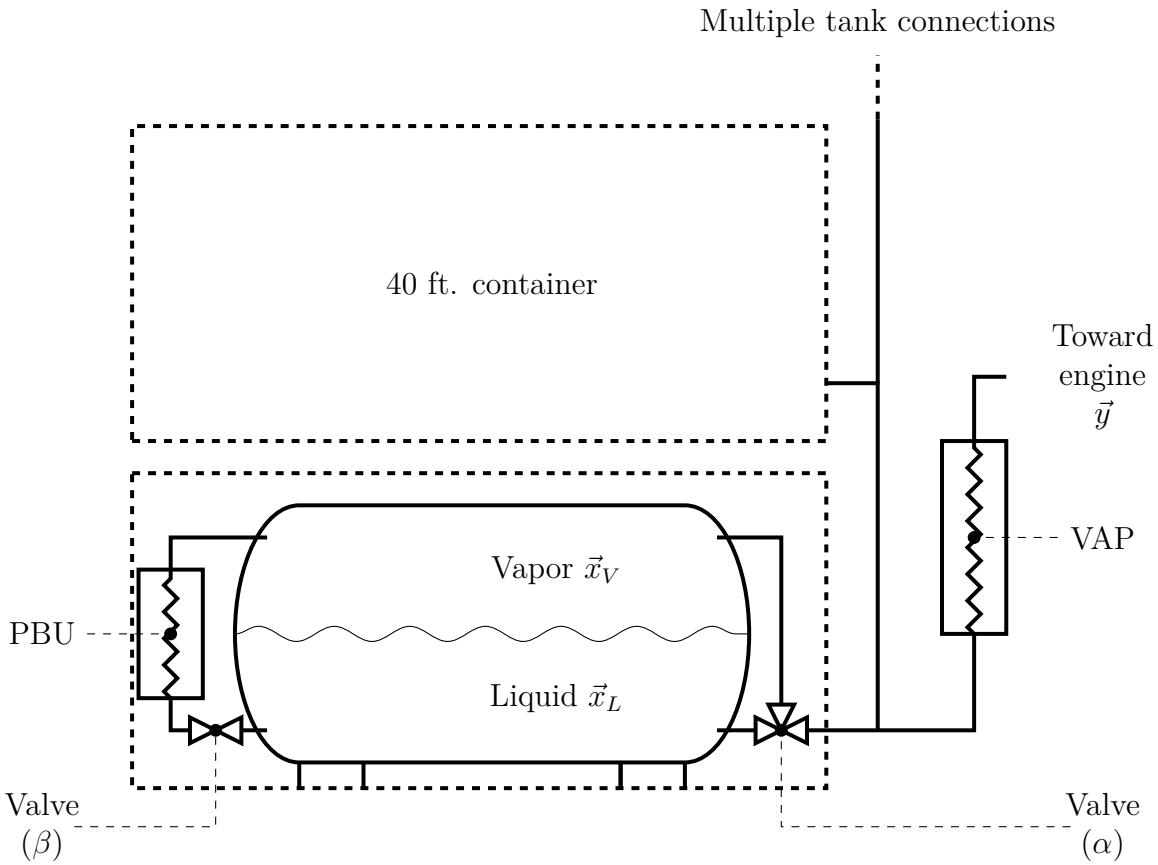

Figure 2.5: Diagram of the fuel system

Figure 2.6: Containerized LNG tank illustration, courtesy of LNG Trainer

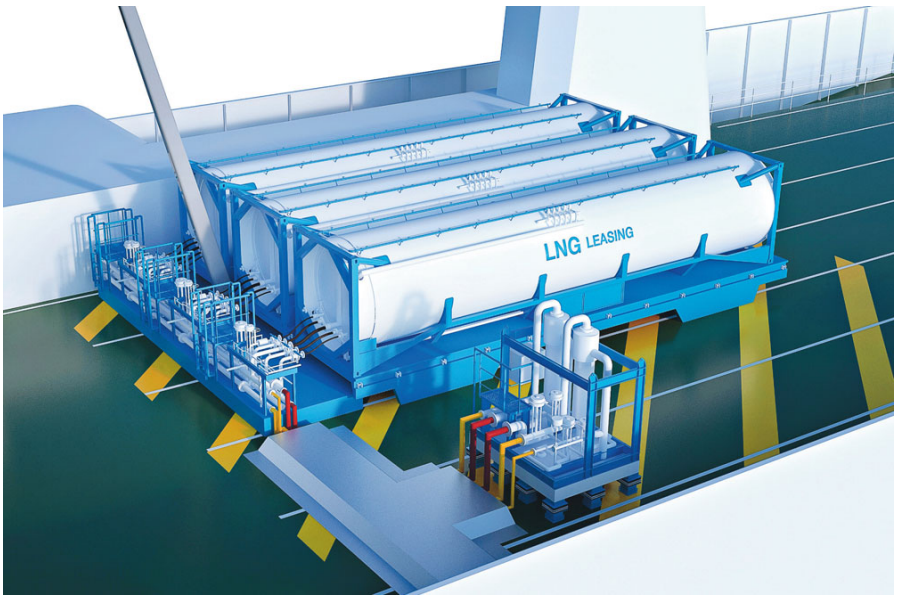

Figure 2.7: Containerized LNG tank illustration, courtesy of Wärtsilä

Equations

The mass flow rate toward engine inlet ($\dot{m}$) is the sum of the tank liquid and vapor output mass flow rates ($\dot{m}_{L_{out}}$ and $\dot{m}_{V_{out}}$ respectively):

$$\dot{m} = \dot{m}_{L_{out}} + \dot{m}_{V_{out}} \tag{2.1}$$

To model the three-way-valve, a mixing variable (α) is introduced such that:

$$\dot{m}_{L_{out}} = \alpha \cdot \dot{m} \qquad \alpha \in [0, 1] \tag{2.2}$$

Assuming each tank is operated the same way, the mass flow rate toward engine inlet is imposed by the energy profile such that:

$$\dot{m} = \frac{\dot{E}}{\alpha \cdot LHV_L + (1 - \alpha) \cdot LHV_V} \tag{2.3}$$

where $\dot{E}$ is the energy need divided by the number of containers. The PBU vaporizes LNG but the matter remains in the system. The action of the PBU can be modeled as an extra heat ingress ($\delta\dot{Q}_{PBU}$). The vaporizing rate is controlled by a valve. This valve is modeled by a variable (β) such that:

$$\beta = \frac{\delta\dot{Q}_{PBU}}{\delta\dot{Q}} \tag{2.4}$$

It is to note β is unrestricted in the model but, just to give an idea, an average PBU vaporizing rate of 0.16 kg/s in a similar tank was reported in [100]. The energy balance is:

$$\dot{U} = \delta\dot{Q}_{PBU} + \delta\dot{Q} - \dot{m}_L \cdot h_L - \dot{m}_V \cdot h_V \tag{2.5}$$

And at each time step the compositions in the tank ($\vec{x}$) and toward engine ($\vec{y}$) are updated. For brevity's sake, in equation 2.6 the compositions are expressed as mass fractions.

$$\begin{aligned} \vec{x} &= \frac{\vec{x}_L((1 - \chi) \cdot m - \alpha \cdot \dot{m} \cdot \Delta t) + \vec{x}_V(\chi \cdot m - (1 - \alpha) \cdot \dot{m} \cdot \Delta t)}{m - \dot{m} \cdot \Delta t} \\ \vec{y} &= \frac{\vec{x}_L \cdot \alpha \cdot \dot{m} \cdot \Delta t + \vec{x}_V \cdot (1 - \alpha) \cdot \dot{m} \cdot \Delta t}{\dot{m} \cdot \Delta t} \end{aligned} \tag{2.6}$$

The liquid level notation (lvl) is introduced such that:

$$lvl = \frac{m \cdot (1 - \chi)}{V \cdot \rho_L} \tag{2.7}$$

Once the energy, mass and composition balance performed, the fluid thermodynamic properties are updated as follow:

$$[P, T, \chi, \vec{x}_L, \vec{x}_V, LHV_L, LHV_V, h_L, h_V, \rho_L] = f(U, m, \vec{x}) \tag{2.8}$$

Control strategy

The ship can use two fuels: LNG or MDO. When the ship uses MDO, the LNG tanks experience self-pressurization by natural heat leaks as described in the previous part. When the ship uses LNG, a small portion (1% on an energy basis in the model) of MDO is used for ignition of the natural gas mixture (Otto cycle) and the chain of actions is the following:

1. To feed the engines, mass must be removed from the tank and sent to the VAP.
2. Withdrawing mass from the tank reduces its service pressure.
3. The BOG formation by natural heat leaks increases the service pressure but not enough to compensate for the pressure drop induced by the mass removal.
4. Preserving the service pressure above 0.6 MPa is crucial to insure a sufficient flow rate at engine inlet. To maintain the service pressure, the operator faces two options:
    - Increase the PBU flow rate. In our model, this is done by increasing variable β.
    - Increase the liquid fraction of the output flow rate. Indeed, the pressure drop will be reduced if more liquid is withdrawn compared to vapor. This is done by increasing variable α.

At each time step, three variables are set to fulfill objectives. The three variables are:

- whether the ship is running on LNG or MDO;

And if it runs on LNG:

- the value of α;
- the value of β.

The objectives to fulfill are:

1. the tank pressure remains between 0.6 and 0.9 MPa;
2. the MN at engine inlet (linked to the composition $\vec{y}$) remains above 80.

The tuning of the three variable is done by trial and error. Also, a trivial objective is that the number of containers should be sufficient so that the liquid level (lvl) remains above 10% (safety margin).

Bunkering scenarios

Bunkering is possible in NLWAL and GFDDC. For flexibility issues, the ship will keep a MDO capacity of 600 m^3. The company is willing to install a maximum of 9 containers on deck. This is the result of a former study and a trade off with cargo payload space. Quotes have been realized for LNG prices in NLWAL and GFDDC. LNG price in GFDDC includes transportation of the containers to and from a filling station in Dominican Republic. Since LNG is not a liquid market, the quotes are only estimations and should be further investigated.

LNG prices are often expressed as a price in dollar per "$t_{MDO\,eq}$": it is the price of the mass of LNG containing the same amount of energy as 1 t of MDO (42,700 MJ). Prices for MDO in NLWAL are available online[2]. MDO is not available in GFDDC but very near in Paramaribo. It is expected to be marginally more expensive than in NLWAL. Four scenarios have been considered:

- **scenario A:** The ship will do her rotation using only MDO. This case is used as a price reference.
- **scenario B:** The ship loads MDO at FRLEH (270 t) and LNG at NLWAL (9 containers). The 9 containers are unloaded in GFDDC and replaced by 7 new fully loaded containers for the return trip (from GFDDC to NLWAL).
- **scenario C:** The ship loads MDO at FRLEH (145.5 t) and GFDDC (155.3 t). 9 LNG containers are loaded in NLWAL. The 9 containers are unloaded in GFDDC and replaced by 7 new fully loaded containers for the return trip (from GFDDC to NLWAL).
- **scenario D:** The ship loads MDO at FRLEH (133.5 t) and GFDDC (281.8 t). 9 LNG containers are loaded in NLWAL. The 9 containers are unloaded in GFDDC and not replaced. The return trip toward NLWAL is performed on MDO only. The empty containers are returned to NLWAL on a regular line.

[2]https://shipandbunker.com/

LNG in NLWAL is assumed[3] to have a Qatar-like composition (see table 6). LNG in GFDDC is assumed to have a Trinidad and Tobago-like composition. For each composition, the mass of fuel in one full tank is computed according to [98] (Article 6.8.1). Indeed, storage tanks shall not be filled to more than a volume equivalent to 98% full at the reference temperature. The reference temperature means the temperature corresponding to the vapor pressure of the fuel in a fuel tank at the set pressure of the PRV. Moreover, holding time from service pressure to the PRV pressure with hotel load consumption only should be at least 15 days (article 6.9.1.1) and computations shall be done considering an ambient air temperature (T_{amb}) of 318.15 K (article 6.9.2.1). For more details regarding the computation of the maximum loading level for compliance, the reader is kindly referred to [101]. The prices assumptions are:

- 580$/t for MDO in FRLEH;
- 590$/t for MDO near GFDDC;
- 486$/$t_{\text{MDO eq}}$ for LNG in NLWAL (16.8 t in one full tank);
- 654$/$t_{\text{MDO eq}}$ for LNG in GFDDC (16.3 t in one full tank).

Finally, the fuel rotation price is computed for each scenario:

Scenario	Rotation price (k€)	Variation
A	331.3	ref.
B	349.9	+6%
C	351.4	+6%
D	329.3	-0.6%

Table 2.3: Rotation price for each scenario

The last scenario (D) is retained. It is to note, it does not account for the price of the return trip of the empty containers on a regular line. The next section presents the results.

[3]Qatar is the biggest LNG supplier of Europe

Results

Once all the parameters and initial values are set, the spreadsheet provides in few minutes (Δt =1 hour[4]) the figure below.

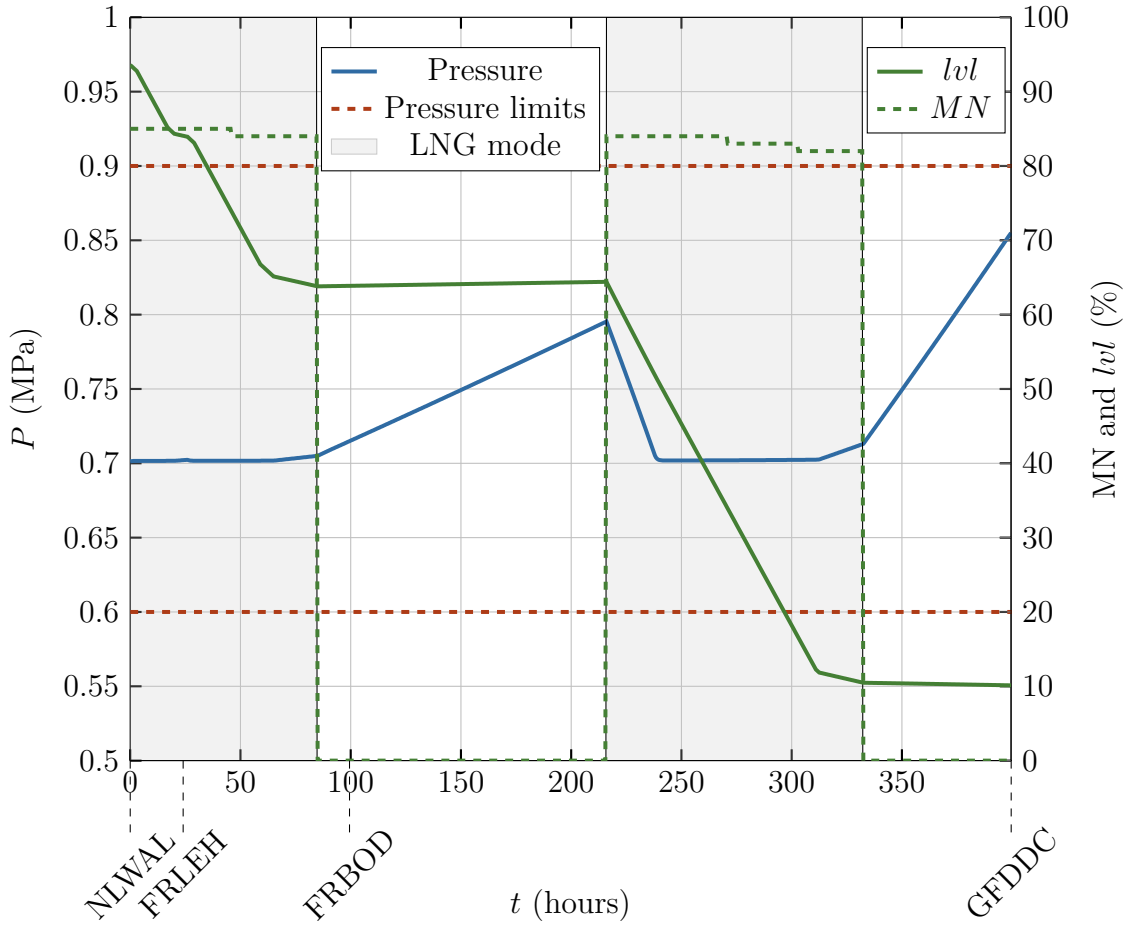

Objectives	
$P \in [0.6, 0.9]$	✓
MN $\geq$ 80	✓
$lvl \geq 10\%$	✓

Figure 2.8: Results - pressure, liquid level and MN evolution

[4]time convergence checked

Figure 2.8 shows:

- **the pressure evolution between NLWAL and GFDDC.** When the LNG mode is "on", mass is withdrawn and the pressure is kept around 0.7 MPa (acting on α or β). When the LNG mode is stopped, the pressure increases by self-pressurization. The pressure remains between the set thresholds (0.6 and 0.9 MPa).
- **the liquid level evolution between NLWAL and GFDDC.** When the LNG mode is "on", the liquid level (lvl) drops since liquid is withdrawn from the tank and sent toward the engines. The liquid level decrease is not linear since it is linked to the energy need: when the need is low (for instance at berth), the liquid level slowly diminishes and when the need is high (at open sea) the liquid level drops faster. When the LNG mode is stopped, the liquid level slightly increases by heat expansion. In the end, at GFDDC the liquid level is at 10%; the containers are almost empty and they can be unloaded.
- **the MN evolution between NLWAL and GFDDC.**When the LNG mode is "on", the MN at inlet drops because heavy hydrocarbons evaporate after methane (at higher temperatures). However the value remains above 80 so the objective is fulfilled. A solution if the MN drops below 80 is to increase the vapor ratio of the outlet flow (reduce α) while boosting the PBU vaporizing rate (increase β). Naturally, this mitigation technique is limited: if the MN in the vapor phase is below 80 or if the maximum PBU vaporizing rate is reached, derating is unavoidable. More details about this mitigation technique are provided in [102].

The LNG mode is split in two to make sure the maximum pressure is never reached. If all the LNG is consumed from start, the minimum liquid level is reached before arrival. Then the ship trips to MDO but self-pressurization occurs rapidly in the almost empty tanks and the maximum pressure is reached. To avoid over-pressure, vapor at low MN (below 80) will have to be withdrawn and sent toward engines. This is an unwanted event.

Conclusions

This thesis presents the research and development work done over the past three years. The main contributions of this thesis can be summarized in the following points:

- The introduction highlights the fact that LNG as a fuel is perceived as a solution to curb harmful emissions in shipping and that its quick uptake is now significant. The lack of tools and methods for the concept design of LNG fuel systems often places a break, however, on this trend. This is especially true in medium size design offices working on ships up to around 100 m length.
- In the first part, models are presented to assess self-pressurization by natural heat leaks in cryogenic tanks. Three models are developed:
  - The first model assumes the tank has no thermal mass and a constant apparent thermal conductivity. The fluid evolves through vapor-liquid equilibrium states and the ambient temperature is constant;
  - The second model assumes the tank has no thermal mass but a variable apparent thermal conductivity. The fluid evolves through vapor-liquid equilibrium states and the ambient temperature evolves through time;
  - The third model assumes the tank has a thermal mass and a constant apparent thermal conductivity. The fluid evolves through vapor-liquid equilibrium states and the ambient temperature is constant.

  The models are compared to experimental data. The second and third models are more accurate than the first one but more complex. Also, they require tuning coefficients. The first model is judged satisfactory for concept design and retained. Then, a LNG ageing model is presented and compared to experimental data. The composition evolution in the liquid and the vapor phase is well predicted. From those predictions, two key values are computed: the net heating value and the methane number. The variations amplitude is of:

  - 5.5% for the net heating value in the liquid phase;
  - 6.4% for the net heating value in the vapor phase;
  - 4.3% for the methane number in the liquid phase;
  - 9.6% for the methane number in the vapor phase.

  In the last section, a methane number meta-model is proposed. This is done to compute easily (in a spreadsheet) and dynamically the methane number at engine inlet. The meta-model is built from an online tool using mapping and multivariate interpolation methods. Two multivariate interpolation techniques have been compared:

  - an inverse distance weighting method;
  - a neural network method.

  The neural network interpolation method shows better results and is retained.

- In the second part, the models are put together for a case study. The case study is provided by a freight company. The input is the ship's operational profile. First, various bunkering scenarios are compared regarding fuel costs. One scenario is retained for further investigations. The goal is to ascertain the following conditions:

  - the tank pressure will never reach the maximum allowable working pressure;
  - the methane number at engine inlet will remain above 80.

  The results are presented showing all conditions are fulfilled.

In the end, the methods and tools provide an accurate, fast and easy-to-iterate approach to produce highly informative content, such as the required tank capacity on-board, the fuel grade evolution, the tank pressure development and the fuel OPEX. Finally, the thesis calls for new developments:

- To model de-rating, low MNs should produce feedback loops impacting the ship's power output/speed. Indeed according to figure 9, a MN below 80, should impact the operational profile. More precisely, it should either impact:

  - The energy need at a given speed (see figure 2.3);
  - The speed and hence the rotation duration.

Moreover, other fuel grade indicators such as the Wobbe index could be considered.

- The method could be further developed to assess LNG cold energy recovery (at the PBU and the VAP). For example, on fishing vessels, the LNG cold energy could be used for freezing. It can be a source of cooling power for reefers. Also, the cold energy could be used for air-cooling before engine intake. At first glance, this is convenient since the LNG vaporizing rate evolves like the air flow rate at engine intake. Moreover, the cold energy from LNG regasification can be used in the air separation process, the freeze desalination process, or to improve the capacity of adsorbed natural gas tanks. LNG can also be used as a heat sink in a power cycle using ambient or waste heat as the heat source. The most popular cold power cycles are: the direct expansion cycle, the Rankine cycle, the Brayton cycle, the absorption power cycle, the Stirling cycle and combined cycles. In most existing cryogenic plants, the recovery method for LNG exergy is based on direct expansion and organic Rankine cycles.

- A lack of consensus on the vapor-liquid equilibrium assumption domain of validity has been identified. Therefor it should be investigated experimentally with a strong focus on the following parameters:

  - the tank geometry;
  - the free surface area;
  - the liquid level;
  - the tank motions;
  - the heat flow.

Scientific productions

International journal submissions

- Jonas Thiaucourt, Jean-François Hetet, Pierre Marty, Pascal Robert, Etienne Delaire,"A zonal non-equilibrium approach to model temperature gradients during ventless bottom filling of pressurized cryotanks for natural gas-powered ships", *Energy*, 2019

- Jonas Thiaucourt, Pierre Marty, Jean-François Hetet,"Impact of natural gas quality on engine performances over a journey using a thermodynamic fuel system model", submitted to *Energy Special Issue* and being reviewed

Conference proceedings

- Jonas Thiaucourt, Pierre Marty, Jean-François Hetet,"Impact of natural gas quality on engine performances over a journey using a thermodynamic fuel system model", proceedings of MOSES2019 conference, 2^{nd} International Conference on Modeling and Optimization of Ship Energy Systems, 2019, Glasgow

- Jonas Thiaucourt, Jean-François Hetet, Etienne Delaire, Pascal Robert,"LNG Ageing Prediction Model", proceedings of ISOPE, International Ocean and Polar Engineering Conference, 2018, Sapporo

Congress proceedings

- Jonas Thiaucourt, Jean-François Hetet,"Impact of Liquefied Natural Gas Quality and Weathering on Engine Performances over a Journey Using a Thermodynamic Fuel System Model", proceeding of CIMAC2019 congress, International Council on Combustion Engines, 2019, Vancouver

- Jonas Thiaucourt, Kilian Le Bail, Jean-François Hetet,"Impact of charged liquefied natural gas on its dynamic behaviour in a pressurized tank", proceeding of COFRET'18 congress, COlloque FRancophone en Energie, Environnement, Economie et Thermodynamique, 2018, Strasbourg

- Jonas Thiaucourt, Jean-François Hetet, Victor Depoers, "A thermodynamic approach to assess the minimum energy consumption required at berth to avoid overpressure on an innovative liquefied natural gas/wind electric hybrid powered ship.", proceeding of SFT congress, Société Française de Thermique, 2019, Nantes

Glossary

ALOSS	Advanced LNG Onboard Storage System
BOG	Boil-Off Gas
BOR	Boil-Off gas Rate
C_2H_4	ethylene
C_2H_6	ethane
C_3H_8	propane
C_4H_{10}	butane
CAA	Clean Air Act
CAPEX	Capital Expenditure
CH_4	methane
CIMAC	International Council on Combustion Engines
CO	carbon monoxide
CO_2	carbon dioxide
CO_2 *eq.*	equivalent carbon dioxide
DEBRE	Bremen
DLL	Dynamic Linked Library
DNV-GL	Det Norske Veritas and Germanischer Lloyd
DOE	Department Of Energy
EEDI	Energy Efficiency Design Index
EGR	Exhaust Gas Re-circulation
EOS	Equations Of State
EPA	Environmental Protection Agency
ESI	Environmental Ship Index
FEM	Finite Element Method
FRBOD	Bordeaux
FRLEH	Le Havre

GCU	Gas Combustion Unit
GERG	European Gas Research Group
GFDDC	Dégrad-des-Cannes
GHG	Greenhouse Gas
GIIGNL	International Group of Liquefied Natural Gas Importers
GRG	Generalized Reduced Gradient
GRI	Gas Research Institute
GTI	Gas Technology Institute
GUI	Graphical User Interface
HFO	Heavy Fuel Oil
HHV	High Heating Value
IDW	Inverse Distance Weighting
IGF	International code of safety for ships using Gases or other low-flashpoint Fuels
IMO	International Maritime Organization
IPCC	Intergovernmental Panel on Climate Change
LAR	Liquefied Argon
LHV	Low Heating Value
LIN	Liquefied Nitrogen
LNG	Liquefied Natural Gas
LOX	Liquefied Oxygen
MARPOL	International Convention for the Prevention of Pollution from Ships
MAWP	Maximum Allowable Working Pressure
MDO	Marine Diesel Oil
MN	Methane Number
MON	Motor Octane Number
N_2	nitrogen
NECA	NO_x Emission Control Area
NIST	National Institute Standards and Technology
NLWAL	Rotterdam
NNET	Neural Network
NO_2	Nitrogen dioxide

NO_x	Nitrogen Oxides
OPEX	Operational Expenditure
PBU	Pressure Build-up Unit
PM	Particulate Matter
PRV	Pressure Relief Valve
R&D	Research and Development
REFPROP	REFerence fluid PROPerties
RMSE	Root Mean Square Error
SECA	Sulfur Emission Control Area
SO_x	Sulfur Oxides
TNO	Netherlands Organization for Applied Scientific Research
TRL	Technology Readiness Level
ULSFO	Ultra Low Sulfur Fuel Oil
UN	United Nations
UNEP	United Nations Environment Program
UNFCCC	United Nations Framework Convention on Climate Change
VAP	vaporizer
VOC	Volatile Organic Compounds
WHO	World Health Organization
WMO	World Meteorological Organization
WPSP	World Ports Sustainability Program

Nomenclature

In some cases, it is unavoidable or simply practical to give symbols multiple definitions. From the context or subscripts it will be clear which definition applies.

Roman letters

b	bias	
C	minimum number of fixed-composition mixtures that could be used to prepare each phase individually	
C	capacitance	
c_p	specific heat	$\mathrm{J{\cdot}kg^{-1}{\cdot}K^{-1}}$
$\dot{E}$	energy need	MW
e	tank insulation thickness	m
f	function	
F	degree of freedom	
H	enthalpy	J
h	specific internal enthalpy	$\mathrm{J{\cdot}kg^{-1}}$
K	tank heat flux coefficient	$\mathrm{W{\cdot}K^{-1}}$
k	tank heat flux coefficient	$\mathrm{W{\cdot}m^{-2}{\cdot}K^{-1}}$
L	length	m
m	mass	kg
$\dot{m}$	mass flow rate	$\mathrm{kg{\cdot}s^{-1}}$
n	engine rated speed	rpm
N	number of combinations or samples	
P	pressure	MPa, bar
Ph	number of phases	
q	heat flux	$\mathrm{W{\cdot}m^{-2}}$
R	radius	m
R	electrical resistance	

S	tank internal surface	m^2
T	temperature	K
t	time	s (or hour or day)
U	internal energy	J
u	specific internal energy	$J \cdot kg^{-1}$
V	volume	m^3
w	weights	

Greek letters

α	three way valve mixing variable	$\in [0, 1]$
β	the pressure built-up unit flow rate variable	-
κ	coefficient of heat conduction	$W \cdot m^{-1} \cdot K^{-1}$
χ	vapor mass fraction	kg/kg

Vectors

$\vec{x}$	composition in the tank	$mol \cdot mol^{-1}$
$\vec{y}$	composition at engine inlet	$mol \cdot mol^{-1}$
$\vec{M}$	molar mass of each component	$kg \cdot mol^{-1}$
$\vec{q}$	heat flux	$W \cdot m^{-2}$

Subscripts

$_L$	property of the liquid phase
$_V$	property of the vapor phase
$_{PBU}$	property of the Pressure Build-up Unit (PBU)
$_{in}$	quantity entering the system
$_{out}$	quantity leaving the system
$_{init}$	initial value
$_{amb}$	ambient
$_{vac}$	vacuum
$_t$	tank

Superscripts

The superscript notation is for time indices (for instance X^t is the value of X at time t).

Other symbols

$\tilde{L}$	specific heat of vaporization	$\mathrm{J{\cdot}kg^{-1}}$
lvl	liquid level in the tank	$\in [0, 1]$
δQ	heat	J
$\delta \dot{Q}$	heat flow rate	W
Δt	time step	s (or hour or day)
δW	work	J
$\circ$	Hadamard product	

Bibliography

[1] E. W. Lemmon, I. H. Bell, M. L. Huber, and M. O. McLinden, "NIST Standard Reference Database 23: Reference Fluid Thermodynamic and Transport Properties-REFPROP, Version 10.0, National Institute of Standards and Technology," 2018.

[2] DNV-GL, "LNGi Comprehensive insights on worldwide LNG bunkering availability and market data on LNG as fuel for ships," 2018.

[3] D. N. Mavris and D. A. DeLaurentis, "Methodology for Examining the Simultaneous Impact of Requirements, Vehicle Characteristics, and Technologies on Military Aircraft Design," in *22nd Congress of the International Council on the Aeronautical Sciences*, Georgia Institute of Technology, 2000.

[4] C. Hulsbosch-Dam, B. Atli-Veltin, J. Kamperveen, H. Velthuis, J. Reinders, M. Spruijt, and L. Vredeveldt, "Thermodynamic aspects of an LNG tank in fire and experimental validation," in *EPJ Web of Conferences* (P. Dančová, ed.), vol. 143, p. 02039, EDP Sciences, may 2017.

[5] M. Kraack, "LNG Infrastructure and Shipbuilding," 2015.

[6] J. P. Kamperveen, M. P. N. Spruijt, and J. E. A. Reinders, "Heat load resistance of cryogenic storage tanks – Results of LNG Safety Program," tech. rep., 2016.

[7] Cummins Westport Inc, "Advanced LNG onboard storage system (ALOSS)," tech. rep., 2013.

[8] K. Kountz, "Weathering of LNG in on-board Storage Tanks," tech. rep., Institute of Gas technology, 1999.

[9] IPCC, "Fifth Assessment Report - Mitigation of Climate Change," tech. rep., 2015.

[10] L. Mouillard, "Marine propulsion lecture," 2017.

[11] F. Burel, R. Taccani, and N. Zuliani, "Improving sustainability of maritime transport through utilization of Liquefied Natural Gas (LNG) for propulsion," *Energy*, vol. 57, pp. 412–420, 2013.

[12] International Group of Liquefied Natural Gas Importers, "GIIGNL Annual Report," tech. rep., 2017.

[13] Trifleet, "TRIFLEET LNG SPEC 2017-10R2," 2017.

[14] IPCC, "Climate Change 2014 Synthesis Report Summary for Policymakers," tech. rep., 2015.

[15] UNFCCC Conference of the Parties (COP), "United Nations Framework Convention on Climate Change," 1992.

[16] IMO, "Third IMO Greenhouse Gas Study 2014 - Executive Summary," tech. rep., 2014.

[17] M. L. Melamed, J. Schmale, and E. Von Schneidemesser, "Sustainable policy—key considerations for air quality and climate change," *Current Opinion in Environmental Sustainability*, vol. 23, pp. 85–91, dec 2016.

[18] Airuse, "The control of shipping emissions," tech. rep., 2016.

[19] M. Vianaa, P. Hammingh, and A. Colette, "Impact of maritime transport emissions on coastal air quality in Europe," *Atmospheric Environment*, vol. 90, pp. 96–105, 2014.

[20] United Nations, "The Ocean conference factsheet," 2017.

[21] J. J. Corbett, J. J. Winebrake, E. H. Green, P. Kasibhatla, V. Eyring, and A. Lauer, "Mortality from Ship Emissions: A Global Assessment," *Environmental Science & Technology*, vol. 41, pp. 8512–8518, dec 2007.

[22] Transport & Environment, "Statistical analysis of the energy efficiency performance (EEDI) of new ships," tech. rep., 2017.

[23] H. Winnes and E. Fridell, "Particle Emissions from Ships: Dependence on Fuel Type," *Journal of the Air & Waste Management Association*, vol. 59, pp. 1391–1398, dec 2009.

[24] Caroline Britz, "Emissions : La France soutiendra une zone SECA en Méditerranée | Mer et Marine," 2017.

[25] Deltamarin Ltd, "Turnkey hybrid scrubber system installation," 2017.

[26] Ship&Bunker, "By 2020 Ships Will Have Option to Desulfurize HFO Onboard to Meet 0.50% Sulfur Regs, Says Oil Tech Company," 2017.

[27] R. Estrada Villanueva Jr, *The emerging role of the classification society as an extension of the flag state administration.* PhD thesis, World Maritime University, 2004.

[28] P. Balcombe, J. Brierley, C. Lewis, L. Skatvedt, J. Speirs, A. Hawkes, and I. Staffell, "How to decarbonise international shipping: Options for fuels, technologies and policies," *Energy Conversion and Management*, vol. 182, pp. 72–88, feb 2019.

[29] D. Topali and H. N. Psaraftis, "The enforcement of the global sulfur cap in maritime transport," *Maritime Business Review*, apr 2019.

[30] DNV-GL, "Assessment of selected alternative fuels and technologies," tech. rep., 2018.

[31] DNV-GL, "In focus- LNG as ship fuel. Latest developments and projects in the LNG industry," 2015.

[32] J. Zelenka, G. Kammel, K. Pichikala, and W. Tritthart, "The Quality of Gaseous Fuels and Consequences for Gas Engines," in *Internationale Energiewirtschaftstagung*, 2017.

[33] J. Zelenka and C. Hoff, "Large Engines Competence Center Meeting the Challenges for Tomorrow ' s Power Generation Using Variable Intake Valve Train for Gas Engines The role of the gas engine in power generation," tech. rep., CIMAC Cascades Helsinki, 2017.

[34] W. Müller and J. Reeh, "Variation of Natural Gas Composition Challenges for Power Generation CIMAC Circle Presentation," tech. rep., Caterpillar, 2014.

[35] H. Tu, *Options and Evaluations on Propulsion Systems of LNG Carriers.* IntechOpen, feb 2019.

[36] V. Bolbot, *Storage, Handling and Boil-off of LNG on Ships.* PhD thesis, NTUA, 2014.

[37] Safety4sea, "New project to adapt space technology to LNG shipping," 2018.

[38] International Institute of Marine Surveying, "LATTICE Technology secures first commercial sale of its on-board LPV LNG Fuel tank," 2018.

[39] "ABS, OceanFinance and SSLC join forces introducing space tech to LNG shipping | LNG World News."

[40] "Prismatic Pressure Vessel [image] | EurekAlert! Science News."

[41] SEA\LNG and SGMF, "Life Cycle GHG Emission Study on the Use of LNG as Marine Fuel," tech. rep., 2019.

[42] M. Anderson, K. Salo, and E. Fridell, "Particle- and Gaseous Emissions from a LNG Powered Ship," *Environmental Science & Technology*, vol. 49, pp. 12568–12575, oct 2015.

[43] M. Leduc, "The Diesel engine and its development: A historical timeline."

[44] J. Babicz, *Wärtsilä encyclopedia of ship technology*. Wärtsilä corporation, 2015.

[45] M. Rozmarynowska-Mrozek, "The Development of the LNG-Fuelled Fleet and the LNG-Bunkering Infrastructure within the Baltic and North Sea Region," *Ekonomiczne Problemy Usług*, vol. 119, pp. 23–40, 2015.

[46] J. Ferreiro, "LNG fueled vessels – A history of firsts," 2015.

[47] E. P. Orue, "Membrane or Type C tanks in small scale LNG ships?," 2017.

[48] Q.-S. Chen, J. Wegrzyn, and V. Prasad, "Analysis of temperature and pressure changes in liquefied natural gas (LNG) cryogenic tanks," *Cryogenics*, vol. 44, no. 10, pp. 701–709, 2004.

[49] M. M. F. Hasan, A. M. Zheng, and I. A. Karimi, "Minimizing Boil-Off Losses in Liquefied Natural Gas Transportation," *Industrial & Engineering Chemistry Research*, vol. 48, pp. 9571–9580, nov 2009.

[50] E. Adom, S. Z. Islam, and X. Ji, "Modelling of Boil-Off Gas in LNG Tanks: A Case Study," *International Journal of Engineering and Technology*, vol. 2, no. 4, pp. 292–296, 2010.

[51] R. Bossier, *Numerical Simulations of LNG Flow in a Two-Tank System using REFPROP*. PhD thesis, Eindhoven University of Technology, 2011.

[52] E. L. Grotle, V. Aesoy, and E. Pedersen, "Modelling of LNG fuel systems for simulations of transient operations," *Maritime-Port Technology and Development - Proceedings of the International Conference on Maritime and Port Technology and Development, MTEC 2014*, pp. 205–215, 2015.

[53] E. L. Grotle and V. Æsøy, "Numerical Simulations of Sloshing and the Thermodynamic Response Due to Mixing," *Energies*, vol. 10, p. 1338, sep 2017.

[54] E. L. Grotle and V. Æsøy, "Dynamic modelling of the thermal response enhanced by sloshing in marine LNG fuel tanks," *Applied Thermal Engineering*, vol. 135, pp. 512–520, may 2018.

[55] Y. Shao, Y. Lee, H. Kang, Y. Shao, Y. Lee, and H. Kang, "Dynamic Optimization of Boil-Off Gas Generation for Different Time Limits in Liquid Natural Gas Bunkering," *Energies*, vol. 12, p. 1130, mar 2019.

[56] T. Włodek, "Analysis of boil-off rate problem in Liquefied Natural Gas (LNG) receiving terminals.," in *IOP Conference Series: Earth and Environmental Science*, 2019.

[57] E. Lisowski and W. Czyzycki, "Transport and storage of LNG container tanks," *Journal of KONES Powertrain and Transport*, vol. 18, 2011.

[58] E. Singstad Paulsen, *Analysis of the Boil-Off Phenomenon in Relation to Ambient Conditions*. PhD thesis, Norwegian University of Science and Technology, 2017.

[59] S. Mer, *Stockage d'ergol cryogénique pour l'exploration spatiale : étude expérimentale, modélisation et optimisation d'un système de contrôle thermodynamique à échappement*. PhD thesis, Université Grenoble Alpes, 2016.

[60] A. Van Foreest, "Modeling of cryogenic sloshing including heat and mass transfer," in *46th AIAA/ASME/SAE/ASEE Joint Propulsion Conference & Exhibit*, (Reston, Virigina), American Institute of Aeronautics and Astronautics, jul 2010.

[61] J. M. Shah and J. J. Aarts, "Effect of Weathering of LNG in Storage Tanks," in *Advances in Cryogenic Engineering*, pp. 253–260, Boston, MA: Springer US, 1995.

[62] H. Doyer and J. Sainson, "LNG behavior during shipping," in *LNG Conferences*, p. 8, 1998.

[63] G. G. Dimopoulos and C. A. Frangopoulos, "A dynamic model for liquefied natural gas evaporation during marine transportation," *International Journal of Thermodynamics*, vol. 11, no. 3, pp. 123–131, 2008.

[64] M. Faou, S. Roche, C. H. Jin, P. Corrignan, P. Marty, and C. Wandji, "Studies of the new generation of LNG ships," in *ATMA*, 2016.

[65] M. Miana, R. del Hoyo, V. Rodrigálvarez, J. R. Valdés, and R. Llorens, "Calculation models for prediction of Liquefied Natural Gas (LNG) ageing during ship transportation," *Applied Energy*, vol. 87, no. 5, pp. 1687–1700, 2010.

[66] L. A. Pellegrini, S. Moioli, F. Brignoli, and C. Bellini, "LNG Technology: The Weathering in Above-Ground Storage Tanks," *Industrial & Engineering Chemistry Research*, vol. 53, pp. 3931–3937, mar 2014.

[67] M. Miana, R. del Hoyo, and V. Rodrigálvarez, "Comparison of evaporation rate and heat flow models for prediction of Liquefied Natural Gas (LNG) ageing during ship transportation," *Fuel*, vol. 177, pp. 87–106, aug 2016.

[68] C. Migliore, C. Tubilleja, and V. Vesovic, "Weathering prediction model for stored liquefied natural gas (LNG)," *Journal of Natural Gas Science and Engineering*, vol. 26, pp. 570–580, sep 2015.

[69] C. Migliore, A. Salehi, and V. Vesovic, "A non-equilibrium approach to modelling the weathering of stored Liquefied Natural Gas (LNG)," *Energy*, vol. 124, pp. 684–692, apr 2017.

[70] F. Huerta and V. Vesovic, "A realistic vapour phase heat transfer model for the weathering of LNG stored in large tanks," *Energy*, vol. 174, pp. 280–291, may 2019.

[71] K. Arrhenius, A. Karlsson, A. Hakonen, L. Ohlson, H. Yaghooby, and O. Büker, "Variations of fuel composition during storage at Liquefied Natural Gas refuelling stations," *Journal of Natural Gas Science and Engineering*, vol. 49, pp. 317–323, jan 2018.

[72] A. Benito, "Accurate determination of LNG quality unloaded in Receiving Terminals : An Innovative Approach," in *World Gas Congress*, pp. 1–20, 2009.

[73] CIMAC WG17 Gas Engines, "Impact of Gas Quality on Gas Engine Performance," tech. rep., 2015.

[74] International Group of Liquefied Natural Gas Importers, "Position paper on the impact of including methane number in natural gas regulation," tech. rep., 2015.

[75] GIE, "Position Paper on impact of including Methane Number in the European Standard for Natural Gas," tech. rep., 2012.

[76] M. Kyratsoudi, "Quality & quantity verification processes across the LNG as a fuel bunkering," tech. rep., 2017.

[77] B. S. Institution, "BSI Standards Publication Natural gas — Calculation PD ISO/TR 22302:2014," tech. rep., 2014.

[78] H. B. Callen, *Thermodynamics and an Introduction to Thermostatistics*. 4th print ed., 1985.

[79] W. Wagner, "Software for the Reference Equation of State GERG-2008 for Natural Gases and Other Mixtures."

[80] O. Kunz, R. Klimeck, W. Wagner, and M. Jaeschke, "The GERG-2004 Wide-Range Equation of State for Natural Gases and Other Mixtures," tech. rep., GERG, 2007.

[81] O. Kunz and W. Wagner, "The GERG-2008 Wide-Range Equation of State for Natural Gases and Other Mixtures: An Expansion of GERG-2004," *Journal of Chemical & Engineering Data*, vol. 57, pp. 3032–3091, nov 2012.

[82] T.-V. Nguyen and B. Elmegaard, "Assessment of thermodynamic models for the design, analysis and optimisation of gas liquefaction systems," *Applied Energy*, vol. 183, pp. 43–60, dec 2016.

[83] G. Morrison and M. McLinden, "Application of a hard sphere equation of state to refrigerants and refrigerant mixtures," tech. rep., 1986.

[84] Promat, "International fire curves - PRTC."

[85] A. Sharafian, O. E. Herrera, and W. Merida, "Performance analysis of liquefied natural gas storage tanks in refueling stations," *Journal of Natural Gas Science and Engineering*, vol. 36, pp. 496–509, 2016.

[86] M. Kang, *Experimental Investigation of Influence of Thermal Stratification on Operation of Cryogenic Tanks*. PhD thesis, Korea Advanced Institute of Science and Technology, 2017.

[87] C. Montsarrat, *Fluid motion analysis in the cryogenic tanks of the upperstage of Ariane 5 during the ascent phase*. PhD thesis, 2019.

[88] A. Van Foreest, *Modeling of cryogenic sloshing including heat and mass transfer*. PhD thesis, 2014.

[89] M. J. Daigle, V. N. Smelyanskiy, J. Boschee, and M. Foygel, "Temperature Stratification in a Cryogenic Fuel Tank," *Journal of Thermophysics and Heat Transfer*, vol. 27, pp. 116–126, jan 2013.

[90] S. Gursu, S. A. Sherif, T. N. Veziroglu, and J. W. Sheffield, "Analysis and Optimization of Thermal Stratification and Self-Pressurization Effects in Liquid Hydrogen Storage Systems Part 1: Model Development," *Journal of Energy Resources Technology*, vol. 115, no. 3, p. 221, 1993.

[91] M. Vietze, C. Mundt, and S. Weiland, "Investigation of Thermal Characteristics of Sandwich Common Bulkhead Equipped Launcher Tank," *Journal of Spacecraft and Rockets*, vol. 54, pp. 67–74, jan 2017.

[92] B. Sakowski, "Sinda/Fluint Stratfied Tank Modeling," tech. rep., NASA, 2014.

[93] B. Gieseking and A. S. Brown, "Novel algorithm for calculating the methane number of liquefied natural gas with defined uncertainty," *Fuel*, vol. 185, pp. 932–940, dec 2016.

[94] International Group of Liquefied Natural Gas Importers, "GIIGNL Annual Report," tech. rep., 2018.

[95] A. Chouai, S. Laugier, and D. Richon, "Modeling of thermodynamic properties using neural networks: Application to refrigerants," *Fluid Phase Equilibria*, vol. 199, pp. 53–62, jun 2002.

[96] Matlab, "Deep Learning Toolbox: User's Guide," tech. rep., MathWorks.

[97] International Maritime Organization, "MEPC 70/18/Add.1 Annex 9," tech. rep., 2016.

[98] International Maritime Organization, "IGF Code," 2017.

[99] M. Chorowski, P. Duda, J. Polinski, and J. Skrzypacz, "LNG systems for natural gas propelled ships," *IOP Conference Series: Materials Science and Engineering*, vol. 101, dec 2015.

[100] J. DiRenzo, *Investigation of an LNG fuel system for a Norwegian coast guard ship: Undersøkelse av LNG drivstoffsystem for skip i den norske kystflåten.* PhD thesis, 2014.

[101] J. Thiaucourt, K. Le Bail, and J.-F. Hetet, "Impact of charged lng on its dynamic behaviour in a pressurized tank," in *COFRET 2018*, 2018.

[102] J. Thiaucourt, P. Marty, and J.-F. Hetet, "Impact of natural gas quality on engine performances over a journey using a thermodynamic fuel system model," in *International Conference on Modeling and Optimisation of Ship Energy Systems (MOSES)*, 2019.

UNIVERSITE BRETAGNE SCIENCES LOIRE POUR L'INGENIEUR

CENTRALE NANTES

Titre : Méthodes et modèles pour l'étude de faisabilité des navires propulsés au gaz naturel liquéfié

Mots clés : Gaz Naturel Liquéfié (GNL), Navire gaz, Code IGF, Boil-off, Combustible cryogénique

Résumé :

Rapporté à la tonne de fret, le trafic maritime est un mode de transport relativement « propre ». Néanmoins, par l'intensification des échanges mondiaux, sa part dans les émissions de Gaz à Effet de Serre (GES) au niveau mondial est appelée à augmenter. Conscients des effets néfastes associés aux GES, les pays membres des nations unies, via l'organisation maritime internationale, imposent le cadre réglementaire pour que ce secteur, vital dans une économie mondialisée, demeure écologiquement acceptable. Des objectifs ambitieux sont établis à court (2020) et moyen terme (2050). Or, d'après l'hypothèse faible de Porter, fixer des objectifs environnementaux sans imposer les moyens à mettre en œuvre favorise l'innovation. Aussi, dans l'industrie du « shipping », les solutions fleurissent au premier rang desquelles figure l'emploi du Gaz Naturel Liquéfié (GNL) en tant que combustible.

D'un point de vue thermodynamique, les inévitables infiltrations thermiques à travers les parois des réservoirs cryogéniques entraînent une variation de la pression dans le réservoir et des fluctuations de la qualité du gaz à l'admission moteur.

Selon le schéma d'exploitation navire, ces deux phénomènes impactent significativement la pertinence de l'option GNL.

En réponse, cette thèse propose un ensemble de modèles 0D pour, à partir d'un profil opérationnel, évaluer :

1. l'évolution de la pression dans les réservoirs ;
2. l'évolution de la qualité du gaz à l'admission moteur.

Dans une première partie, des modèles sont proposés pour simuler les infiltrations thermiques à travers le réservoir, l'évaporation du GNL, son vieillissement (altération des propriétés du gaz par évaporation différenciée des composés) et l'évolution du taux de méthane à l'admission moteur. Puis, les modèles sont assemblés à travers une étude de cas apportée par un acteur du transport maritime.

Title : Methods and models for the concept design of liquefied natural gas fuel systems on ships

Keywords : Liquefied Natural Gas (LNG), Natural gas fueled ships, IGF Code, Boil-off, Cryogenic fuel.

Abstract :

In proportion to the ton of cargo, shipping is a relatively "clean" transportation mode. Nevertheless, due to global trade intensification, its share in the global greenhouse gas (GHG) emissions should increase. Aware that GHG adverse effects are a major concern for humanity, united nation member states impose, via the international maritime organization, a regulatory framework so that this vital sector in a global economy remains sustainable. Short (2020) and medium (2050)-term goals are set. According to the weak version of Porter's hypothesis, strict environmental regulations encourage innovations. Hence, in the shipping industry solutions flourish among which the use of Liquefied Natural Gas (LNG) as a fuel.

On a thermodynamic basis, the unavoidable heat leaks into the cryogenic tanks cause variations of the tank pressure and the natural gas quality at engine inlet.

Depending on the ship's operational profile, those two phenomena will impact significantly the LNG as a fuel option relevance. One major bottleneck slowing the uptake of LNG as a marine fuel is the lack of methods and models to perform, at a concept design level, the feasibility study.

In response, this thesis proposes 0D models to assess from the operational profile:

1. the tank pressure evolution;
2. the gas quality evolution at engine inlet.

In the first part, models are proposed to simulate heat leaks into the tanks, LNG vaporization, ageing (the alteration of natural gas thermophysical properties by a differentiate vaporization of its compounds) and methane number evolution at engine inlet. Then, the models are put together and applied on a case study. The ship concept is proposed by a freight company.